The Role of Divalent Metal Ions in Enzymatic DNA Ligation

by

Mark Robert Taylor

A dissertation submitted in partial fulfillment
of the requirements for the degree of
Doctor of Philosophy
(Biological Chemistry)
in the University of Michigan
2014

Doctoral Committee:

Associate Professor Patrick J. O'Brien, Chair
Professor David R. Engelke
Professor Carol A. Fierke
Associate Professor Bruce A. Palfey
Associate Professor Thomas E. Wilson

Dedication

“If I have seen further, it is because I stand on the shoulders of giants.”

-Sir Isaac Newton

This thesis is a testament to all those that have helped me along my path,
who have picked me up when I have stumbled,
and have pushed me forward when I have stubbornly sat still.

Acknowledgements

This work could not have been accomplished without the help of countless people in my life. None of this would have been possible without the support of my family, my friends, my coworkers, and my peers in graduate school. Each of them has my eternal gratitude.

While I can't hope to acknowledge everyone's individual role in helping get this work done, certain people deserve special mention for their contributions to the work presented herein. Work by Daniel Wahl and John Conrad during rotations in the O'Brien lab was instrumental in getting the DNA ligation assay working and in providing preliminary data that helped guide my work. Neha Bokil performed the majority of the E720Q and D570N experiments as an undergraduate researcher under my guidance andTom Jurkiw performed most of the E621Q experiments while a rotation student in our lab. Both of these students truly astonished me with their quick grasp of the concepts of kinetics and their dedication to science. This work could not have been done so well or so quickly without them.

Table of Contents

Dedication.....ii

Acknowledgements.....iii

List of Figures.....v

List of Tables.....vii

Chapter 1: Background on Enzymatic DNA Ligation.....1

Chapter 2: Kinetic Mechanism of Human DNA Ligase I Reveals Magnesium-dependent Changes in the Rate-limiting Step that Compromise Ligation Efficiency.....14

Appendix A: Figures, Tables and Experimental Methods to Accompany Chapter 2.....39

Chapter 3: Comparison of Manganese and Magnesium as Cofactors for Human DNA Ligase I.....50

Appendix B: Figures and Tables to Accompany Chapter 3.....73

Chapter 4: Role of Conserved Active Site Carboxylates in Enzymatic DNA Ligation.....78

Chapter 5: Conclusions and Future Directions.....102

Appendix: Berkeley-Madonna Code for Reaction Fitting.....110

List of Figures

Figure 1-1: ATP dependent DNA ligase domain structure....2
Figure 1-2: Steps of enzymatic DNA ligation....4
Figure 1-3: Crystal structure of hLIG1 reveals 2 potential metal binding site....6
Figure 2-1: Reaction pathway for ligation by eukaryotic DNA ligase....16
Figure 2-2: Ligation assay using fluorescently labeled DNA....23
Figure 2-3: Pre-steady state ligation reaction under burst conditions....25
Figure 2-4: Magnesium dependence of single-turnover ligation....25
Figure 2-5: ATP dependence of LIG1....27
Figure 2-6: Magnesium dependence of multiple-turnover ligation....29
Figure 2-7: Evidence for the release of adenylylated intermediate during multiple-turnover ligation....31
Figure 2-8: Minimal kinetic mechanism of LIG1....32
Figure 2-9: Pathways for repair of 5'-adenylylated DNA resulting from abortive ligation....36
Figure A-1: Evaluation of different quenching solutions....44
Figure A-2: Representative single-turnover ligation kinetics indicate that the concentration of LIG1 employed is far above the K_d for substrate binding....44
Figure A-3: Active-site titration to determine the concentration of active (adenylylated) LIG1....45
Figure A-4: Stability of LIG1 in reaction buffer....45
Figure A-5: DNA concentration dependence of the multiple-turnover ligation reaction....46
Figure A-6: Multiple-turnover ligation is linearly dependent upon the concentration of LIG1....46
Figure A-7: Representative initial rates for steady state ligation by LIG1....47
Figure A-8: Binding of Mg^{2+} to ATP decreases the concentration of free Mg^{2+} available to LIG1....47

Figure A-9: Kinetic and thermodynamic constants obtained from fits of the ATP concentration dependencies with the two magnesium model for LIG1.....48
Figure A-10: Measurement of k_{cat}/K_M for utilization of ATP $(k_{cat}/K_M)^{ATP}$ by LIG1.....48
Figure 3-1: Multiple-turnover ligation with Mn2+ and saturating ATP and DNA.....61
Figure 3-2: Multiple-turnover ligation with Mn^{2+} and sub-saturating ATP.....62
Figure 3-3: Mn^{2+} is a noncompetitive inhibitor of Mg^{2+}-dependent ligation.....63
Figure 3-4: Mn^{2+} dependence of single-turnover ligation.....65
Figure 3-5: Mn^{2+} is a noncompetitive inhibitor of adenylyl transfer, but not nick-sealing.....66
Figure B-1: LIG1 is stable under standard manganese reaction conditions.....73
Figure B-2: Determination of proper quench solution for rapid-mixing experiments.....74
Figure B-3: Evidence of DNA saturation during manganese stimulated multiple-turnover ligation.....75
Figure B-4: ATP saturation of manganese stimulated multiple-turnover ligation.....75
Figure B-5: LIG1 saturation of manganese stimulated single-turnover ligation.....77
Figure 4-1: Metal binding sites revealed by hLIG1 structure.....81
Figure 4-2: Active-site titration of D570N and E720Q LIG1 mutants.....89
Figure 4-3: E621Q exhibits extremely slow single-turnover ligation.....90
Figure 4-4: E621Q shows no significant decrease in substrate binding activity.....91
Figure 4-5: Single-turnover ligation by D570N and E720Q.....92
Figure 4-6: Representative steady-state time-course.....94
Figure 4-7: D570N and E720Q display wild-type substrate binding.....95
Figure 4-8: D570N and E720Q show greatly weakened metal binding during multiple-turnover reactions.....97

List of Tables

Table 3-1: Comparison of kinetic constants for LIG1 measured in the presence of magnesium or manganese.....69

Table B-1: 800 nM LIG1 saturates single-turnover reactions under all tested reaction conditions.....77

Table 4-1: Comparison of kinetic constants measured with wild-type LIG1 to D570N and E720Q.....99

Chapter 1: Background on Enzymatic DNA Ligation

The simultaneous discovery of DNA ligases by the Gellert, Hurwitz, Lehman and Richardson groups in 1967 was a milestone in biology [1-4]. Identification of an enzyme capable of joining two DNA molecules filled a fundamental gap in the process of discontinuous DNA replication posited by Okazaki, *et al*. a year prior [5]. The ability to easily mend breaks formed in a DNA molecule also encouraged the idea of a dynamic genome, where DNA molecules continually experience transient breaks which are quickly mended. We now know this genomic dynamism to be essential to genomic integrity, as DNA breaks are continually formed and resealed during repair of DNA damage [6]. In addition to their importance in genomic maintenance, DNA ligases have proven an invaluable scientific tool. The ability to stitch together different DNA molecules enabled the technique of molecular cloning, which has proven essential to the advancement of the biomedical sciences. DNA ligases remain widely used today for many biotechnology and molecular biology applications.

Domain architecture of ATP-dependent DNA ligases

DNA ligases are a classic example of divergent evolution, with ATP dependent DNA ligases from viruses to bacteria to humans all sharing a conserved catalytic core [7] (Figure 1-1). This core consists of three independently folding domains; the DNA binding domain, the adenylylation domain, sometimes also referred to as the nucleotidyl transferase (NTase) domain, and the oligonucleotide binding (OB)-fold domain. Closest to the N-terminus is the DNA binding domain. This domain displays the largest size variability among DNA ligases, ranging from the nearly 300 residue domain of human DNA ligase I to the miniscule 20 residue "latch" of the Chlorella virus DNA ligase [8, 9]. True to its name, this domain displays the majority of DNA binding activity for the mammalian DNA ligases, and carries no residues required for

catalysis [9]. Next to the DNA binding domain lies the adenylylation domain. This domain contains the active-site lysine that becomes adenylylated, as well as the AMP binding pocket and numerous catalytic residues [10-13]. The C-terminal OB-fold domain contains the remainder of the residues required for catalysis. The OB-fold and adenylylation domains together display sufficient DNA binding activity to enable catalysis in the absence of the DNA binding domain [9]. Higher eukaryotes encode specialized DNA ligases which contain additional domains that appear to assist in substrate binding [14-16]. In addition to these core domains, most DNA ligases contain additional, non-catalytic residues at the N- and/or C-terminus that play a role in protein-protein interactions and cellular localization.

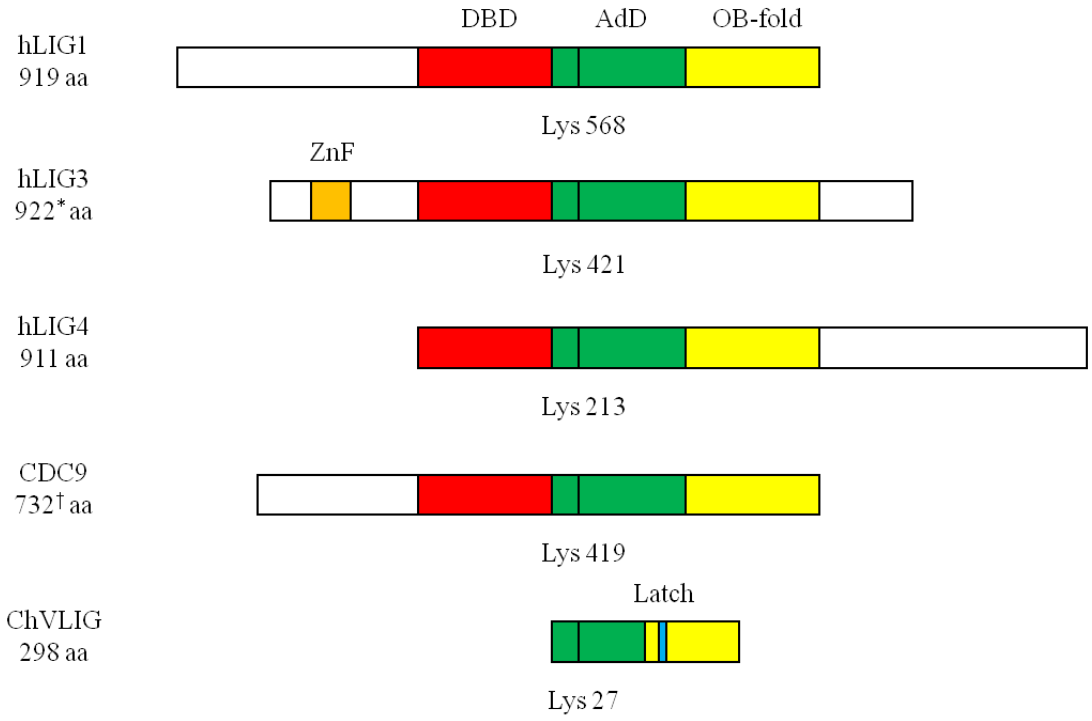

Figure 1-1: ATP dependent DNA ligase domain structure. Alignment of the domains present in human DNA ligase I (hLIG1), DNA ligase III (hLIG3), and DNA ligase IV (hLIG4), *Saccharomyces cerevisiae* DNA ligase (CDC9), and Chlorella Virus DNA ligase (ChVLIG). The adenylylation domain (AdD, green) and oligonucleotide binding-fold (OB-fold, yellow) domains which make up the core catalytic domains are highlighted along with the DNA binding domain (DBD, red). The position of the active-site that becomes adenylylated is listed for each protein. ChVLIG does not have a large DBD, but instead contains a small, 20 amino acid "latch" (Latch, blue) within the OB-fold that aids DNA binding. The zinc finger domain (ZnF, orange) unique to LIG3 is also pictured. N- and C-terminal protein-interaction motifs and cellular localization signals are not pictured.

Mechanism of Enzymatic DNA Ligation

All known DNA ligases follow a conserved reaction mechanism involving 3 independent phosphoryl transfers [17] (Figure 1-2). The reaction mechanism begins with enzyme adenylylation, where the enzyme catalyzes covalent attachment of an adenylyl group to an active-site lysine, using either NAD^+ or ATP as the AMP donor. During the next step, adenylyl transfer, the protein catalyzes transfer of the AMP group from the adenylylated lysine to an exposed 5' phosphate in DNA. The reaction completes with the nick-sealing step when the 3' hydroxyl of an adjacent DNA strand attacks the adenylylated 5' phosphate, resulting in phosphodiester bond formation. Each of these steps requires at least one divalent metal cofactor, with magnesium presumably the physiologically relevant cofactor. Throughout the reaction, the high energy of the original phosphoanhydride bond of ATP/NAD^+ is stored within intermediates, first as a phosphoramidate on the adenylylated lysine and then as a phosphoanhydride on the adenylylated DNA. This pathway effectively links the original energy of ATP/NAD^+ cleavage with formation of a phosphodiester bond. Though each of these steps is inherently reversible, hydrolysis of the pyrophosphate formed during enzyme adenylylation renders the overall reaction essentially irreversible.

Mammalian DNA Ligases

There are three identified mammalian DNA ligases. DNA ligase I (LIG1) accomplishes most of the most of the measured DNA ligation activity within a cell [18]. Found only in the nucleus and with robust activity toward single-strand breaks, LIG1 is predicted to be the main DNA ligase for resolving single-strand breaks formed during nuclear DNA replication and repair [19-21]. Immortalized cells originating from a patient with mutations in both LIG1 alleles suffer retarded Okazaki fragment joining, as well as general growth and genome stability defects [22, 23]. The patient herself suffered from developmental retardation as well as hypersensitivity to DNA damage and other developmental abnormalities [24]. Similar problems occur in mouse models containing LIG1 mutations [25]. Altogether these results suggest that LIG1 plays an essential role in nuclear genomic maintenance.

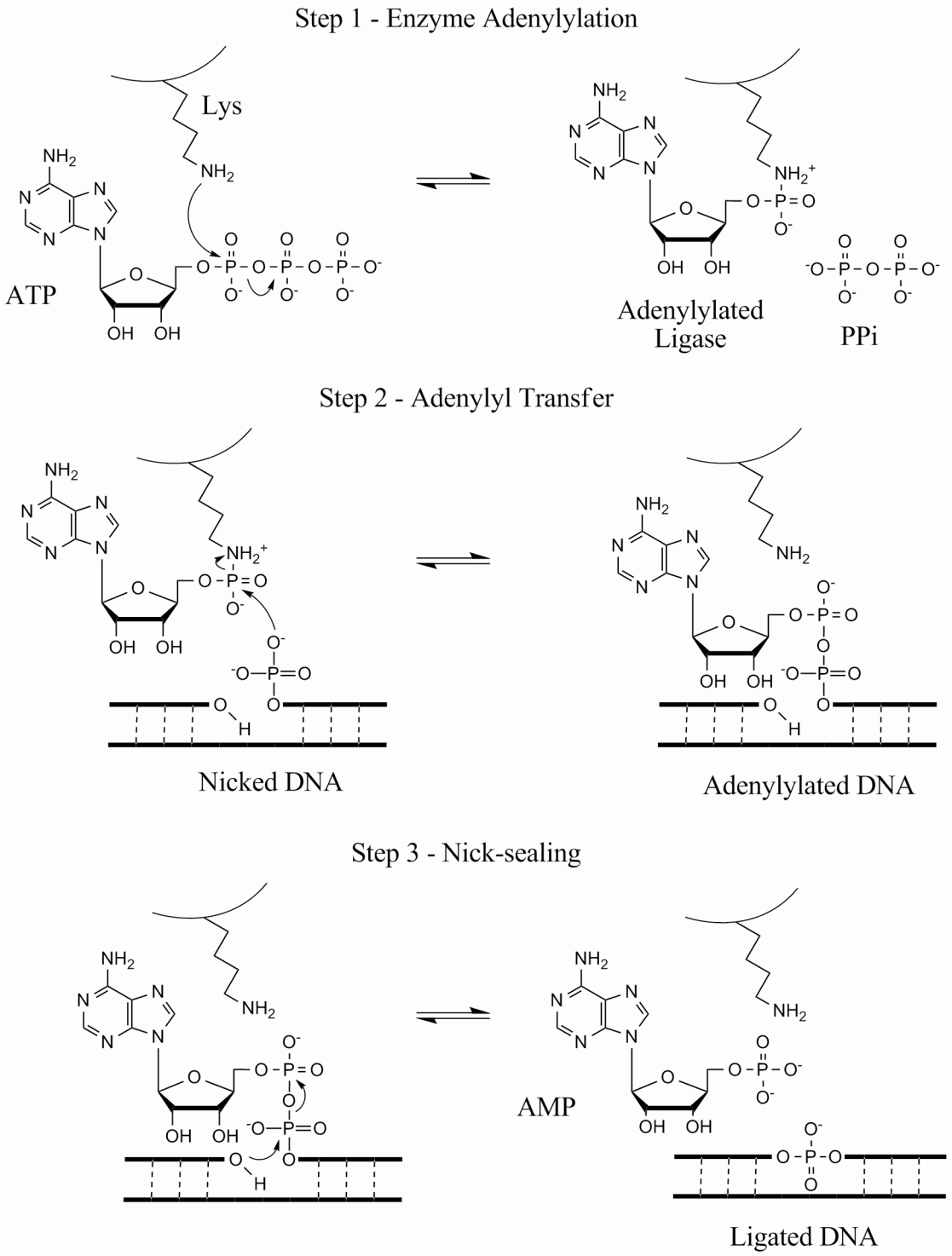

Figure 1-2: Steps of enzymatic DNA ligation. The three steps of enzymatic DNA ligation are pictured. The side-chain of the active-site lysine that becomes transiently adenylylated is pictured. Metal ions required for each reaction step are not pictured.

DNA ligase III (LIG3) is the sole DNA ligase in mitochondria and as such is essential for all mitochondrial DNA repair [26, 27]. Consistent with this role, LIG3 displays robust activity toward both single- and double-strand break repair. Loss of mitochondrial LIG3 results in abnormal mitochondrial structure and function, eventually leading to loss of the organelle and cell death [28]. LIG3 is also expressed in the nucleus, however its function within the nucleus is currently unknown. Numerous studies indicate LIG3 capable of participating in single- and double-strand nuclear DNA repair pathways, however cells without nuclear LIG3 appear normal. This suggests that LIG3 may assist in some nuclear DNA repair, but it is not essential and likely serves as an emergency backup to the other DNA ligases.

DNA ligase IV (LIG4) is responsible for nuclear double-strand break repair. Much of the activity of LIG4 is observed during non-homologous end joining (NHEJ) where two separate DNA molecules are joined end-to-end using little to no sequence homology [29]. Accurate NHEJ requires the activity of over half a dozen proteins including LIG4, and resolves otherwise catastrophic damage to the genome [30]. In addition to combating double-strand breaks formed as a result of DNA damage, NHEJ plays an essential role during immune system development by ligating together the immunoglobulin genes during V(D)J recombination [31]. Inappropriate NHEJ can cause chromosomal fusions and translocations, leading to severe cellular dysfunction and cancer [32]. Overexpression of LIG3 leads to an increase in the rate of chromosomal aberrations, suggesting that the double-strand break repair of LIG3 is more error prone than that of LIG4.

DNA Ligase Structure

In 2004, the first crystal structure of a human DNA ligase was solved by Pascal *et al.* [9] (Figure 1-3A). The crystal captures a truncated form of human LIG1 in complex with an adenylylated DNA nick. The truncation removes the N-terminal 231 residues of LIG1 which contain the nuclear localization signal and protein-interaction motifs. Loss of these residues does not seem to affect basic enzyme catalysis, as this form of the enzyme displays identical activity to the wild-type protein under *in vitro* conditions. Capture of the enzyme in complex with adenylylated

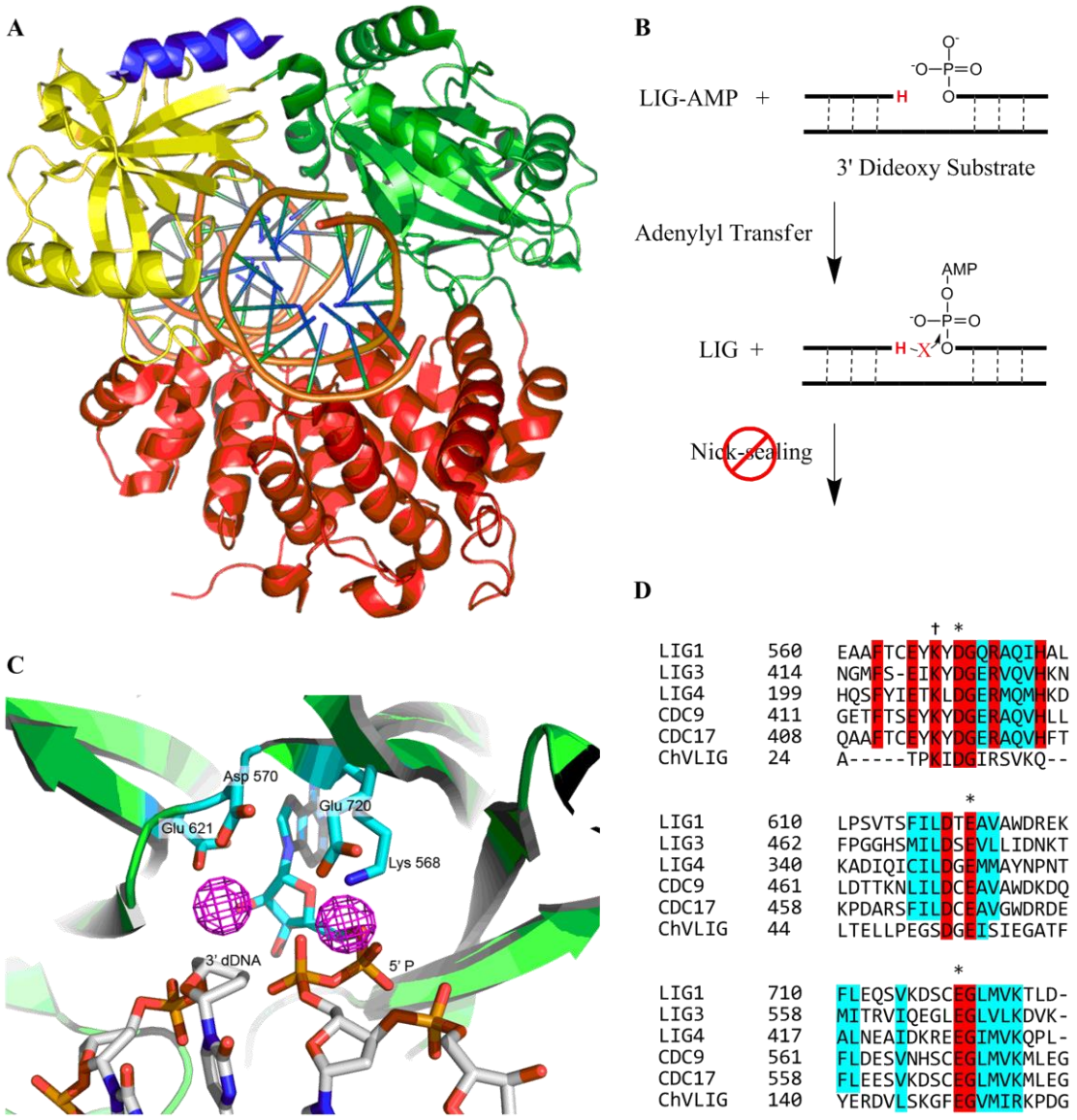

Figure 1-3: Crystal structure of hLIG1 reveals 2 potential metal binding sites. A Crystal structure of hLIG1 in complex with adenylylated DNA substrate [9]. DNA binding domain (red), adenylylation domain (green) and OB-fold domain (yellow) of hLIG1 completely encircle DNA substrate. Motif VI residues of the OB-fold domain (blue) which contain residues essential for enzyme adenylylation are oriented toward solvent. **B** The absence of a 3' hydroxyl group on the 5' side of the nick prevents nick-sealing. **C** Close-up view of hLIG1 active site. Magenta lattices indicate location of potential metal binding sites. Free 5' and 3' groups at the nick and residues involved in metal binding are labeled along with active-site lysine. **D** Protein sequence alignment of the three human DNA ligases with ligase from *Saccharomyces cerevisiea* (CDC9), *Schizosaccharomyces pombe* (CDC17) and Chlorella Virus DNA (ChVLIG) reveal strong conservation within the active-site. Alignment performed with default settings in ClustalX using truncated versions of each protein that include only the catalytic core domains. * indicates a residue involved in coordination of proposed active-site metal sites. † indicates Lys 568.

DNA was accomplished through the use of a DNA substrate containing a 3' dideoxy nucleotide at the nick. Without the 3' hydroxyl required for catalysis during nick-sealing, the enzyme is forced to stall between the adenylyl transfer and nick-sealing steps (Figure 1-3B). At this stage, the enzyme has fully encircled the DNA at the nick, with contacts between the N-terminal DNA binding domain and C-terminal OB-fold stabilizing the toroidal structure.

The difference in electron density between the crystal soaked in magnesium and manganese reveals two potential metal binding sites within the active-site (Figure 1-3C). These sites are coordinated by universally conserved residues that align very similarly in other DNA ligase structures (Figure 1-3C,D) [8, 33, 34]. Both of these sites have excellent coordination geometry for magnesium, and each is located in a position suitable for catalysis. The site on the 3' end of the nick, coordinated by E720 and the phosphate groups of the 5' adenylylate, positions a metal ion for activation of the 5' hydroxyl for nucleophilic attack on the adenylylated lysine during adenylyl transfer, and would also stabilize AMP as a leaving group during nick-sealing. The site on the 5' end of the nick, coordinated by E621 and D570, places a metal ion in position to activate the 3' hydroxyl for attack during nick-sealing. Each of these amino acid residues is universally conserved among LIG1 homologues, suggesting they serve an important role in LIG1 function. Mutations of the corresponding residues in Chlorella virus DNA ligase have large effects on both metal affinity during catalysis and maximal catalytic rate.

Impact of DNA Ligase Research

The essential role of DNA ligases in everyday genomic maintenance make them fascinating enzymes to study. The existence of multiple DNA ligases in humans with partially overlapping function raises the possibility that different DNA repair pathways could be targeted by specifically inhibiting individual DNA ligases. Used alone or combined with other DNA damaging agents that target certain DNA repair processes, DNA ligase inhibitors could then be potent chemotherapeutic agents. Recent research has identified some early small molecule candidates for DNA ligase inhibitors specific to each of the three human DNA ligases [35, 36]. One LIG3 inhibitor has proven specifically interesting, as early studies have shown certain

cancer cell lines display an increased sensitivity to DNA damaging agents in the presence of sub-toxic levels of the inhibitor. Though LIG1 specific inhibitors remain to be tested, these could be an excellent tool against tumors such as glioblastomas which grow around senescent neurons. Inhibition of LIG1 would preferentially harm cells going through replication, while normal DNA repair within the cells could be accomplished by LIG3.

There are few reported clinical cases of acute hLIG1 dysfunction, presumably because such dysfunction usually results in an extremely shortened lifespan. There are, however, multiple avenues by which slow onset, chronic hLIG1 dysfunction may occur. As one example, previous research has shown that different metals can inhibit the enzyme, and that this inhibition occurs under concentrations similar to those observed in cells during heavy metal poisoning [37]. On a cellular level, heavy metal poisoning leads to persistent DNA breaks, suggesting DNA ligases may be unable to seal breaks under these conditions [38]. There is also evidence that dysfunction of DNA ligases leads to neuronal dysfuntion in the disease Ataxia with Oculomotor Apraxia 1 (AOA1). Patients with AOA1 display late-onset, cumulative motor-neuron death, caused by loss of the protein Aprataxin [39, 40]. Aprataxin catalyzes the removal of adenylyl groups from 5' phosphates in DNA, whose only known mechanism of formation is abortive ligation by DNA ligases [41]. Thus understanding the basics of DNA ligase function may give insight into these and other diseases.

In addition to these clinically relevant reasons to study hLIG1, the importance of pursuing basic research cannot be overstated. Only by understanding the basics of how enzymes work can scientists begin to formulate the more important questions of how these enzymes relate to known and unknown diseases. For example, it is only because we characterized the kinetic mechanism of human LIG1 that we now know the adenylylated DNA problematic in AOA1 can be formed by LIG1 under normal cellular conditions, and not just during acute cellular stress. Though there is currently a popular push to pursue only the most relevant, immediately applicable research, we cannot rationally claim to know biology well enough to suggest we know the direct path toward any important discovery. In fact, the seemingly unimportant basic science research often leads to some of the most important breakthroughs in history. In this manner, the focus of this thesis is

the basic science of human DNA ligase I. Here I report my investigations into the metal dependence of enzymatic DNA ligation through kinetic characterization and active-site mutation.

The work in Chapter 2 characterizes the kinetic mechanism of hLIG1 in the presence of magnesium, the presumptive physiological metal cofactor. The main purpose of this work is to establish a kinetic framework for the function of hLIG1 against which future investigations can be compared. LIG1 is found to perform flawlessly under most conditions, converting single-strand nicks into ligated DNA. However, when magnesium concentrations are lowered, a detectable amount of abortive ligation occurs. Abortive ligation by a DNA ligase essentially exacerbates the damage at a nick, as the 5' adenylylated DNA that is formed is not easily rebound by ligase, and the nick becomes a persistent DNA break until other repair pathways can remove the adenylylated nucleotide. This type of damage is expected to play a role in the disease Ataxia with Oculomotor Apraxia 1, where the protein that directly removes 5' adenylyl groups, aprataxin, suffers loss of function.

Chapter 3 compares magnesium and manganese as cofactors for hLIG1. Full characterization of the kinetic mechanism of hLIG1 in the presence of manganese reveals that manganese alone can stimulate each step of the ligation reaction. The two metals display remarkable similarities with similar metal affinities and maximal rate constants for each step of the reaction. One startling difference between magnesium and manganese, however, is the presence of a lower affinity inhibitory manganese binding site. This inhibition has the peculiar trait of inhibiting enzyme adenylylation and adenylyl transfer, but not nick-sealing. The inhibitory metal site(s) also appear to be specific for manganese over magnesium, as the inhibitory metal ion(s) cannot be competed away with saturating levels of magnesium.

Chapter 4 investigates the effect of conservative mutations on the residues chelating the potential metal sites observed in the hLIG1 crystal structure. The goal of this investigation was to identify the role of each metal site during catalysis, and potentially whether one or two metals are required for catalysis. The E621Q mutation results in greatly diminished enzyme activity, creating an enzyme that is more than 10,000-fold slower than the wild-type. The enzyme appears to still be adenylylated and is technically capable of DNA ligation, but does so at a greatly

decreased rate. The D570N and E720Q mutations result in very similar effects on the enzyme. Both mutations weaken the magnesium affinity during adenylyl transfer and nick-sealing by ~10 fold. The mutations also decrease the maximal rate constants for adenylyl transfer and nick-sealing, resulting in an ~40-fold decrease in adenylyl transfer and ~100-fold decrease in nick-sealing for either mutation. These mutations also appear to affect the rate of enzyme adenylylation, suggesting that the metal sites play a role in both the DNA and ATP dependent reactions.

This body of work greatly deepens our understanding of the kinetic mechanism of enzymatic DNA ligation, and provides new insight into the role of meal ions during catalysis. Future research can build upon the information provided here to deepen our understanding of how metal ions play a role in the individual reaction steps, and how the enzyme engages the DNA substrate. The recent wide-spread availability of next-generation DNA sequencing technology allows the possibility to ask new questions about DNA ligases that would have been technically impossible a decade ago, like how does the sequence at a nick affect the rate, fidelity or efficiency of enzymatic DNA ligation.

References

1. Gellert, M., *Formation of covalent circles of lambda DNA by E. coli extracts.* Proc Natl Acad Sci U S A, 1967. **57**(1): p. 148-55.
2. Gefter, M.L., A. Becker, and J. Hurwitz, *The enzymatic repair of DNA. I. Formation of circular lambda-DNA.* Proc Natl Acad Sci U S A, 1967. **58**(1): p. 240-7.
3. Olivera, B.M. and I.R. Lehman, *Linkage of polynucleotides through phosphodiester bonds by an enzyme from Escherichia coli.* Proc Natl Acad Sci U S A, 1967. **57**(5): p. 1426-33.
4. Weiss, B. and C.C. Richardson, *Enzymatic breakage and joining of deoxyribonucleic acid, I. Repair of single-strand breaks in DNA by an enzyme system from Escherichia coli infected with T4 bacteriophage.* Proc Natl Acad Sci U S A, 1967. **57**(4): p. 1021-8.
5. Sakabe, K. and R. Okazaki, *A unique property of the replicating region of chromosomal DNA.* Biochim Biophys Acta, 1966. **129**(3): p. 651-4.
6. Sancar, A., et al., *Molecular mechanisms of mammalian DNA repair and the DNA damage checkpoints.* Annu Rev Biochem, 2004. **73**: p. 39-85.
7. Shuman, S. and B. Schwer, *RNA capping enzyme and DNA ligase: a superfamily of covalent nucleotidyl transferases.* Mol Microbiol, 1995. **17**(3): p. 405-10.
8. Nair, P.A., et al., *Structural basis for nick recognition by a minimal pluripotent DNA ligase.* Nat Struct Mol Biol, 2007. **14**(8): p. 770-8.
9. Pascal, J.M., et al., *Human DNA ligase I completely encircles and partially unwinds nicked DNA.* Nature, 2004. **432**(7016): p. 473-8.
10. Kodama, K., D.E. Barnes, and T. Lindahl, *In vitro mutagenesis and functional expression in Escherichia coli of a cDNA encoding the catalytic domain of human DNA ligase I.* Nucleic Acids Res, 1991. **19**(22): p. 6093-9.
11. Sriskanda, V. and S. Shuman, *Mutational analysis of Chlorella virus DNA ligase: catalytic roles of domain I and motif VI.* Nucleic Acids Res, 1998. **26**(20): p. 4618-25.
12. Sriskanda, V., et al., *Mutational analysis of Escherichia coli DNA ligase identifies amino acids required for nick-ligation in vitro and for in vivo complementation of the growth of yeast cells deleted for CDC9 and LIG4.* Nucleic Acids Res, 1999. **27**(20): p. 3953-63.
13. Sriskanda, V. and S. Shuman, *Role of nucleotidyl transferase motif V in strand joining by chlorella virus DNA ligase.* J Biol Chem, 2002. **277**(12): p. 9661-7.
14. Mackey, Z.B., et al., *DNA ligase III is recruited to DNA strand breaks by a zinc finger motif homologous to that of poly(ADP-ribose) polymerase. Identification of two functionally distinct DNA binding regions within DNA ligase III.* J Biol Chem, 1999. **274**(31): p. 21679-87.
15. Taylor, R.M., et al., *Role of the DNA ligase III zinc finger in polynucleotide binding and ligation.* Nucleic Acids Res, 1998. **26**(21): p. 4804-10.
16. Taylor, R.M., C.J. Whitehouse, and K.W. Caldecott, *The DNA ligase III zinc finger stimulates binding to DNA secondary structure and promotes end joining.* Nucleic Acids Res, 2000. **28**(18): p. 3558-63.

17. Lehman, I.R., *DNA ligase: structure, mechanism, and function.* Science, 1974. **186**(4166): p. 790-7.
18. Soderhall, S. and T. Lindahl, *Mammalian DNA ligases. Serological evidence for two separate enzymes.* J Biol Chem, 1975. **250**(21): p. 8438-44.
19. Levin, D.S., et al., *An interaction between DNA ligase I and proliferating cell nuclear antigen: implications for Okazaki fragment synthesis and joining.* Proc Natl Acad Sci U S A, 1997. **94**(24): p. 12863-8.
20. Montecucco, A., et al., *DNA ligase I is recruited to sites of DNA replication by an interaction with proliferating cell nuclear antigen: identification of a common targeting mechanism for the assembly of replication factories.* EMBO J, 1998. **17**(13): p. 3786-95.
21. Levin, D.S., et al., *Interaction between PCNA and DNA ligase I is critical for joining of Okazaki fragments and long-patch base-excision repair.* Curr Biol, 2000. **10**(15): p. 919-22.
22. Barnes, D.E., et al., *Mutations in the DNA ligase I gene of an individual with immunodeficiencies and cellular hypersensitivity to DNA-damaging agents.* Cell, 1992. **69**(3): p. 495-503.
23. Prigent, C., et al., *Aberrant DNA repair and DNA replication due to an inherited enzymatic defect in human DNA ligase I.* Mol Cell Biol, 1994. **14**(1): p. 310-7.
24. Webster, A.D., et al., *Growth retardation and immunodeficiency in a patient with mutations in the DNA ligase I gene.* Lancet, 1992. **339**(8808): p. 1508-9.
25. Bentley, D.J., et al., *DNA ligase I null mouse cells show normal DNA repair activity but altered DNA replication and reduced genome stability.* J Cell Sci, 2002. **115**(Pt 7): p. 1551-61.
26. Simsek, D., et al., *Crucial role for DNA ligase III in mitochondria but not in Xrcc1-dependent repair.* Nature, 2011. **471**(7337): p. 245-8.
27. Gao, Y., et al., *DNA ligase III is critical for mtDNA integrity but not Xrcc1-mediated nuclear DNA repair.* Nature, 2011. **471**(7337): p. 240-4.
28. Shokolenko, I.N., et al., *Mitochondrial DNA ligase is dispensable for the viability of cultured cells but essential for mtDNA maintenance.* J Biol Chem, 2013. **288**(37): p. 26594-605.
29. Wilson, T.E., U. Grawunder, and M.R. Lieber, *Yeast DNA ligase IV mediates non-homologous DNA end joining.* Nature, 1997. **388**(6641): p. 495-8.
30. van Gent, D.C. and M. van der Burg, *Non-homologous end-joining, a sticky affair.* Oncogene, 2007. **26**(56): p. 7731-40.
31. Grawunder, U., et al., *DNA ligase IV is essential for V(D)J recombination and DNA double-strand break repair in human precursor lymphocytes.* Mol Cell, 1998. **2**(4): p. 477-84.
32. Deriano, L. and D.B. Roth, *Modernizing the nonhomologous end-joining repertoire: alternative and classical NHEJ share the stage.* Annu Rev Genet, 2013. **47**: p. 433-55.
33. Ochi, T., X. Gu, and T.L. Blundell, *Structure of the catalytic region of DNA ligase IV in complex with an Artemis fragment sheds light on double-strand break repair.* Structure, 2013. **21**(4): p. 672-9.
34. Cotner-Gohara, E., et al., *Human DNA ligase III recognizes DNA ends by dynamic switching between two DNA-bound states.* Biochemistry, 2010. **49**(29): p. 6165-76.
35. Zhong, S., et al., *Identification and validation of human DNA ligase inhibitors using computer-aided drug design.* J Med Chem, 2008. **51**(15): p. 4553-62.

36. Chen, X., et al., *Rational design of human DNA ligase inhibitors that target cellular DNA replication and repair.* Cancer Res, 2008. **68**(9): p. 3169-77.
37. Yang, S.W., F.F. Becker, and J.Y. Chan, *Inhibition of human DNA ligase I activity by zinc and cadmium and the fidelity of ligation.* Environ Mol Mutagen, 1996. **28**(1): p. 19-25.
38. Li, H., R. Swiercz, and E.W. Englander, *Elevated metals compromise repair of oxidative DNA damage via the base excision repair pathway: implications of pathologic iron overload in the brain on integrity of neuronal DNA.* J Neurochem, 2009. **110**(6): p. 1774-83.
39. Date, H., et al., *Early-onset ataxia with ocular motor apraxia and hypoalbuminemia is caused by mutations in a new HIT superfamily gene.* Nat Genet, 2001. **29**(2): p. 184-8.
40. Moreira, M.C., et al., *The gene mutated in ataxia-ocular apraxia 1 encodes the new HIT/Zn-finger protein aprataxin.* Nat Genet, 2001. **29**(2): p. 189-93.
41. Ahel, I., et al., *The neurodegenerative disease protein aprataxin resolves abortive DNA ligation intermediates.* Nature, 2006. **443**(7112): p. 713-6.

Chapter 2: Kinetic Mechanism of Human DNA Ligase I Reveals Magnesium-dependent Changes in the Rate-limiting Step that Compromise Ligation Efficiency

Abstract

DNA ligase I (Lig1) catalyzes the ligation of single-strand breaks to complete DNA replication and repair. The energy of ATP is used to form a new phosphodiester bond in DNA via a reaction mechanism that involves three distinct chemical steps; enzyme adenylylation, adenylyl transfer to DNA and nick-sealing. We used steady state and pre-steady state kinetics to characterize the minimal mechanism for the reactions catalyzed by human Lig1. The ATP dependence of the reaction indicates that Lig1 requires multiple Mg^{2+} ions for catalysis and that an essential Mg2+ ion binds more tightly to ATP than to the enzyme. Further dissection of the magnesium ion dependence of individual reaction steps revealed that the affinity for Mg^{2+} changes along the reaction coordinate. At saturating concentrations of ATP and Mg^{2+} ions, the three chemical steps occur at similar rates and the efficiency of ligation is high. However, under conditions of limiting Mg^{2+}, the nick-sealing step becomes rate-limiting and the adenylylated DNA intermediate is prematurely released into solution. Subsequent adenylylation of enzyme prevents rebinding to the adenylylated DNA intermediate comprising an Achilles' heel of Lig1. These ligase-generated 5'-adenylylated nicks constitute persistent breaks that are a threat to genomic stability if left unrepaired. The kinetic and thermodynamic framework determined here for Lig1 provides a starting point for understanding the mechanism and specificity of mammalian DNA ligases.

*This work was done with the help of Daniel Wahl and John A. Conrad. DW and JC performed early experiments to determine proper reaction conditions for hLIG1, and collect early data on the kinetics of hLIG1 in the presence of multiple metals. Mark Taylor collected and analyzed all data reported herein with help from Patrick O'Brien.

Citation for this published work: Taylor, M.R., et al., Journal of Biological Chemistry, 2011. **286**(26): p. 23054-62.

Introduction

Breaks in DNA result from spontaneous hydrolysis of the phosphodiester backbone and are formed as transient intermediates during DNA replication and repair pathways. Mammals have three genes encoding DNA ligases that seal these breaks and restore the continuous nature of chromosomes. DNA Ligase I (Lig1) is essential for ligation of single-strand breaks in the nucleus, including the ligation of Okazaki fragments during discontinuous DNA replication [1]. DNA ligase III (Lig3) is required for mitochondrial DNA replication and repair. Although Lig3 has been assumed to play essential roles in nuclear DNA repair, it was recently shown to be dispensable for nuclear genomic maintenance [2, 3]. DNA ligase IV (Lig4) is specialized for repair of nuclear double-strand breaks, and is required for nonhomologous end joining and V(D)J recombination [4, 5].

The overall reaction catalyzed by DNA ligases involves the formation of a phosphodiester bond between an adjacent 3' hydroxyl and a 5' phosphate in DNA. The reaction proceeds via a universally conserved pathway [6-8] (Figure 2-1). First, the apoenzyme catalyzes transfer of the AMP group from a nucleotide cofactor to an active site lysine, forming an adenylylated enzyme intermediate. Eukaryotic ligases use ATP as the adenylyl group donor, whereas bacterial ligases utilize either ATP or NAD^+. After binding a nicked DNA substrate, the adenylylated enzyme catalyzes transfer of the adenylyl group to the 5'-phosphate present at the nick, forming an adenylylated DNA intermediate. In the final step of the reaction, DNA ligase catalyzes the nucleophilic attack of the 3'-hydroxyl on the adenylylated 5'-phosphate to form a new phosphodiester bond and to release AMP. Although enzyme adenylylation and nick-sealing are known to be reversible in the presence of a large excess of pyrophosphate or AMP, these steps are effectively irreversible in their absence. All of the chemical steps catalyzed by ligase have been shown to require magnesium, but the number of magnesium ions and their affinities during each step have not been determined [9].

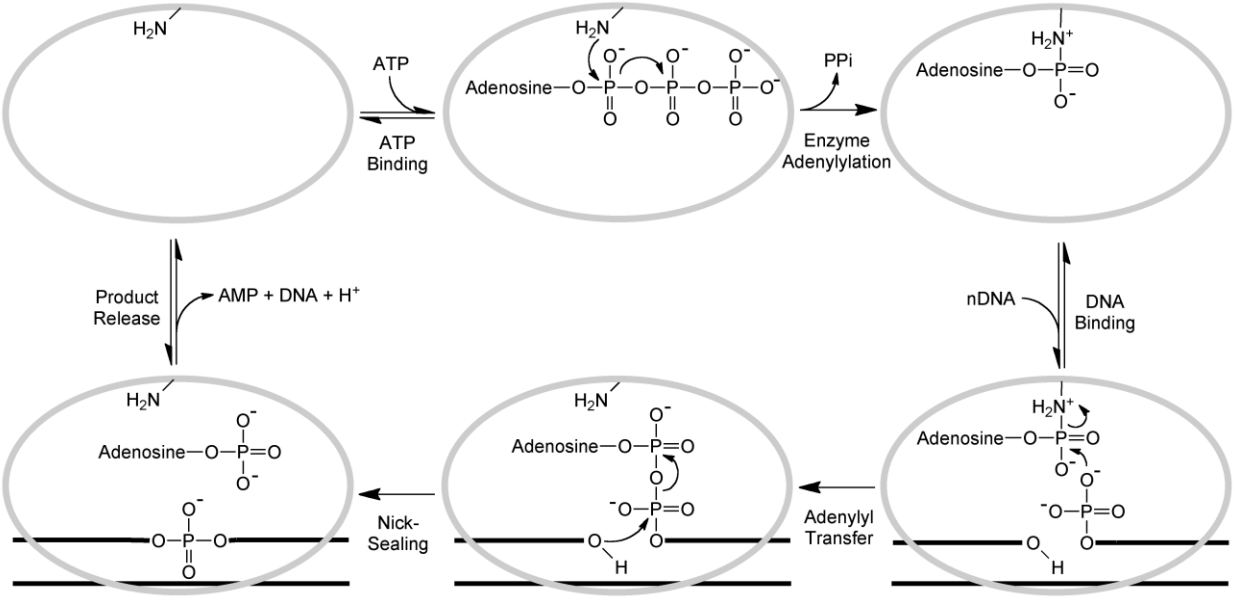

Figure 2-1. Reaction pathway for ligation by a eukaryotic DNA ligase. Cleavage of the phosphoanhydride bond of ATP provides the energy required to form a phosphodiester bond in DNA. This is achieved by the initial formation of an adenylyl-lysine covalent intermediate with the release of inorganic pyrophosphate (PPi), subsequent transfer of the AMP group to the 5'-phosphate of the nicked DNA (nDNA), and finally the attack of the 3'-hydroxyl to seal the nick and release AMP. All three of these chemical steps require Mg^{2+} ions (not shown).

The crystal structure of human Lig1 in complex with an adenylylated DNA intermediate revealed that three distinct domains of the enzyme encircle the DNA substrate [10]. Extensive interactions distort the DNA and allow the two ends of the nick to be juxtaposed in the active site of the enzyme. The overall structure of the Lig1 complex is expected to be similar for both the adenylyl transfer and nick-sealing steps, although the active site may require rearrangement to reposition the reactive phosphoryl group between these two steps. In contrast, the enzyme must undergo a large conformational change to allow for enzyme adenylylation [10-12]. The crystallized ligase lacks the N-terminal 232 amino acids that contain the nuclear localization signal and contribute to protein-protein interactions [7, 13, 14]. We chose to use the same form that was crystallized for our biochemical studies, because this truncated enzyme is fully active as a ligase *in vitro* [10] and is able to complement ligase-deficient bacteria [15].

We have determined the minimal kinetic mechanism for ligation of a single-strand break by human Lig1 and have examined the magnesium dependence of the individual steps. These experiments revealed that the rate-limiting step changes as a function of magnesium

concentration and exposed an Achilles' heel of Lig1, whereby low magnesium concentrations cause release of the adenylylated DNA intermediate to form a persistent DNA break. This observation provides a rationale for the existence of the aprataxin pathway for repair of adenylylated DNA intermediates and implies that magnesium deficiency could cause defects in DNA repair and replication.

Experimental Procedures

Recombinant DNA Ligase I

The catalytic domain of human Lig1 (residues 232-919) was expressed in *E. coli* and purified as previously described [10]. Cells were lysed in the presence of 1 mM EDTA to preserve the adenylylated form of the enzyme, and subsequently purified over a phosphocellulose column and a NTA-nickel column. The His tag was removed with Prescission protease, and Lig1 was further purified with Q-sepharose. The final purified fractions were combined and dialyzed into storage buffer (25 mM Tris•Cl, pH 7.6, 150 mM NaCl, 1 mM DTT, and 0.1 mM EDTA). Aliquots were snap-frozen and stored at -80 ^{o}C. Purity was greater than 95% as judged by SDS-PAGE. Initial concentrations were estimated from the absorbance at 280 nm, using the calculated extinction coefficient. The concentration of active, adenylylated enzyme was determined by titration with nicked DNA substrate, as described below, and this active concentration is reported throughout.

DNA Substrates

Oligonucleotides were synthesized by Integrated DNA Technologies or by the Keck Center at Yale University and were purified on denaturing polyacrylamide gels. The portion of the gel containing the full-length oligonucleotide was excised and crushed, and DNA was extracted by soaking overnight in 500 mM NaCl and 1 mM EDTA. The extracted oligonucleotides were desalted by binding to a C18 reverse phase column (Sep-pak, Waters) and eluted with 30% (v/v) acetonitrile. Concentrations were obtained from the absorbance at 260 nm using the calculated extinction coefficients. The three oligonucleotides used in this study had sequences 5'-CCGAATCAGTCCGACGACGCATCAGCAC, 5'-GTGCTGATGCGTC, and 5'-P-GTCGGACTGATTCGG-FAM (P indicates 5' phosphorylation and FAM indicates the presence

of a 3’ fluorescein). The nicked, double-stranded DNA substrate (nDNA) was formed by mixing equimolar amounts of the three oligonucleotides in 10 mM NaMES pH 6.5 and 50 mM NaCl and cooling the mixture from 90 °C to 4 °C at a rate of 3 °C per minute.

Gel-based Ligation Assay

Ligation reactions were performed at 37 °C. Unless otherwise indicated, the standard buffer contained 50 mM NaMOPS pH 7.5 (measured at 25 °C), 1 mM dithiothreitol, 0.05 mg/mL BSA, and sufficient NaCl to maintain a constant ionic strength of 150 mM. The amounts of ATP, $MgCl_2$, nDNA, and Lig1 varied, as indicated below. Preincubation controls established that Lig1 retains 100% of its activity after 1 hr in this standard buffer, and all of the kinetic data was collected within this window of time (Appendix Figure A-4). Reactions were quenched in formamide/EDTA (30 mM EDTA in 94% formamide), heated to 95 °C for 5 min to denature the DNA and resolved on 20% (w/v) denaturing polyacrylamide gels containing 8 M Urea. Fluorescein-labeled oligonucleotides were detected with a Typhoon Trio$^+$ imager (GE Healthcare) with excitation at 488 nm and emission through a 520 nm band-pass filter. The images were analyzed using ImageQuantTL (GE Healthcare). The intensity of the individual DNA species was corrected for background fluorescence, and the fraction of the total fluorescence was determined by dividing the fluorescence intensity for the desired species by the signal for all other species in the sample. When necessary, this fraction was converted into its concentration by multiplying by the total concentration of DNA in the reaction.

Rapid Quench Experiments

Rapid mixing experiments were performed in a Kintek RFQ-3 quench-flow apparatus. One sample loop contained Lig1 and the other contained nDNA, each at double the reaction concentration. The samples were in 1x reaction buffer with the desired magnesium concentration and the drive syringes contained the same solution. Loaded reactants were allowed to equilibrate for 90 seconds to reach the correct temperature. Reactions were initiated by mixing of 20 µL of

each sample and were quenched at the desired times by mixing with 20 µL of 50 mM EDTA in 90% formamide. Samples were analyzed with the standard gel-based ligation assay. Unless otherwise indicated, the typical concentrations of nDNA and Lig1 were 80 nM and 600 nM, respectively. The data were imported into the program Berkeley-Madonna (www.berkeleymadonna.com) and the curve fitting function was used to globally fit the levels of intermediate and product by the scheme represented in Figure 2-1 (see Appendix A for additional details). Fitting of the data to a model including reversible chemical steps did not produce significantly different results (data not shown). Fits of reactions from individual experiments provided values for the rate constants for adenylyl transfer and nick-sealing and the reported values reflect the average rates determined from at least three independent experiments at each concentration of magnesium. These rate constants were plotted versus the concentration of magnesium ions and fit by a hyperbolic binding curve (Equation 2-1), in which k_{obs} is the observed rate constant at a given concentration of Mg^{2+}, k_{max} is the maximal rate constant at saturating Mg^{2+}, and K_{Mg} is the concentration of Mg^{2+} at which k_{obs} is equal to one half k_{max} (Kaleidagraph, Synergy Software).

$$k_{obs} = k_{max}[Mg^{2+}]/(K_{Mg} + [Mg^{2+}]) \qquad \text{Equation 2-1}$$

Multiple-Turnover Ligation Assays

Steady state kinetic analysis was performed in the standard ligation buffer and the temperature was maintained at 37 °C in a circulating water-bath. Reaction mixtures were preincubated for 5 min prior to addition of enzyme. Reactions were arrested by quenching a 4 µL aliquot in 15 µL of a quench solution (50 mM EDTA in 95% formamide), and the extent of ligation was determined as described above. The initial rates were determined from the linear rate of substrate disappearance within the first 10% of the reaction. When both intermediate and product were observed, the rate of formation of each species was determined. Values reported represent the average of at least three experiments. The dependence on substrate concentration was fit by the Michaelis-Menten equation (Equation 2-2) and the magnesium concentration dependence was fit by Equation 2-3, in which K_{Mg} is the concentration of Mg^{2+} required to reach half of the maximal

rate of reaction. The full ATP dependence at 0.2 and 1 mM Mg^{2+} was fit by the equation for a random, bi-reactant system that accounts for the depletion of one substrate by the other (see Appendix A Additional Methods).

$$V_{init}/[E] = V_{max}[S]/(K_M + [S]) \qquad \text{Equation 2-2}$$

$$V_{init}/[E] = V_{max}[Mg^{2+}]/(K_{Mg} + [Mg^{2+}]) \qquad \text{Equation 2-3}$$

The efficiency of ligation was defined as the partitioning between nick-sealing and release of adenylylated DNA, and was determined by dividing the steady-state rate of product formation by the sum of the rates of formation of product and intermediate Equation 2-4. See the Appendix A materials for additional information including the equation used for fitting the Mg^{2+} dependence for the efficiency of ligation.

$$\text{Efficiency} = V_{prod}/(V_{prod} + V_{int}) \qquad \text{Equation 2-4}$$

Results

Gel-based Ligation Assay

We characterized the enzymatic activity of Lig1 on a synthetic 28mer oligonucleotide duplex that contained a nick with a 3'-hydroxyl and a 5'-phosphate (Figure 2-2A). This substrate is identical to the oligonucleotide that was crystallized in complex with Lig1 [10] except for the addition of a fluorescein label at the 3' end of the downstream 15mer. The fluorescein label enables detection of the AMP-DNA intermediate and is not expected to alter reaction kinetics, because the downstream end of this DNA does not contact Lig1 in the crystal structure. In order to measure the pre-steady state kinetics for the Lig1-catalyzed reaction, we used a rapid-quench apparatus. Under optimal conditions the enzymatic DNA ligation occurs on the second time scale, requiring a rapid and efficient quench that traps all of the intermediates. Therefore, we tested several chemical quenches, including EDTA/formamide, urea, and concentrated sodium hydroxide, and found that EDTA/formamide and sodium hydroxide are equally effective in stopping the ligation reaction (Appendix Figure A-1). In contrast, a urea quench solution takes significantly longer to inactivate Lig1 and results in greater amounts of intermediate and product than either the EDTA or hydroxide quench solutions. Samples quenched in EDTA/formamide can be directly analyzed by gel electrophoresis, making this a convenient quench. A representative time course for a single-turnover ligation reaction is shown in Figure 2-2. Greater than 95% of the nicked DNA is ligated within two seconds and the build-up and break-down of the adenylylated DNA intermediate can be readily quantified. The concentration of Lig1 was varied in excess over the concentration of DNA to establish that the concentrations employed were far above the dissociation constant for DNA binding and that the maximal single-turnover rates were determined (Appendix Figure A-2). This gel-based assay allows both pre-steady state and steady state kinetics of the Lig1-catalyzed reaction to be monitored.

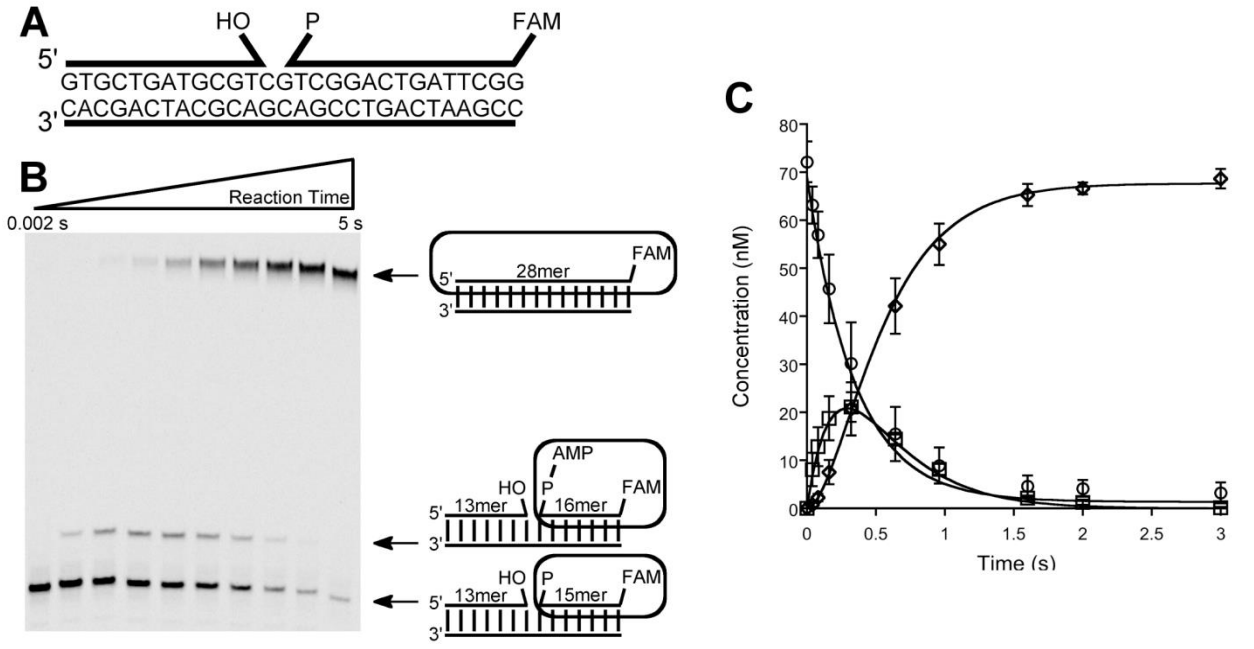

Figure 2-2. Ligation assay using fluorescently-labeled DNA. A, Schematic of the 28mer nicked DNA substrate. The 3'-hydroxyl (OH), 5'-phosphate (P), and 3'-fluorescein (FAM) label are shown. **B**, Representative denaturing 20% acrylamide gel of a single-turnover ligation reaction with 80 nM nDNA, 600 nM Lig1, and 1 mM $MgCl_2$. Shown to the right of the gel are the species represented in each band with the fluorescent molecule highlighted. **C**, Results of quantification and fitting of substrate (○), intermediate (□) and product (◊) from three separate experiments, including the example shown in B. The error bars indicate one standard deviation from the mean. The lines indicate the global fit of all three species by Berkeley-Madonna using the reaction mechanism from Figure 2-1. The rate constants for adenylyl transfer and nick-sealing are determined from these data.

Pre-steady State Burst and Active Site Titration of Ligase

Recombinant Lig1 was purified from *E. coli* in the fully adenylylated form [10, 16]. Therefore, we titrated Lig1 against a fixed concentration of DNA in the absence of ATP and allowed the ligation reaction to proceed to completion. The amount of active enzyme is indicated by the amount of DNA that was ligated, because each enzyme molecule can turn over only once (Appendix Figure A-3). This analysis assumes that 100% of the enzyme is in the adenylylated form, which was confirmed by carrying out burst experiments in which enzyme was preincubated with ATP and Mg^{2+} prior to the addition of nicked DNA substrate (Figure 2-3). When 80-fold molar excess of ATP (4 μM) is present, the burst phase is followed by a steady state phase. The burst amplitude is identical within error to the amount of DNA that is ligated in the absence of added ATP, indicating that all of the Lig1 molecules are adenylylated (Figure 2-

3). The observation of burst kinetics indicates that a step up to or including enzyme adenylylation is rate-limiting at low concentrations of ATP. In contrast, when the concentration of ATP is increased to 150 μM, the burst phase is almost eliminated (Figure 2-3, ◊). This indicates that the rate constant for enzyme adenylylation with saturating ATP is similar in magnitude to the rate constant for adenylyl transfer from the enzyme to the DNA.

Mg^{2+}-dependence of Single-turnover Ligation

To investigate the steps of adenylyl transfer and nick-sealing, we performed single-turnover ligation reactions at a range of Mg^{2+} concentrations. As Lig1 is fully adenylylated, it was not necessary to add ATP to these reactions. The advantage of using single-turnover conditions with excess enzyme over DNA is that neither the enzyme adenylylation nor product release steps are monitored. The concentration of enzyme was far above the K_d for DNA binding and therefore DNA binding is much faster than the subsequent steps (Appendix Figure A-2). Thus, the rate constants for both adenylyl transfer and nick-sealing can be determined from this analysis (see Figure 2-2C for representative data). These microscopic rate constants are plotted as a function of magnesium concentration and the data are fit by a simple hyperbolic binding equation (Figure 2-4). This fit yields the maximal rate at saturating Mg^{2+} (k_{max}) and the concentration that is necessary to reach half of the maximal rate (K_{Mg}). EDTA rapidly inactivates all Lig1-catalyzed reactions, suggesting that Mg^{2+} binding is in rapid equilibrium. Therefore, K_{Mg} is expected to be equal to the dissociation constant for the weakest essential Mg^{2+} ion. It is striking that the adenylyl transfer reaction shows a much higher affinity for magnesium than the nick-sealing reaction (K_{Mg} of 0.15 and 2.6 mM respectively; Figure 2-4). With saturating magnesium, the nick-sealing step is significantly faster than the adenylyl transfer rate with k_{max} values of 12 s^{-1} and 2.6 s^{-1}, respectively. However, because of the lower affinity for magnesium during the nick-sealing reaction, the nick-sealing step becomes rate-limiting at very low concentrations of Mg^{2+}. This leads to an increase in the lifetime of the adenylylated DNA intermediate.

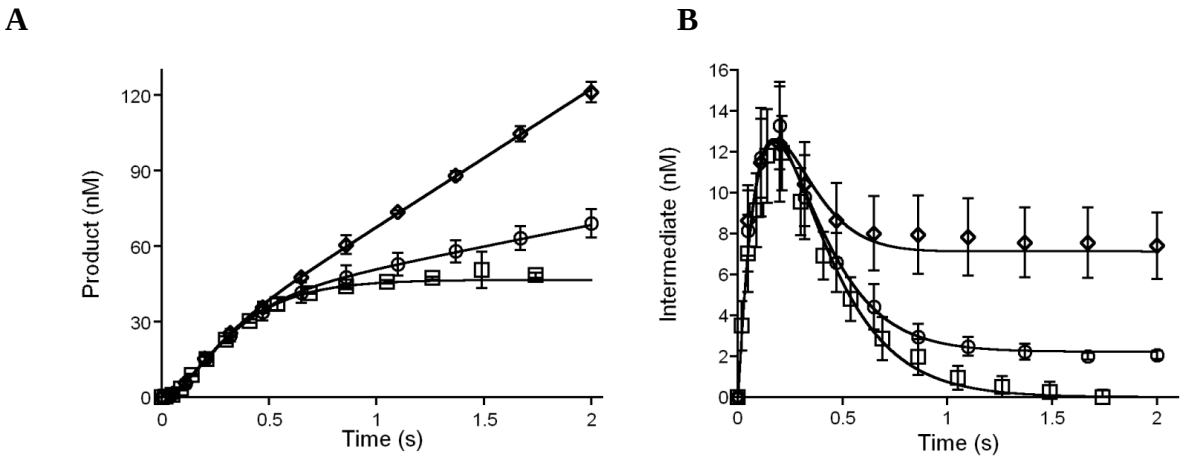

Figure 2-3. Pre-steady state ligation reaction under burst conditions. Formation of DNA product (A) and adenylylated intermediate (B) were monitored during single and multiple-turnover reactions containing 50 nM ligase, 500 nM nDNA, and 10 mM $MgCl_2$ in the absence of ATP (□), or in the presence of 4 μM (○) or 150 μM ATP (◊). In reactions containing ATP, Lig1 was preincubated with ATP to allow for enzyme adenylylation. The identical burst amplitude observed for multiple-turnover and single-turnover reactions indicates that all of the active ligase is already adenylylated. At saturating ATP the steady state rate is only slightly slower than the pre-steady state rate and the burst is poorly defined. This demonstrates that enzyme adenylylation and adenylyl transfer occur at similar rates when the enzyme is saturated with Mg^{2+} ions and ATP and DNA substrates. The steady state level of adenylylated DNA intermediate is at almost 20% the level of total enzyme when ATP is saturating (150 μM, ◊), providing additional evidence that the nick-sealing step is partially rate-limiting under these conditions.

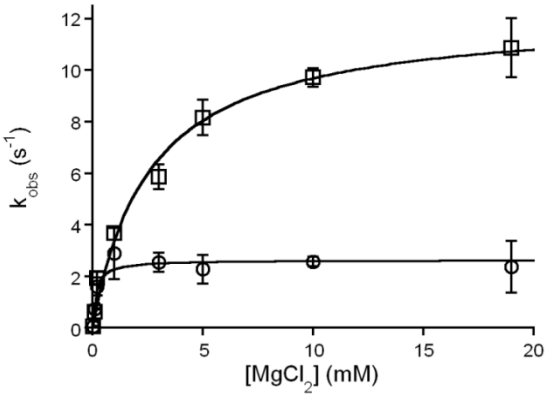

Figure 2-4. Magnesium dependence of single-turnover ligation. Reactions containing 80 nM nDNA, 600 nM Lig1, and Mg^{2+} concentrations that ranged from 0.02 to 19 mM were monitored by quenched-flow. The time-dependent changes in the concentration of DNA product and intermediate were fit by the minimal kinetic scheme to obtain the rate constants for adenylyl transfer (○) and nick-sealing (□). Both rates increase as a function of Mg^{2+} concentration and the curves shown are fits to a binding hyperbola. These hyperbolic fits yield maximal rate constants of 2.6 ± 0.6 s^{-1} for adenylyl transfer and 12 ± 2 s^{-1} for nick-sealing. The K_{Mg} value for the adenylyl transfer step (0.15 ± 0.06 mM) is much lower than the value observed for nick-sealing (2.6 ± 0.9 mM). Due to the difference in affinity, adenylyl-transfer is mostly rate-limiting at high concentrations of $MgCl_2$, but the two steps become more closely matched at low concentrations of $MgCl_2$.

ATP Dependence of Steady State Ligation

In order to characterize multiple-turnover ligation, we first measured the dependence of the Lig1-catalyzed reaction on the concentration of ATP. Initial rates were measured with saturating concentration of DNA (1 μM) and three different concentrations of Mg^{2+}. Under all conditions, the initial rate portion of the reaction progress curves is linear (Appendix Figure A-7). At a high concentration of Mg^{2+} (30 mM), the ATP dependence follows Michaelis-Menten behavior with a K_M value of 12 μM and a k_{cat} value of 0.74 s^{-1} (Figure 2-5A). In contrast, at 1 mM Mg^{2+} the velocity shows a biphasic dependence on the concentration of ATP (Figure 2-5B). The expected Michaelis-Menten behavior is observed at low concentrations of ATP, but strong inhibition is observed at higher concentrations of ATP. A similar biphasic ATP dependence is observed in reactions with 0.2 mM Mg^{2+}, but the inhibitory phase is shifted to a lower concentration of ATP than in the reactions performed at 1 mM Mg^{2+} (Figure 2-5C). The inhibition can be explained by the model in which Lig1 requires two Mg^{2+} ions for enzyme adenylylation, with one metal coming from ATP•Mg^{2+} and the other coming from solution (Figure 2-5D). The dissociation constant for ATP binding to Mg^{2+} under similar conditions has been reported to be 10–30 μM [17, 18], and thus the concentration of free Mg^{2+} is predicted to be dramatically decreased by the presence of stoichiometric ATP (Appendix Figure A-8). Similar inhibition has been observed for other ATP-dependent enzymes [19, 20]. Although the ATP concentration dependence could be readily fit by the requirement for two Mg^{2+} ions at both 1 and 0.2 mM $MgCl_2$ (Figure 2-5B, C), these fits gave slightly different estimates for the Mg^{2+} affinity and the maximal rate of ligation (Appendix Figure A-9). The discrepancy between different data sets could be due to experimental error or to additional complexities such as inhibition by free ATP. Therefore, we independently measured the Mg^{2+} dependence of k_{cat}/K_M and k_{cat} under conditions in which magnesium was always in excess over ATP.

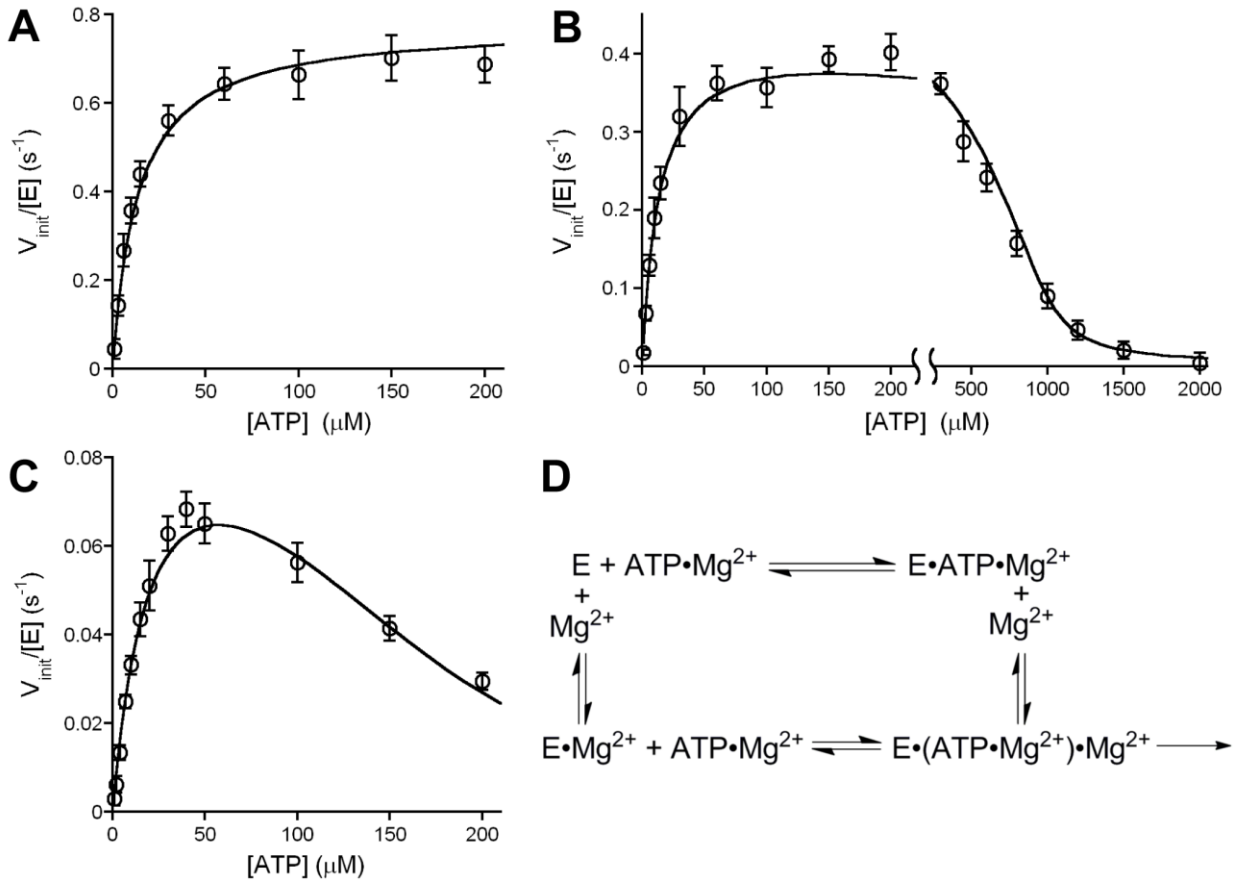

Figure 2-5. ATP dependence of Lig1. Multiple-turnover ligation assays were performed with saturating nDNA (1 μM) and with varying concentration of ATP and Mg^{2+}. *A*, The initial rates determined with 30 mM $MgCl_2$ are plotted as a function of ATP concentration. These data were fit by the Michaelis-Menten equation which yields a k_{cat} value of 0.74 ± 0.09 s^{-1} and a K_M for ATP of 11 ± 3 μM. *B*, The ATP dependence with 1 mM $MgCl_2$. The low concentrations of ATP can be fit by the Michaelis-Menten equation (not shown) to yield a k_{cat} value of 0.4 ± 0.06 s^{-1} and a K_M value of 13 ± 4 μM. *C*, The ATP dependence at 0.2 mM $MgCl_2$. *D*, The kinetic model describing the requirement of Lig1 for two Mg^{2+} ions in the enzyme adenylylation step. The biphasic concentration dependence shown in panel B and C was fit by the model in D and takes into consideration the depletion of free Mg^{2+} due to the presence of excess ATP (see Appendix A).

Mg^{2+} Dependence of Steady State Ligation

The magnesium dependence for k_{cat} was determined with saturating DNA and ATP substrates. In order to account for the binding of Mg^{2+} ions to ATP, which decreases the concentration of free Mg^{2+} available for binding to the second site on Lig1, we calculated the free Mg^{2+} ion concentration for each steady state reaction (Figure 2-6A). The steady state k_{cat} value showed a

simple hyperbolic dependence on Mg^{2+} ions, with an apparent dissociation constant for Mg^{2+} (K_{Mg}) of 0.71 mM. The metal binding affinity cannot be ascribed to any single step, because the rate-limiting step changes as a function of Mg^{2+} concentration. The maximal turnover number (k_{cat}) of 0.81 s^{-1} was used along with the independently determined microscopic rate constants for adenylyl transfer and nick-sealing to calculate the microscopic rate constant for enzyme adenylylation of 1.3 s^{-1} (see Appendix A Materials). This rate constant is very similar to the rate constant for adenylyl transfer of 2.6 s^{-1} and explains why the burst phase is poorly defined in pre-steady state reactions with saturating ATP (Figure 2-3).

In order to determine the affinity of Lig1 for Mg^{2+} during enzyme adenylylation, we monitored the steady state reaction with saturating DNA, but sub-saturating ATP (k_{cat}/K_M^{ATP}). This apparent second-order rate constant for the utilization of ATP can be limited by steps up to and including enzyme adenylylation. To avoid the problem of Mg^{2+} ion chelation that occurs at high concentrations of ATP, Mg^{2+} was in excess of ATP. The dependence of the steady state rate on the concentration of ATP is linear (Appendix Figure A-10). The resulting k_{cat}/K_M values show a simple hyperbolic dependence on the concentration of Mg^{2+} and yield a K_{Mg} value of 1.4 mM for an essential Mg^{2+} ion in the enzyme adenylylation step (Figure 2-6B). As discussed above, this metal ion is in addition to the Mg^{2+} ion that is already associated with the ATP molecule that is bound from solution (Figure 2-5D). At saturating Mg^{2+} the k_{cat}/K_M value for ATP is 6.2×10^4 $M^{-1}s^{-1}$, which is in reasonable agreement with the k_{cat}/K_M value of ~6.7×10^4 $M^{-1}s^{-1}$ determined by varying ATP at saturating Mg^{2+} (Figure 2-5A). This number is significantly lower than the k_{cat}/K_M value for the DNA substrate of ~3×10^7 $M^{-1}s^{-1}$ (Appendix Figure A-5B).

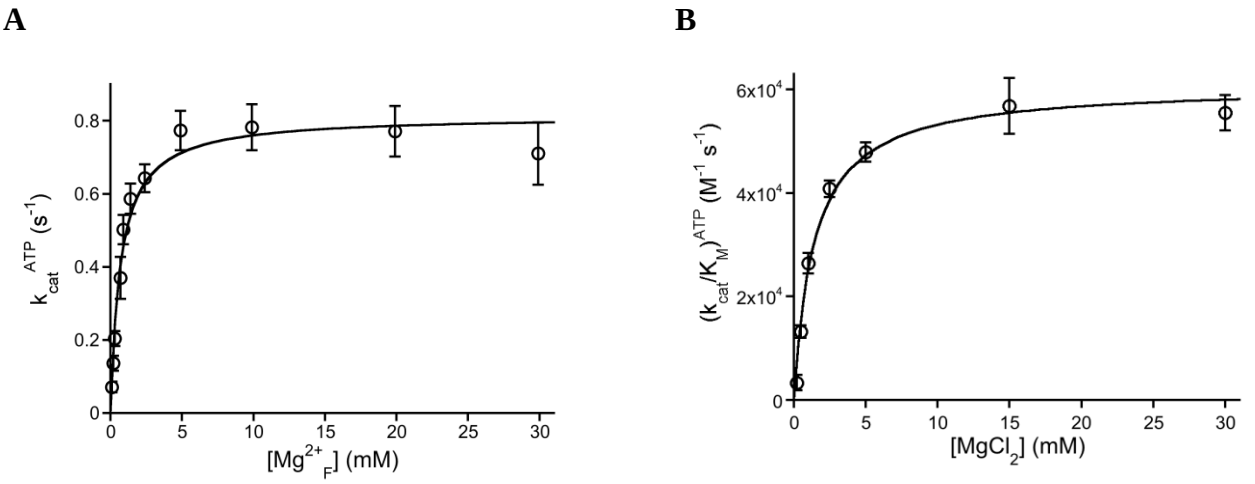

Figure 2-6. Magnesium dependence of multiple-turnover ligation. A, Reactions contained saturating nDNA (1 μM) and ATP (100 μM) and the concentration of $MgCl_2$ was varied (0.2-30 mM). The concentration of free Mg^{2+} ion was calculated using the dissociation constant for the ATP•Mg^{2+} complex determined from the ATP dependence fits (12 μM). Fitting of the data by a hyperbolic binding curve yields a maximal k_{cat} value of 0.81 ± 0.1 s^{-1} and a value of K_{Mg} of 0.71 ± 0.2 mM. **B**, The values of $(k_{cat}/K_M)^{ATP}$ were determined with sub-saturating concentrations of ATP at the indicated Mg^{2+} concentrations between 0.2 and 30 mM. The magnesium dependence of $(k_{cat}/K_M)^{ATP}$ was fit by a binding hyperbola yielding a maximal $(k_{cat}/K_M)^{ATP}$ value of 6.2 ± 1.1×10^4 $M^{-1}s^{-1}$ and a K_{Mg} value of 1.8 ± 0.5 mM.

Dead-end Ligation Intermediates

To investigate whether the long lifetime of the adenylylated DNA intermediate that is observed in single-turnover reactions at very low Mg^{2+} concentrations results in off-pathway events, we looked more closely at multiple-turnover reactions performed under similar conditions. The dissociation of Lig1 from an adenylylated DNA intermediate is expected to be irreversible under multiple-turnover conditions, because the free enzyme can adenylylate itself and is unable to rebind the adenylylated DNA intermediate. Indeed, multiple-turnover reactions containing 0.2 mM $MgCl_2$ show a significant build-up of adenylylated DNA intermediate (data not shown). Given the complex interplay between ATP and free magnesium concentrations, we expected that a similar situation would occur even at higher concentrations of total magnesium. To test this possibility, we followed steady state ligation reactions with saturating DNA, 1 mM $MgCl_2$, and high levels of ATP. Under these conditions, the depletion of free Mg^{2+} results in significant off-pathway release of the adenylylated DNA intermediate (Figure 2-7A, right panel). The level of intermediate that is formed greatly exceeds the enzyme concentration, indicating multiple-

turnover release of the intermediate. In contrast, similar reactions with less than 200 μM ATP that proceed to equivalent levels of product formation produce no detectable intermediate (Figure 2-7A, left panel). We measured the initial rates for steady state formation of adenylylated DNA intermediate and ligated product in order to quantify the efficiency of ligation. As ligase can take either the productive pathway of nick-sealing or the nonproductive pathway of release of adenylylated DNA (Figure 2-7B), this efficiency is calculated from the ratio of the rate for product formation divided by the sum of the rates for product and intermediate formation (Equation 2-4). Over the range of ATP concentrations tested, the efficiency of ligation falls from near 100% under optimal conditions to 60% with 1 mM Mg^{2+} and 2 mM ATP (Figure 2-7B). Although the truncated enzyme that lacks the amino terminal 232 amino acids appears to be fully active as a ligase, we were concerned that the removal of this portion of the protein might affect the rate of dissociation from the adenylylated DNA intermediate. Therefore, we prepared full-length Lig1 and measured the efficiency of ligation with 1 mM Mg^{2+} and 2 mM ATP. We observed that the full-length enzyme had essentially the same efficiency of ligation as the truncated enzyme under these conditions (Appendix Figure A-11).

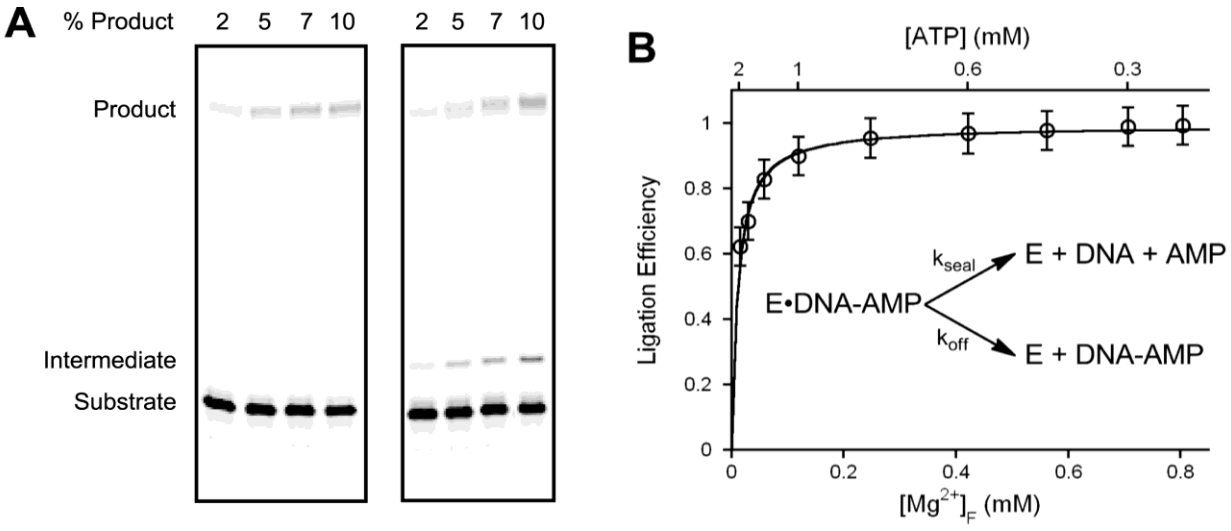

Figure 2-7. Evidence for the release of adenylylated intermediate during multiple-turnover ligation. A, Representative gels analyzing multiple-turnover ligation with 1 mM $MgCl_2$ and 0.2 mM (left) or 2 mM (right) ATP. Time-points follow the first 10% of product formation. At low ATP concentration no noticeable intermediate was formed (left), whereas at high ATP concentration the intermediate accumulates in excess of enzyme concentration, indicating substantial release of intermediate (right). **B**, Ligation efficiency as a function of free Mg^{2+} under conditions of stoichiometric ATP and Mg^{2+}. Steady state rates of formation of intermediate and product were determined for reactions containing 1 mM $MgCl_2$ and 0.2–2 mM ATP. The concentration of ATP is indicated on the upper x-axis and the calculated concentration of free Mg^{2+} is shown on the lower x-axis. The concentration of free Mg^{2+} was determined using a K_d value of 12 μM for the ATP•Mg complex (Figure 2-5 and Appendix Figure A-9). Data in panel B were fit by the simple partitioning scheme shown as an inset, using the independently determined values of k_{seal} and the associated K_{Mg} for this step allowing a Mg^{2+}-independent value for k_{off} of 0.05 s^{-1} to be determined (see Appendix A and Appendix Equation A-12).

Discussion

This work constitutes the first comprehensive kinetic analysis of a human DNA ligase and provides new insight into the multi-step reaction. We report the pre-steady state and steady state kinetic parameters for the ligation of a single-strand DNA break by human Lig1. Furthermore, we have investigated the Mg^{2+} dependence of individual steps in the ligase reaction. These experiments revealed that the affinity of Lig1 for Mg^{2+} ions varies along the reaction coordinate, and that the rate-limiting step and the efficiency of ligation depend on the concentration of Mg^{2+}.

A

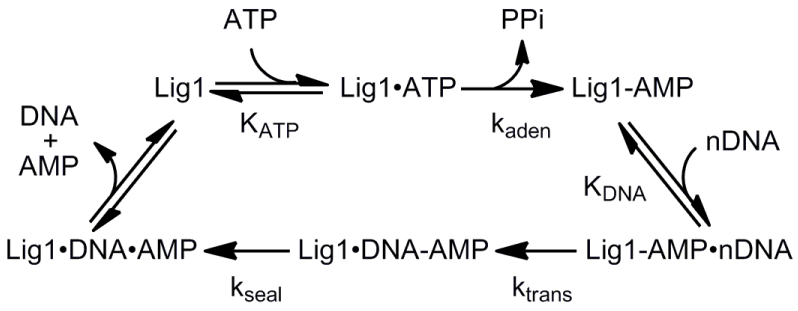

B

Step	K_d (µM)	k_{max} (s^{-1})	K_{Mg} (mM)
ATP binding	12 ± 4	-	-
Enzyme adenylylation	-	1.3 ± 0.3	1.8 ± 0.5
DNA binding	$\leq$ 0.03	-	-
Adenylyl transfer	-	2.6 ± 0.6	0.15 ± 0.06
Nick-sealing	-	12 ± 2	2.6 ± 0.9

Figure 2-8. Minimal kinetic mechanism for Lig1. A, Reaction scheme illustrating the minimal number of steps for DNA ligation. The substrate binding steps are assumed to be in rapid equilibrium, whereas the chemical steps are irreversible under the conditions employed. **B**, Summary of individual rate and equilibrium constants at saturating Mg^{2+}. The apparent dissociation constant for Mg^{2+} (K_{Mg}) was determined for individual steps of the reaction.

Minimal kinetic framework for Lig1

The minimal kinetic mechanism for Lig1 is presented in Figure 2-8A. The three chemical steps of ligase are essentially irreversible in the presence of excess ATP. The rates of enzyme adenylylation and adenylyl transfer are evenly matched when the nicked DNA substrate is saturating. The multiple-turnover rate constant (k_{cat}) is 0.8 s^{-1} in this case. However, it is important to note that DNA ligation occurring in excision repair pathways may not require multiple-turnover ligation. We found that the recombinant Lig1 that we purified from *E. coli* is fully adenylylated and extremely stable. The pool of adenylylated ligase may be sufficient for ligation of low numbers of single-strand DNA breaks, and there may not be a strong driving force to increase the rate of enzyme activation. When Mg^{2+} is saturating, the nick-sealing step is significantly faster than the DNA adenylylation step, which would help to ensure efficient coupling between nick recognition and nick-sealing. However, the lower affinity of Mg^{2+} in the nick-sealing step leaves Lig1 vulnerable to uncoupling of these two chemical steps, which has biological implications (see below).

Although the catalytic core is universally conserved in all ligases, there are additional domains that vary between different isoforms in a given organism and between ligases from different organisms. Therefore, it is interesting to compare the ligation activity of human Lig1, which is one of the largest ligases, with the ligase from Chlorella virus, which is one of the smallest ligases. Recent pre-steady state analysis of the Chlorella virus DNA ligase revealed almost identical rate constants for adenylyl transfer and nick-sealing as we have observed for human Lig1 [21]. Consistent with their similar kinetic parameters *in vitro*, both enzymes are able to rescue the growth of yeast lacking cdc9, the replicative DNA ligase [22, 23].

DNA ligases require divalent metal ions for catalysis, therefore we have investigated the magnesium dependence of the different steps in the Lig1-catalyzed reaction. The complex behavior observed when ATP and Mg^{2+} concentrations are similar strongly suggests that Lig1 requires two Mg^{2+} ions for adenylylation (Figure 2-5D). One Mg^{2+} ion is expected to be bound along with the ATP substrate, but a second is required that has much weaker affinity (K_{Mg} = 1.4

mM). A similar conclusion was reached in a study of the T4 bacteriophage DNA and RNA ligases [24]. The use of more than one metal ion for phosphoryl and nucleotidyl transfer appears to be quite common, with examples ranging from protein kinases [19] to DNA polymerases and nucleases [25]. It is likely that subsequent steps also involve more than one metal ion, and there is evidence of two metal ion binding sites in the structure of the adenylylated DNA intermediate (*10*). The magnesium dependencies for adenylyl transfer and nick-sealing can be explained by a single catalytic metal ion, but are also consistent with two metal ions that have different affinity. In this case, the value of K_{Mg} that we have determined corresponds to the binding of the weakest essential Mg^{2+} ion. Our experiments reveal that the affinity for this metal ion changes significantly between different steps of the ligation reaction, increasing by an order of magnitude between the enzyme adenylylation step and the adenylyl transfer step and then decreasing by a similar degree in the nick-sealing step (Figure 2-8B). These changes in Mg^{2+} affinity could be explained by conformational changes in the substrate or enzyme, or could indicate that unique metal binding sites are involved in different steps of the reaction. Additional work is required to determine the identity and catalytic roles of these Mg^{2+} ions. In many phosphoryl transfer enzymes, Mg^{2+} ions play roles in activating the nucleophile and stabilizing the development of negative charge.

Biological Implications of the Lig1 Magnesium Dependence

The decreased affinity of Lig1 for Mg^{2+} ions in the final nick-sealing step of the reaction renders Lig1 susceptible to changes in the concentration of free Mg^{2+} ions. Lig1 faithfully completes ligation at high concentrations of magnesium, however, low concentrations of magnesium cause the enzyme to abort ligation. The released adenylylated DNA intermediate cannot be ligated, because Lig1 reacts quickly with ATP and the occupancy of the AMP-binding pocket precludes rebinding. Thus, repair pathways are needed to remove the 5'-blocking adenylyl group to allow another opportunity for ligation. In the context of oxidative DNA damage, it has been suggested that mammalian DNA ligases attempt to ligate nicks lacking 3'-hydroxyl groups [26]. Our finding that low Mg^{2+} or high ATP concentration can lead to significant abortive ligation on a normal DNA nick provides an additional possibility. If a DNA break is repaired under conditions

of imbalanced Mg^{2+} or Mg^{2+}-binding metabolites, then there is a significant risk that Lig1 will fail to complete ligation. The abundance of Mg^{2+} (total concentration 10-40 mM) and similarity to other metal ions has made it difficult to directly measure free Mg^{2+} concentration in the cell, however the data that are available for several different cell types suggest that the majority of Mg^{2+} is bound and the free Mg^{2+} is in the range of 0.2–3 mM [27]. The *in vitro* ligation experiments show that this range of Mg^{2+} ion concentration is where Lig1 becomes susceptible to abortive ligation and even slight decreases in the availability of free Mg^{2+} will further increase the burden (Figure 2-7). Thus, abortive ligation intermediates could be frequently generated in a wide variety of cellular contexts.

Although this abortive ligation was observed for a truncated form of Lig1 that lacks the first 232 amino acids, we observed that the amino terminus of Lig1 does not change the efficiency of ligation under conditions of limiting Mg^{2+} in vitro (Appendix Figure A-11). However, this portion of the protein is important for nuclear localization and for interactions with other proteins, including the sliding clamp PCNA (*7,13,14*). It remains to be tested whether protein-protein interactions alter the efficiency of Lig1 in the cell, but the existence of dedicated repair pathways for adenylylated DNA suggest that abortive ligation does occur (*26*).

There are two pathways that would enable the repair of adenylylated DNA intermediates (Figure 2-9). The first pathway is the direct repair catalyzed by aprataxin. Aprataxin is a hydrolase that catalyzes the removal of the AMP group from adenylylated DNA nicks to regenerate the 5'-phosphate [26, 28]. Defects in aprataxin cause the neurodegenerative disease ataxia with oculomotor apraxia 1, which is characterized by the loss of specific neuronal cells. It has been suggested that the affected neuronal cells either experience higher levels of oxidative damage or lack alternative repair pathways [26]. It is expected that long-patch base excision repair would also be an effective way of repairing an abortive ligation intermediate (Figure 2-9). In this pathway, strand displacement by a replicative polymerase would be followed by flap cleavage by FEN1 to generate a new 5'-phosphate that would be a substrate of DNA ligase (Figure 2-9). In

support of this proposed pathway, strand displacement and FEN1 cleavage has been shown to accept flap substrates with 5' blocking lesions [29].

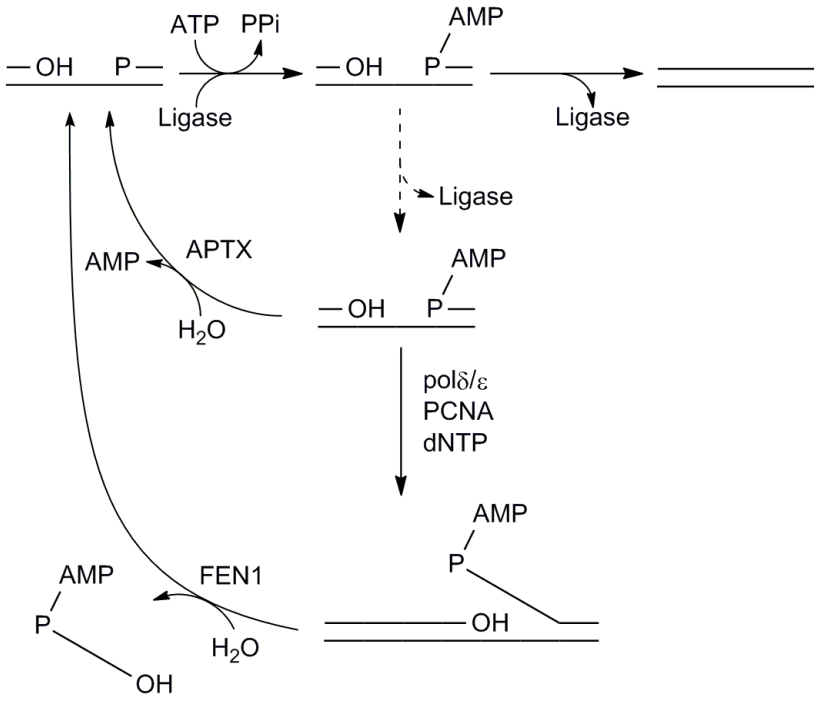

Figure 2-9. Pathways for repair of 5'-adenylylated DNA resulting from abortive ligation. Direct repair of a 5'-adenylylated nick is catalyzed by aprataxin (APTX). Alternatively, strand displacement by a replicative DNA polymerase generates a 5'-flap structure that can be processed by FEN1 to regenerate the adjacent 3'-hydroxyl and 5'-phosphate required by DNA ligase.

Our findings indicate that 3'-blocking lesions are not the only pathway for abortive ligation by human ligases and suggest that there are multiple cellular perturbations that could impact the frequency with which 5'-adenylylated DNA breaks are formed. As persistent DNA breaks are expected to block transcription and to be converted into double-strand breaks upon DNA replication, the formation and repair of 5'-adenylylated DNA is expected to be critical to cellular viability and genomic stability. Additional work is needed to understand the physiological conditions and molecular pathways important for the formation and repair of 5'-adenylylated DNA breaks.

References

1. Petrini, J.H., Y. Xiao, and D.T. Weaver, *DNA ligase I mediates essential functions in mammalian cells.* Mol Cell Biol, 1995. **15**(8): p. 4303-8.
2. Simsek, D., et al., *Crucial role for DNA ligase III in mitochondria but not in Xrcc1-dependent repair.* Nature, 2011. **471**(7337): p. 245-8.
3. Gao, Y., et al., *DNA ligase III is critical for mtDNA integrity but not Xrcc1-mediated nuclear DNA repair.* Nature, 2011. **471**(7337): p. 240-4.
4. Sekiguchi, J., et al., *Genetic interactions between ATM and the nonhomologous end-joining factors in genomic stability and development.* Proc Natl Acad Sci U S A, 2001. **98**(6): p. 3243-8.
5. Barnes, D.E., et al., *Targeted disruption of the gene encoding DNA ligase IV leads to lethality in embryonic mice.* Curr Biol, 1998. **8**(25): p. 1395-8.
6. Lehman, I.R., *DNA ligase: structure, mechanism, and function.* Science, 1974. **186**(4166): p. 790-7.
7. Tomkinson, A.E., et al., *DNA ligases: structure, reaction mechanism, and function.* Chem Rev, 2006. **106**(2): p. 687-99.
8. Shuman, S., *DNA ligases: progress and prospects.* J Biol Chem, 2009. **284**(26): p. 17365-9.
9. Yang, S.W. and J.Y. Chan, *Analysis of the formation of AMP-DNA intermediate and the successive reaction by human DNA ligases I and II.* J Biol Chem, 1992. **267**(12): p. 8117-22.
10. Pascal, J.M., et al., *Human DNA ligase I completely encircles and partially unwinds nicked DNA.* Nature, 2004. **432**(7016): p. 473-8.
11. Sriskanda, V. and S. Shuman, *Specificity and fidelity of strand joining by Chlorella virus DNA ligase.* Nucleic Acids Res, 1998. **26**(15): p. 3536-41.
12. Mackey, Z.B., et al., *DNA ligase III is recruited to DNA strand breaks by a zinc finger motif homologous to that of poly(ADP-ribose) polymerase. Identification of two functionally distinct DNA binding regions within DNA ligase III.* J Biol Chem, 1999. **274**(31): p. 21679-87.
13. Ellenberger, T. and A.E. Tomkinson, *Eukaryotic DNA ligases: structural and functional insights.* Annu Rev Biochem, 2008. **77**: p. 313-38.
14. Song, W., et al., *The DNA binding domain of human DNA ligase I interacts with both nicked DNA and the DNA sliding clamps, PCNA and hRad9-hRad1-hHus1.* DNA Repair (Amst), 2009. **8**(8): p. 912-9.
15. Kodama, K., D.E. Barnes, and T. Lindahl, *In vitro mutagenesis and functional expression in Escherichia coli of a cDNA encoding the catalytic domain of human DNA ligase I.* Nucleic Acids Res, 1991. **19**(22): p. 6093-9.
16. Teraoka, H., et al., *Expression of active human DNA ligase I in Escherichia coli cells that harbor a full-length DNA ligase I cDNA construct.* J Biol Chem, 1993. **268**(32): p. 24156-62.

17. O'Sullivan, W.J. and D.D. Perrin, *The Stability Constants of Metal-Adenine Nucleotide Complexes.* Biochemistry, 1964. **3**: p. 18-26.
18. Phillips, R.C., P. George, and R.J. Rutman, *Thermodynamic studies of the formation and ionization of the magnesium(II) complexes of ADP and ATP over the pH range 5 to 9.* J Am Chem Soc, 1966. **88**(12): p. 2631-40.
19. Waas, W.F. and K.N. Dalby, *Physiological concentrations of divalent magnesium ion activate the serine/threonine specific protein kinase ERK2.* Biochemistry, 2003. **42**(10): p. 2960-70.
20. Cronin, C.N. and K.F. Tipton, *The roles of magnesium ions in the reaction catalysed by phosphofructokinase from Trypanosoma brucei.* Biochem J, 1987. **247**(1): p. 41-6.
21. Samai, P. and S. Shuman, *Functional dissection of the DNA interface of the nucleotidyl transferase domain of Chlorella virus DNA ligase.* J Biol Chem, 2011.
22. Barnes, D.E., et al., *Human DNA ligase I cDNA: cloning and functional expression in Saccharomyces cerevisiae.* Proc Natl Acad Sci U S A, 1990. **87**(17): p. 6679-83.
23. Sriskanda, V., et al., *Mutational analysis of Escherichia coli DNA ligase identifies amino acids required for nick-ligation in vitro and for in vivo complementation of the growth of yeast cells deleted for CDC9 and LIG4.* Nucleic Acids Res, 1999. **27**(20): p. 3953-63.
24. Cherepanov, A.V. and S. de Vries, *Kinetic mechanism of the Mg2+-dependent nucleotidyl transfer catalyzed by T4 DNA and RNA ligases.* J Biol Chem, 2002. **277**(3): p. 1695-704.
25. Steitz, T.A. and J.A. Steitz, *A general two-metal-ion mechanism for catalytic RNA.* Proc Natl Acad Sci U S A, 1993. **90**(14): p. 6498-502.
26. Ahel, I., et al., *The neurodegenerative disease protein aprataxin resolves abortive DNA ligation intermediates.* Nature, 2006. **443**(7112): p. 713-6.
27. Gunther, T., *Concentration, compartmentation and metabolic function of intracellular free Mg2+*. Magnes Res, 2006. **19**(4): p. 225-36.
28. Rass, U., I. Ahel, and S.C. West, *Molecular mechanism of DNA deadenylation by the neurological disease protein aprataxin.* J Biol Chem, 2008. **283**(49): p. 33994-4001.
29. Liu, Y., H.I. Kao, and R.A. Bambara, *Flap endonuclease 1: a central component of DNA metabolism.* Annu Rev Biochem, 2004. **73**: p. 589-615.

Appendix A: Figures, Tables and Experimental Methods to Accompany Chapter 2

Appendix Methods

Fitting of ATP dependence

The ATP dependence of Lig1 suggests that adenylylation of Lig1 follows a random, bireactant system in which there is a requirement for both the ATP•Mg^{2+} complex and a free magnesium ion (Mg^{2+}_F) for activity (Scheme A-1).

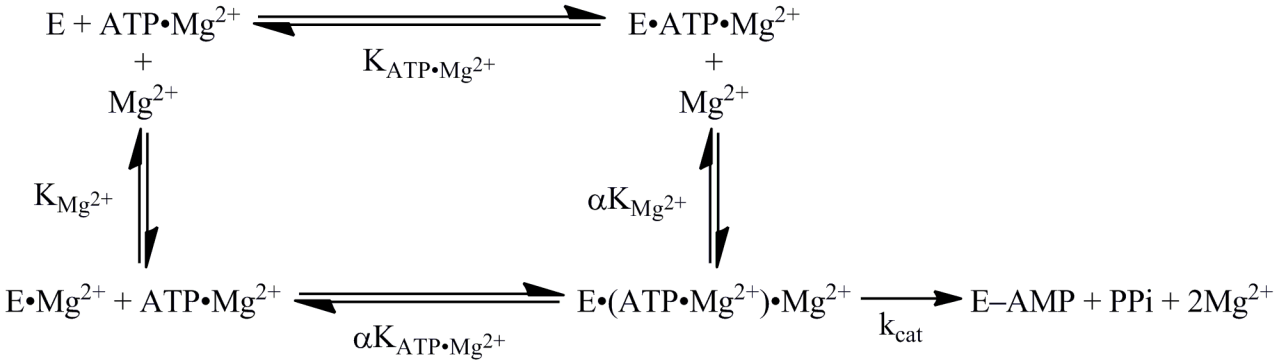

Scheme A-1: Kinetic model describing substrate binding in Lig1.

For simplicity, all of the steps following initial substrate binding have been grouped together into k_{cat}. The term α is the cooperativity constant that represents the change in substrate affinity for the second substrate after the first has already bound. The generic form of this system, where the two substrates are represented by the variables A and B, has been described by Segel (1). The equation describing the system is available as equation VI-2:

$$\frac{v}{V_{\max}} = \frac{[A][B]}{\alpha(K_A)(K_B) + \alpha(K_A)[B] + \alpha(K_B)[A] + [A][B]}$$ Appendix Equation A-1

Designating $V_{max} = k_{cat}[E]_t$:

$$\frac{v}{[E]_t} = \frac{k_{cat}[A][B]}{\alpha(K_A)(K_B) + \alpha(K_A)[B] + \alpha(K_B)[A] + [A][B]}$$ Appendix Equation A-2

For our model, the two substrates for the enzyme are ATP•Mg^{2+} and $Mg^{2+}{}_F$. The concentrations of these species present in our reactions must be determined from the total concentrations of Mg^{2+} and ATP and the dissociation constants for Mg^{2+} and ATP. ATP is known to potentially bind two magnesium atoms, resulting in the equilibrium pictured in Figure A-2.

$$ATP_F + Mg^{2+}{}_F \overset{K_1}{\longleftrightarrow} ATP{\bullet}Mg^{2+} + Mg^{2+}{}_F \overset{K_2}{\longleftrightarrow} ATP{\bullet}(Mg^{2+})_2$$

Scheme A-2: Binding of magnesium by ATP.

Previous studies have shown that the second magnesium ion is bound with much lower affinity than the first (K_2 ~ 20 mM and K_1 ~ 20 μM). This results in a low population of the ATP•$(Mg^{2+})_2$ complex under the conditions that we have employed and we have therefore simplified the analysis by ignoring the negligible binding of the second magnesium ion to ATP•Mg^{2+} from our calculations. Using the definition of the dissociation constant, K_1, and the law of conservation of mass, we can determine relations between the concentrations of ATP•Mg^{2+} and $Mg^{2+}{}_F$ and our known constants. The relation for the dissociation constant K_1:

$$K_1 = \frac{[ATP_F][Mg^{2+}{}_F]}{[ATP{\cdot}Mg^{2+}]}$$ Appendix Equation A-3

From conservation of mass:

$$[ATP_T] = [ATP_F] + [ATP \cdot Mg^{2+}]$$ Appendix Equation A-4

$$[Mg^{2+}{}_T] = [Mg^{2+}{}_F] + [ATP \cdot Mg^{2+}]$$ Appendix Equation A-5

Rearrangement of Appendix Equation A-4 and Appendix Equation A-5 yields Appendix Equation A-6 and Appendix Equation A-7, respectively:

$$[ATP_F] = [ATP_T] - [ATP \cdot Mg^{2+}]$$ Appendix Equation A-6

$$[Mg^{2+}{}_F] = [Mg^{2+}{}_T] - [ATP \cdot Mg^{2+}]$$ Appendix Equation A-7

Substituting Appendix Equation A-6 and Appendix Equation A-7 into Appendix Equation A-3 and rearranging gives the following:

$$0 = [ATP \cdot Mg^{2+}]^2 - [ATP \cdot Mg^{2+}](K_1 + [ATP_T] + [Mg^{2+}{}_T]) + [ATP_T][Mg^{2+}{}_T]$$

Appendix Equation A-8

Which can be input into the quadratic equation to yield an equation for [ATP•Mg^{2+}]:

$$[ATP \cdot Mg^{2+}] = \frac{K_1 + [ATP_T] + [Mg^{2+}{}_T] - \sqrt{(K_1 + [ATP_T] + [Mg^{2+}{}_T])^2 - 4[ATP_T][Mg^{2+}{}_T]}}{2}$$

Appendix Equation A-9

Only the negative root is used in this equation because use of the positive root would result in an ATP•Mg^{2+} concentration greater than the concentration of ATP_T or $Mg^{2+}{}_T$, which is impossible. The $Mg^{2+}{}_F$ concentration can then be calculated from Appendix Equation A-7, using the value of [ATP•Mg^{2+}] obtained from Appendix Equation A-9.

Calculation of rate constant for enzyme adenylylation

We calculated the rate constant for enzyme adenylylation from the measured steady state rate and the separately determined microscopic rate constants for adenylyl transfer and nick-sealing. This analysis assumes that the substrate binding and release steps occur very quickly and that the steady state rate constant (k_{cat}) is controlled by the rate constants for the individual phosphoryl transfer steps. The reciprocal of the overall rate of reaction is given by the sum of the recipricols of the individual steps (2) as shown in Appendix Equation A-10:

$$\frac{1}{k_{cat}} = \frac{1}{k_{adenylylation}} + \frac{1}{k_{transfer}} + \frac{1}{k_{nick-sealing}}$$ Appendix Equation A-10

Rearranging yields Appendix Equation A-11:

$$\frac{1}{k_{adenylylation}} = \frac{1}{k_{cat}} - \frac{1}{k_{transfer}} - \frac{1}{k_{nick-sealing}}$$ Appendix Equation A-11

Using the experimentally determined values of 2.6 s^{-1}, 12 s^{-1} and 0.81 s^{-1} for the adenylyl transfer, nick-sealing and steady-state ligation rate constants, respectively, we determine the enzyme adenylylation rate constant to be 1.3 s^{-1} under saturation conditions.

Analysis of the abortive ligation catalyzed by Lig1 at limiting Mg^{2+}

The simplest model to explain the abortive ligation involves direct partitioning between nick-sealing and release of the adenylylated DNA intermediate (see the inset of Figure 2-7). The Mg^{2+} dependence of the nick-sealing step was determined independently from the single-turnover ligation at high concentration of Mg^{2+} (Figure 2-8, using the data from Figure 2-4). In the absence of direct information regarding the binding affinity of the adenylylated intermediate, we assumed that the rate constant for its release (k_{off}) is independent of Mg^{2+} concentration.

Substitution into the partitioning equation (Equation 2-4) gives Appendix Equation A-12, in which k_{seal} is the rate constant for nick sealing, and K_{Mg} is the apparent dissociation constant for Mg^{2+} in the nick-sealing step.

$$F_{nick-seal} = \frac{\frac{k_{seal} \cdot [Mg^{2+}]_F}{K_{Mg^+}[Mg^{2+}]_F}}{\frac{k_{seal} \cdot [Mg^{2+}]_F}{K_{Mg^+}[Mg^{2+}]_F} + k_{off}}$$

Appendix Equation A-12

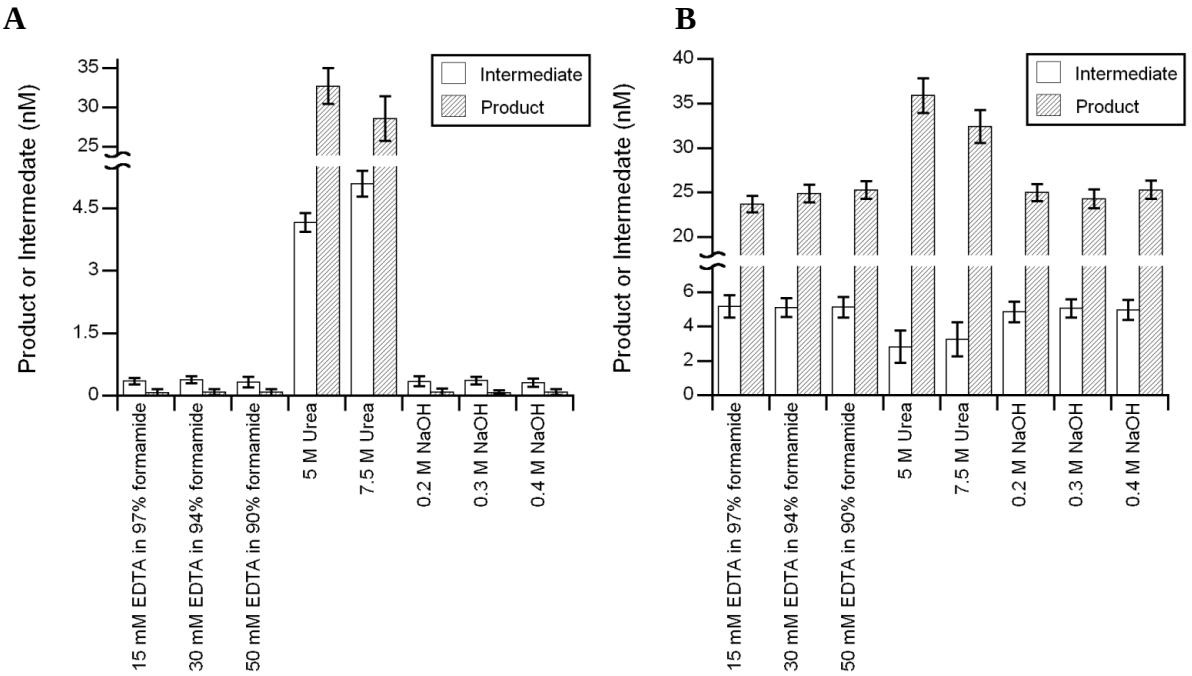

Appendix Figure A-1: Evaluation of different quenching solutions. Single-turnover ligation reactions contained 600 nM Lig1 and 80 nM DNA in standard reaction buffer with 10 mM $MgCl_2$ and were quenched at 4 ms (**A**) or 400 ms (**B**) in the indicated quench solution and the amounts of intermediate and product formed were quantified via the gel-based ligation assay. **A**, Quench solutions that contain either EDTA or concentrated NaOH result in less than 1% formation of intermediate or product when the reaction is quenched at 4 ms. In contrast, urea quench solutions allow the reaction to proceed to roughly 40% completion. **B**, The EDTA and NaOH quench solutions stop the reaction at a similar extent of reaction at 400 ms. Urea quenches appear to act more slowly, allowing for greater product formation and intermediate breakdown.

A

0.015 mM $MgCl_2$

[Lig1]	$k_{transfer}$ (s^{-1})	k_{seal} (s^{-1})
400 nM	0.045 ± 0.013	0.040 ± 0.021
600 nM	0.054 ± 0.008	0.044 ± 0.011
800 nM	0.049 ± 0.020	0.045 ± 0.016

B

10 mM $MgCl_2$

[Lig1]	$k_{transfer}$ (s^{-1})	k_{seal} (s^{-1})
400 nM	2.1 ± 0.8	9.1 ± 1.1
600 nM	2.3 ± 0.4	9.6 ± 0.6
800 nM	2.2 ± 0.7	9.8 ± 1.3

Appendix Figure B-2: Representative single-turnover ligation kinetics indicate that the concentration of Lig1 employed is far above the K_d for substrate binding. The rate constants for adenylyl transfer and nick-sealing were determined for single-turnover reactions containing 80 nM DNA and 400–800 nM Lig1 in standard reaction buffer with 0.015 mM $MgCl_2$ (**A**) or 10 mM $MgCl_2$ (**B**). The rate constants determined for each chemical step are equivalent, within error, across all enzyme concentrations tested, indicating that the single-turnover reaction is saturated with 400 nM Lig1 (K_d >> 400 nM). Unless otherwise indicated, we used 600 nM Lig1 to ensure that the maximal single-turnover rate was measured.

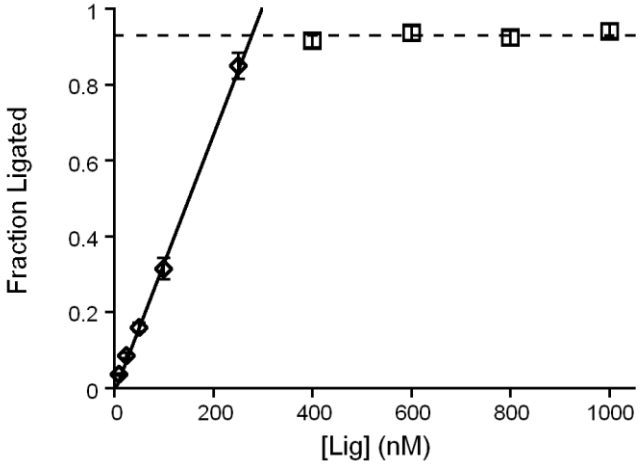

Appendix Figure A-3: Active-site titration to determine the concentration of active (adenylylated) LIG1. Single-turnover reactions were in the standard buffer containing 250 nM DNA and 10 mM $MgCl_2$ and the indicated concentration of Lig1. Reactions were quenched after 10 minutes and the ligation was limited to a single turnover, because no ATP was present. Prior to this experiment, the concentrations of ligase and DNA were based on measurement of the UV-absorbance. According to the titration, 270 nM ligase would be required to fully ligate 250 nM nicked DNA. We adjusted the concentration of the Lig1 stock by 7.4 % to ensure that the concentration of substrate and enzyme were equivalent. A similar titration was performed on enzyme that was loaded into the quench-flow apparatus and this revealed that there was a reproducible loss of ~10% of the enzyme during the rapid-mixing experiments. After this correction we measured identical steady state rate constants from reactions performed either in the quench-flow or with manual mixing on the bench-top.

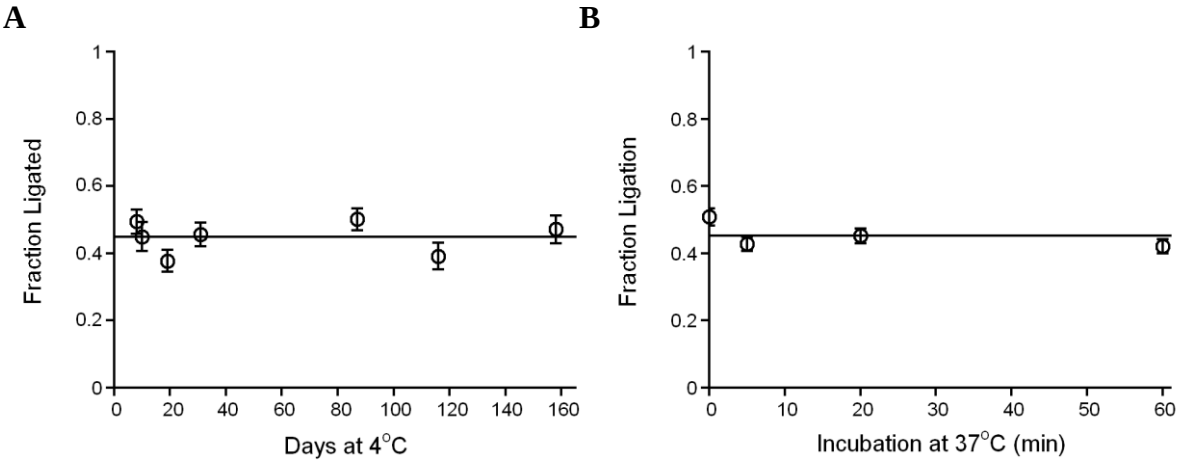

Appendix Figure A-4: Stability of LIG1 in reaction buffer. Reactions containing 20 nM Lig1, 40 nM DNA and 10 mM $MgCl_2$ in standard reaction buffer were quenched after 10 minutes and the fraction of ligated DNA was determined. Because ATP was omitted from the reaction, ligation was limited to a single turnover. 100 nM stock solutions of Lig1 used in the reactions had been incubating at 4 °C (**A**) or 37 °C (**B**) in 1x reaction buffer for various times prior to the experiment. There is no appreciable change in ligation % across the time-span tested under either condition, indicating that ligase is very stable for up to 5 months at 4 °C, or an hour at 37 °C. All kinetic data reported in the accompanying paper was obtained from reactions lasting less than 40 minutes.

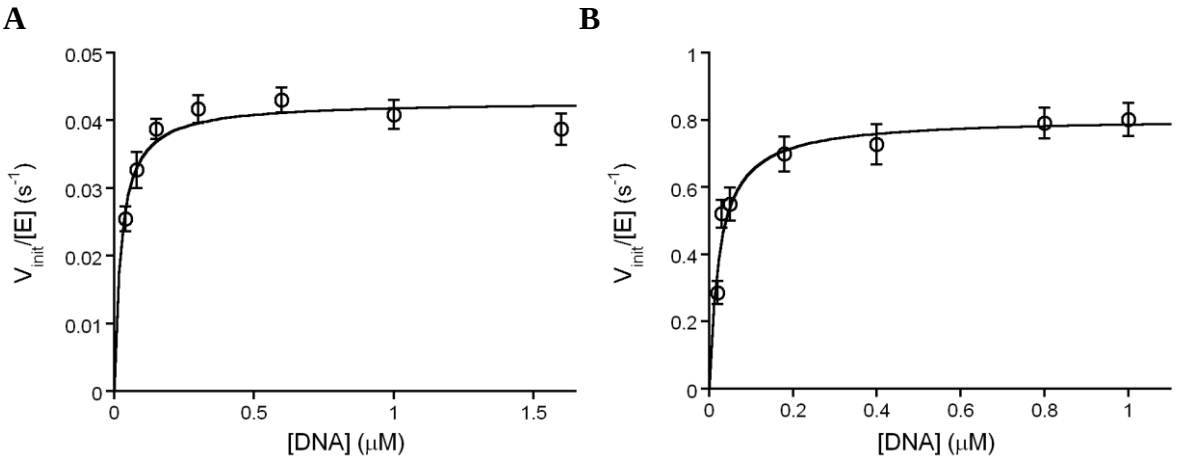

Appendix Figure A-5: DNA concentration dependence of the multiple-turnover ligation reaction. The rate of multiple-turnover ligation was determined across a range of DNA concentrations for reactions containing 1 nM ligase in 1x reaction buffer with 200 μM ATP at either 0.2 mM $MgCl_2$ (**A**) or 10 mM $MgCl_2$ (**B**). Both sets of data fit well to the Michaelis-Menten equation and yield a K_M for DNA of 24 ± 8 nM. Reactions were performed in duplicate.

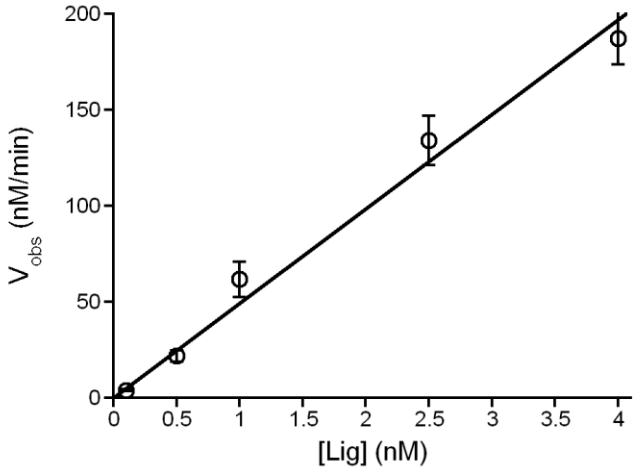

Appendix Figure A-6: Multiple-turnover ligation is linearly dependent upon the concentration of LIG1. The rate of product formation was determined from multiple-turnover reactions containing a range of ligase concentrations and saturating DNA (1 μM) in 1x reaction buffer with 200 μM ATP and 10 mM $MgCl_2$. The linear response of the reaction velocity to enzyme concentration shows that Lig1 does not undergo any concentration dependent changes in activity across this range and that similar reactions performed across this range of ligase concentrations are directly comparable.

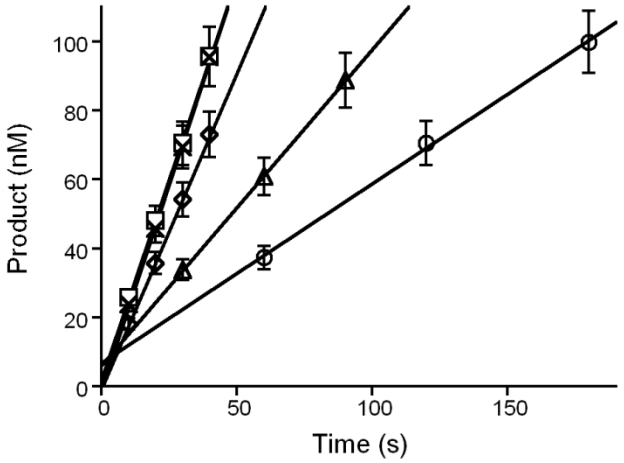

Appendix Figure A-7: Representative initial rates for steady state ligation by LIG1. Product formation was monitored in reactions containing 1 µM DNA, 30 mM $MgCl_2$ and 3 µM (○), 6 µM (Δ), 30 µM (◊), 100 µM (x), or 200 µM (□) ATP. The initial rates were linear up to at least 10% reaction in all cases and steady state kinetics were determined from reaction time courses that were within the first 10% of reaction unless otherwise noted.

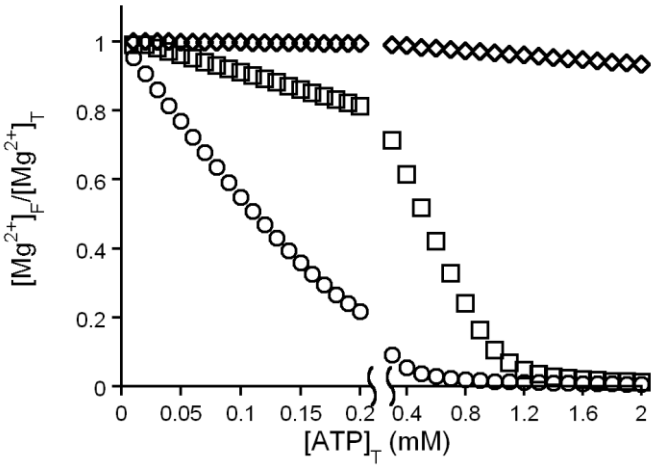

Appendix Figure A-8: Binding of Mg^{2+} to ATP decreases the concentration of free Mg^{2+} available to LIG1. The ratio of the concentration of free magnesium to total magnesium was calculated for solutions with varying levels of ATP and either 0.2 mM (○), 1 mM (□) or 30 mM (◊) $MgCl_2$, using the binding equilibria shown in Scheme S2 and a value of 12 µM for K_1. The concentration of free magnesium drops rapidly in a solution containing only 0.2 mM $MgCl_2$, with a 20% loss of free magnesium at 40 µM ATP. In contrast, a 20% loss of free magnesium in a solution containing 1 mM $MgCl_2$ does not occur until the ATP concentration reaches 200 µM. This trend correlates with the inhibition seen in multiple-turnover reactions as ATP stimulated inhibition of the reaction is delayed in the 1 mM $MgCl_2$ reactions, as compared to the 0.2 mM $MgCl_2$ reactions. The 30 mM $MgCl_2$ reactions are predicted to maintain high levels of free Mg^{2+} over this range of ATP concentrations and we found no evidence of inhibition of Lig1 by ATP under these conditions.

Parameter	0.2 mM $MgCl_2$	1 mM $MgCl_2$	30 mM $MgCl_2$
K_1 (M)	1.2×10^{-5}	1.2×10^{-5}	1.2×10^{-5}
K_{MgF} (M)	6.6×10^{-4}	6.6×10^{-4}	6.6×10^{-4}
$K_{ATP\bullet Mg}$ (M)	5.0×10^{-5}	1.7×10^{-5}	1.1×10^{-5}
k_{cat} (s^{-1})	0.59	0.8	0.8
α	5	5	5

Appendix Figure A-9: Kinetic and thermodynamic constants obtained from fits of the ATP concentration dependencies with the two magnesium model for LIG1. These parameters are from the curve fits shown in the text (Figure 2-5). The ATP concentration dependencies were fit to the equation describing the bisubstrate model of Appendix Scheme A-1 (Appendix Equation A-2) using the program Kaleidagraph. In this equation the species A and B represent the ATP•Mg^{2+} complex and free Mg^{2+} ion, respectively. The expressions describing the concentrations of the ATP•Mg^{2+} complex and free Mg^{2+} ion were derived from the binding equilibria in Appendix Scheme A-2 (Appendix Equation A-9 and A-7) and were substituted into Appendix Equation A-2 for fitting to the known experimental conditions. We were unable to fit all three data sets to common parameters, but reasonable fits were obtained with constant values for the affinity of ATP for Mg^{2+}, Lig1 affinity for free Mg^{2+}, and an α value for cooperative binding of ATP•Mg^{2+} and Mg^{2+}. The resulting best fit values for k_{cat} and the binding affinity of ATP•Mg^{2+} to Lig1 are in reasonable agreement. The failure to obtain a perfect fit to all of the data could indicate experimental error or additional complexities not considered in our model, such as inhibition by free ATP or additional binding sites for Mg^{2+} on Lig1 or the DNA substrate.

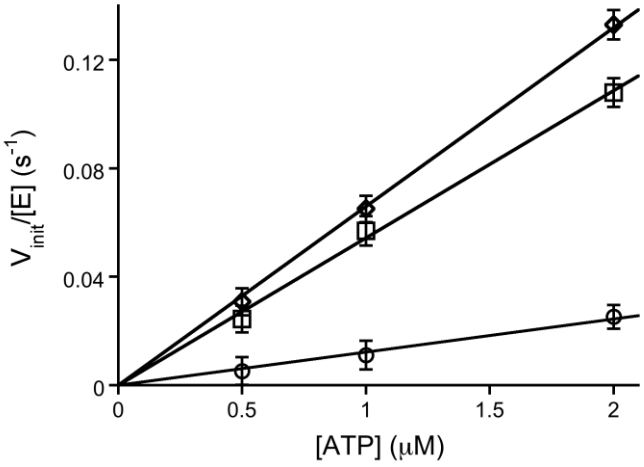

Appendix Figure A-10: Measurement of k_{cat}/K_M for utilization of ATP $(k_{cat}/K_M)^{ATP}$ by LIG1. Representative data are shown for reactions containing 4 nM ligase and 1 μM DNA in the standard reaction buffer with 0.5 μM, 1 μM, and 2 μM ATP and 0.5 mM (○), 5 mM (□) or 15 mM (◊) $MgCl_2$. The linear dependence of the initial rates upon the concentration of ATP indicates that these reactions are sub-saturating for ATP and the value of $(k_{cat}/K_M)^{ATP}$ is given by the slope of the line. All reactions were performed in triplicate and the error bars indicate the standard deviation.

References

1. Segel, I. H. (1975) *Enzyme Kinetics: Behavior and Analysis of Rapid Equilibrium and Steady-State Enzyme Systems*, John Wiley & Sons, Inc., New York
2. Cleland, W. W. (1975) *Biochemistry* **14**, 3220-3224

Chapter 3: Comparison of Manganese and Magnesium as Cofactors for Human DNA Ligase I

Abstract

DNA ligases utilize a catalytic mechanism that involves three phosphoryl transfer reactions. Each of these chemical steps requires the presence of one or more divalent metal cofactors. While most phosphoryl transfer enzymes appear to use magnesium as the physiological cofactor, many are also able to utilize manganese. Metal substitution often results in changes to enzyme catalysis, including changes in substrate specificity and affinity, or the rate of catalysis during metal-dependent steps. Characterization of single and multiple turnover reactions of human DNA ligase I in the presence of manganese have shown that manganese can substitute for magnesium in all steps of the reaction. Surprisingly, low affinity inhibition by manganese exists for some, but not all of the reaction steps. Inhibition is not competitive with magnesium, suggesting that inhibitory metal binding occurs outside of the active-site. This research shows the LIG1 active site has enough plasticity to efficiently accommodate both magnesium and manganese cofactors while also revealing a previously unknown inhibitory metal site.

Introduction

DNA ligases seal breaks in the DNA backbone by catalyzing formation of a phosphodiester bond between adjacent DNA strands [1]. This function is absolutely essential to maintain the integrity of the genome after nicks are formed during DNA repair and replication. Higher eukaryotes encode three different DNA ligases, each specializing in a different area of DNA break repair. DNA ligase I (LIG1) is the most abundant of the three and accomplishes the majority of nuclear single-strand DNA break repair [2]. DNA ligase III exhibits both single- and double-strand break repair activity and accomplishes all DNA repair within the mitochondria [3, 4]. DNA ligase III is also expressed in the nucleus, however this form appears to dispensable for normal cellular function. DNA ligase IV is responsible for nuclear double-strand break repair such as that during non-homologous end-joining [5, 6]. All three ligases share a common catalytic core consisting of three-independently folding domains. It is expected that a comprehensive understanding of LIG1 will provide a useful framework for understanding all human ligases.

Enzymatic DNA ligation follows a reaction pathway that is universally conserved from bacteria to higher eukaryotes (Scheme 3-1) [1]. The pathway consists of 3 independent phosphoryl transfer reactions. The first step of the pathway, enzyme adenylylation, involves attachment of an AMP group to an active site lysine on the enzyme using either ATP or NAD^+ as the nucleotide donor. ATP serves as the nucleotide donor for all mammalian DNA ligases. Enzyme adenylylation requires the presence of two divalent metals, one that comes in with the ATP molecule and another captured from solution [7]. In the second step of the pathway, adenylyl transfer, the enzyme catalyzes attack of the 5' phosphate at the nick on the adenylylated lysine, resulting in transfer of the AMP to the DNA and formation of an adenylylated DNA intermediate. The final step of the reaction involves catalyzing attack of the 3' hydroxyl at the nick on the adenylylated phosphate, forming a phosphodiester bond and sealing the nick. Both DNA dependent steps require the presence of at least one divalent metal ion [8]. A crystal structure of LIG1 in complex with adenlylyated DNA pre-nick-sealing reveals two potential

metal binding sites well-coordinated by universally conserved active-site residues [9]. Metal ions in these sites would interact closely with important substrate chemical groups, however the function of a metal in either site is not known.

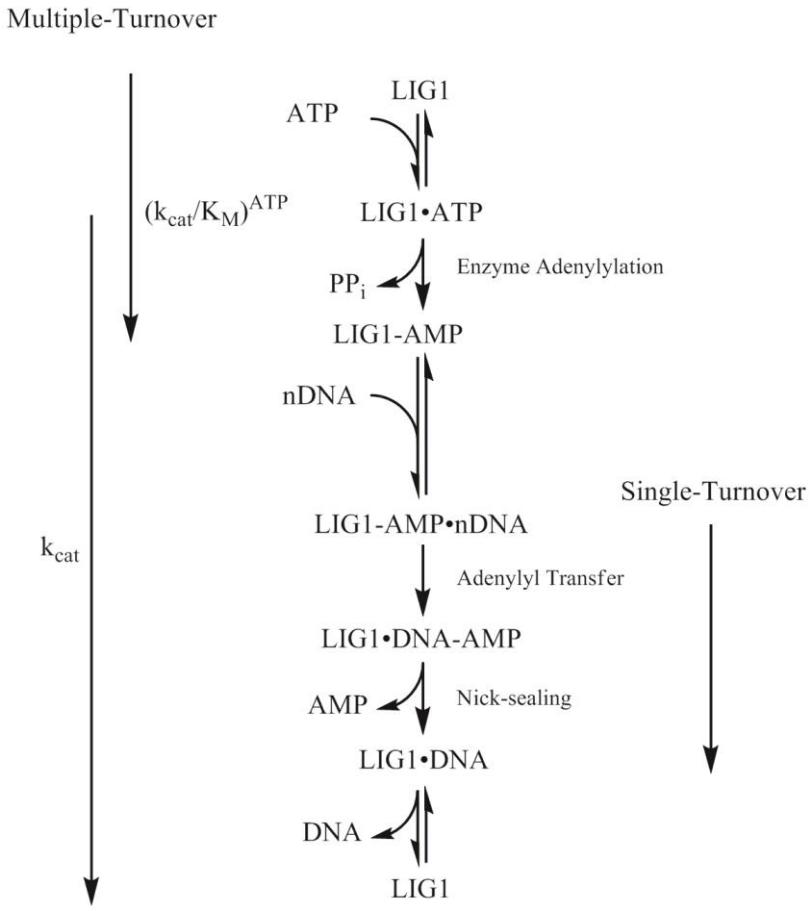

Scheme 3-1: Kinetic mechanism of enzymatic DNA ligation.

We recently characterized the kinetic mechanism of DNA ligation in the presence of magnesium, the presumptive physiological cofactor [7]. Many magnesium-dependent phosphoryl transfer enzymes are able to utilize manganese in place of magnesium as the catalytically required metal cofactor [10-12]. In many cases, study of the differences between reactions catalyzed in magnesium or manganese catalyzed reactions gives functional insight into the role of metal ions during catalysis. We report here a systematic comparison of manganese and magnesium as metal

cofactors for enzymatic ligation by human DNA ligase I. We find manganese is able to substitute for magnesium in every step of the reaction, displaying similar binding affinities and resulting in similar maximal rate constants. We also discover the presence of an inhibitory metal site specific for manganese over magnesium. Surprisingly, inhibition occurs during enzyme adenylylation and adenylyl transfer, but not nick-sealing. More potent inhibition occurs in mixtures of magnesium and manganese, suggesting that ligase activity could be compromised under conditions of manganese metal toxicity.

Methods

Recombinant DNA Ligase I

The catalytic domain of human LIG1 (residues 232-919) was expressed in *E. coli* and purified as previously described [7]. Cells were lysed in the presence of 1 mM EDTA to preserve the adenylylated form of the enzyme, and subsequently purified over a phosphocellulose column and a NTA-nickel column. The His tag was removed with Prescission protease, and LIG1 was further purified with Q-sepharose. The final purified fractions were combined and dialyzed into storage buffer (25 mM Tris•Cl, pH 7.6, 150 mM NaCl, 1 mM DTT, and 0.1 mM EDTA). Aliquots were snap-frozen and stored at -80 ^{o}C. Purity was greater than 95% as judged by SDS-PAGE. Initial concentrations were estimated from the absorbance at 280 nm, using the calculated extinction coefficient. The concentration of active, adenylylated enzyme was determined by titration with nicked DNA substrate, as described previously [7], and this active concentration is reported throughout.

DNA Substrates

Oligonucleotides were synthesized by Integrated DNA Technologies or by the Keck Center at Yale University and were purified on denaturing polyacrylamide gels. The portion of the gel containing the full-length oligonucleotide was excised, crushed, and extracted by soaking overnight in 500 mM NaCl and 1 mM EDTA. The extracted oligonucleotides were desalted by binding to a C18 reverse phase column (Sep-pak, Waters) and eluted with 30% (v/v) acetonitrile. Concentrations were obtained from the absorbance at 260 nm using the calculated extinction coefficients. The three oligonucleotides used in this study had sequences 5'-CCGAATCAGTCCGACGACGCATCAGCAC, 5'-GTGCTGATGCGTC, and 5'-P-GTCGGACTGATTCGG-FAM (P indicates 5' phosphorylation and FAM indicates the presence

of a 3’ fluorescein). The nicked, double-stranded DNA substrate (nDNA) was formed by mixing equimolar amounts of the three oligonucleotides in 10 mM NaMES pH 6.5 and 50 mM NaCl and cooling the mixture from 90 °C to 4 °C at a rate of 3 °C per minute.

Gel-based Ligation Assay

Ligation reactions were performed at 37 °C. Unless otherwise indicated, the standard buffer contained 50 mM NaMOPS pH 7.5 (measured at 25 °C), 1 mM dithiothreitol, 0.05 mg/mL BSA, and sufficient NaCl to maintain a constant ionic strength of 150 mM. The amounts of ATP, $MgCl_2$, $MnCl_2$, nDNA, and LIG1 varied, as indicated below. Preincubation controls established that LIG1 retains 100% of its activity after 1 hr in this standard buffer, and all of the kinetic data was collected within this window of time (Appendix Figure B-1) [7]. Reactions were quenched as described below, heated to 95 °C for 5 min to denature the DNA and resolved on 20% (w/v) denaturing polyacrylamide gels containing 8 M Urea. Fluorescein-labeled oligonucleotides were detected with a Typhoon Trio$^+$ imager (GE Healthcare) with excitation at 488 nm and emission through a 520 nm band-pass filter. The images were analyzed using ImageQuantTL (GE Healthcare). The intensity of the individual DNA species was corrected for background fluorescence, and the fraction of the total fluorescence was determined by dividing the fluorescence intensity for the desired species by the signal for all other species in the sample. When necessary, this fraction was converted into its concentration by multiplying by the total concentration of DNA in the reaction.

Multiple-Turnover Ligation Assays

Steady state kinetic analysis was performed in the standard ligation buffer and the temperature was maintained at 37 °C in a circulating water-bath. Reaction mixtures were preincubated for 5 min prior to addition of LIG1. Reactions were arrested by quenching a 4 µL aliquot in 15 µL of quench solution (50 mM EDTA in 90% formamide), and the extent of ligation was determined as described above. Initial rates were determined from the linear rate of substrate disappearance

within the first 10% of the reaction. When both intermediate and product were formed during the reaction, the rate of formation for each species was determined. Values reported represent the average of at least three experiments. Equations used to fit data are described in the Models of Kinetic Parameters section and in the text. All fitting of multiple-turnover data was done using Kaleidagraph, Synergy Software.

Rapid Quench Experiment

Rapid mixing experiments were performed in a Kintek RFQ-3 quench-flow apparatus. One sample loop contained LIG1 and the other contained DNA, each at double the reaction concentration. The samples were in 1x reaction buffer with the desired metal ion concentration and the drive syringes contained the same solution. Loaded reactants were allowed to equilibrate for 90 seconds to reach the correct temperature. Reactions were initiated by mixing of 20 µL of each sample and were quenched at the desired times by mixing with 20 µL of quench solution, held in the quenching syringe. Data obtained at concentrations above 1 mM manganese with the 50 mM EDTA in 90% formamide quench used previously [7] did not fit well to the 2-step irreversible model (Appendix Figure B-2). Data from identical reactions instead quenched with concentrated HCl do fit well to a 2-step irreversible model. Comparison of the data from EDTA/formamide or HCl quenched reactions reveals that a larger amount of adenylylated DNA intermediate is formed when reactions are quenched with EDTA/formamide. This suggests that the EDTA/formamide quench does not stop the adenylyl transfer step on the sub-millisecond time-scale required for quench-flow experiments. For this reason, 3M HCl was used as the quenching solution for all single-turnover experiments. 5 seconds after quenching, samples were brought to neutral pH by addition of 20 µL of 3 M NaOH. 160 mL of 50 mM EDTA in 90% formamide was added following neutralization and samples were analyzed with the standard gel-based ligation assay. Unless otherwise indicated, the typical concentrations of nDNA and LIG1 were 80 nM and 600 nM, respectively. The data were imported into the program Berkeley-Madonna (www.berkeleymadonna.com) and the curve fitting function was used to globally fit the levels of intermediate and product by the scheme represented in Scheme 3-1. Fitting of the data to a model including reversible chemical steps did not produce significantly different results

(data not shown). Fits of reactions from individual experiments provided values for the rate constants for adenylyl transfer and nick-sealing and the reported values reflect the average rates determined from at least three independent experiments at each metal concentration. These rate constants were plotted versus the concentration of metal ions. Fitting of the data is discussed in the results section.

Models of Kinetic Parameters

$$k_{obs} = \frac{k_A * [A]}{(K_A + [A]) * (1 + \frac{[I]}{K_I})}$$ Equation 3-1

Equation 3-1 describes the non-competitive inhibition model where a reaction is activated by binding of species A to a single stimulatory site and is inhibited by binding of species I to a single inhibitory site. k_{obs} is the observed rate constant for the step being measured, k_A is the maximal rate constant, K_A is the observed affinity for species A during the observed step, and K_I is the observed affinity for species I. Equation 3-1 is used for fitting the manganese data in Figures 3-1B, 3-2B, and 3-3B. It is also used for fitting the data in Figures 3-3A, 3-3B, and 3-5A where manganese is inhibiting the magnesium stimulated reaction. In cases where manganese acts to activate as well as inhibit catalysis, A = I.

$$k_{obs} = \frac{k_A * [A]}{K_A + [A]}$$ Equation 3-2

Equation 3-2 describes the model where a reaction is activated by binding of species A to a single stimulatory site. k_{obs} is the observed rate constant for the step being measured, k_A is the maximal rate constant, and K_A is the observed affinity for species A during the observed step. Equation 3-2 is used for fitting the magnesium data in Figures 3-1B, 3-2B, 3-4A, and 3-4B. It is also used for fitting of the manganese dependence of nick-sealing in Figure 3-4B and takes the form of the Michaelis-Menten equation for the ATP dependence of multiple-turnover in Appendix Figure B-4.

$$k_{obs} = \frac{k_A * \frac{[A]}{K_A} + k_B * \frac{[B]}{K_B}}{1 + \frac{[A]}{K_A} + \frac{[B]}{K_B}}$$ Equation 3-3

Equation 3-3 describes the model where a reaction is activated by competitive binding of species A or species B to a single stimulatory site. k_{obs} is the observed rate constant for the step being measured, k_A and k_B are the maximal rate constants when either species A or B is bound, respectively, and K_A and K_B are the observed affinities for species A and B, respectively, during the observed step. Equation 3-3 is used for fitting the data in Figure 3-5B.

Results

Manganese Stimulated Steady-State Ligation

To evaluate the ability of manganese to stimulate DNA ligation, we performed multiple-turnover reactions at varying concentrations of manganese. These reactions spanned the range of manganese concentrations from 100 μM to 20 mM. The rate of all multiple-turnover reactions were determined from data obtained at less than 10% product formation, ensuring measurement of the steady-state reaction (Figure 3-1A). Observation of identical V/E values for reactions with both 250 nM and 1 μM DNA at both 100 μM and 20 mM manganese indicate that the 1 μM DNA concentration used for the multiple-turnover experiments is saturating (Appendix Figure B-3A, B). Product formation remains linear over the time-course of the reaction requiring the most time (Appendix Figure B-3, B), and pre-incubation of the enzyme under typical reaction conditions without DNA does not affect the rate of reaction (Appendix Figure B-1). These results indicate that LIG1 is stable under these reaction conditions in the presence of manganese, similar to what we have previously seen with magnesium [7]. The dependence of the manganese stimulated steady-state rate on ATP was found to be similar to that observed with magnesium, with a $K_{M,ATP}$ of 12 μM (Appendix Figure B-4).

The maximal multiple-turnover rate constant at saturating DNA and ATP, k_{cat}, displays a biphasic dependence on manganese concentration, increasing from 0 mM to 1 mM manganese and then decreasing above 1 mM manganese (Figure 3-1B). The biphasic dependence of k_{cat} fits well to a noncompetitive inhibition model where one manganese ion activates the enzyme and a second manganese ion inhibits (Equation 3-1). This fit yields a k_{cat} of 1.3 ± 0.1 s^{-1}, with a stimulatory $K_{1/2}$ for manganese, K_{Mn}, of 0.5 ± 0.08 mM and an inhibitory $K_{1/2}$ for manganese, K_I, of 2.1 ± 0.6 mM. These data show that manganese can fulfill all the catalytically required roles of magnesium during ligation. Data previously obtained in the presence of magnesium is plotted alongside the manganese data for comparison (Figure 3-1B, Equation 3-2). Comparison of the

kinetic constants measured with manganese to those measured with magnesium reveals that the two metals bind the stimulatory site with similar affinity and result in a similar reaction rate (0.5 mM and 1.3 s^{-1} vs. 0.71 mM and 0.81 s^{-1} for manganese and magnesium, respectively) (Table 3-1).

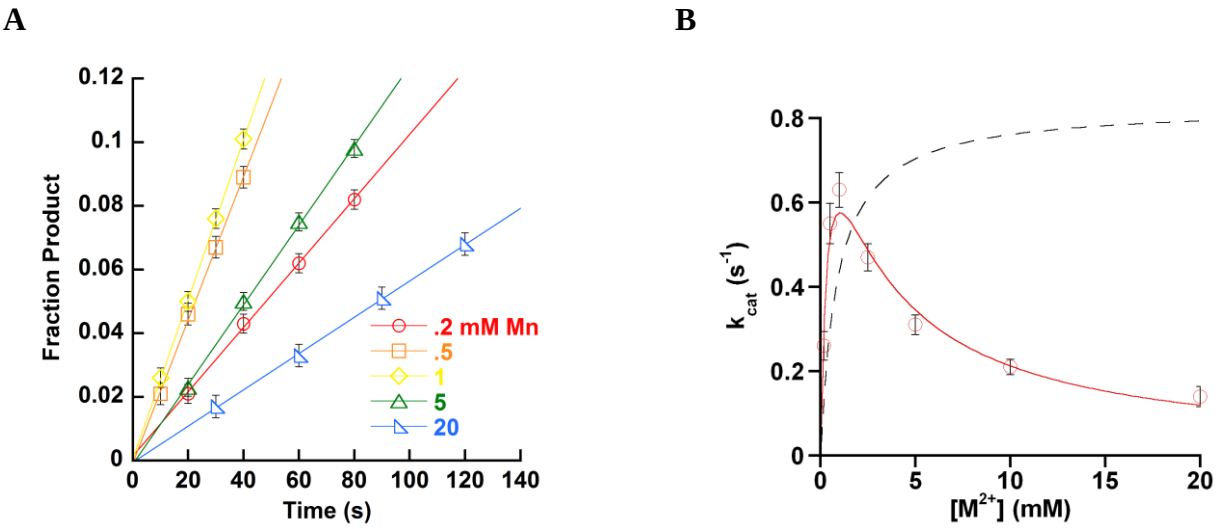

Figure 3-1: Multiple-turnover ligation with Mn^{2+} and saturating ATP and DNA. A, Representative initial rates of DNA ligation with Mn^{2+} as the cofactor. Reactions contained saturating DNA (1 μM) and 4 nM LIG1 and the mean ± SD is shown for 3 independent reactions. **B,** The k_{cat} value for LIG1-catalyzed ligation shows a biphasic dependence on the concentration of Mn^{2+} (○). For comparison, the k_{cat} dependence on magnesium is plotted from [7]. The Mg^{2+} dependence is represented by a single-site binding model (Equation 3-2, dashed black line), the Mn^{2+} dependence is fit by a noncompetitive inhibition model (Equation 3-1, solid red line).

Manganese Stimulation of ATP-dependent Reactions

The use of subsaturating levels of ATP allows monitoring of the ATP dependent steps of the reaction, ATP binding and enzyme adenylylation (Scheme 3-1). Analysis of the second order rate constant for the utilization of ATP ($(k_{cat}/K_M)^{ATP}$) under these conditions allows us to investigate how manganese affects the ATP-dependent reactions for DNA ligation. The linear dependence of the steady-state rate on the concentration of ATP at less than 2 mM ATP confirms that $(k_{cat}/K_M)^{ATP}$ is determined (Figure 3-2A). The value of $(k_{cat}/K_M)^{ATP}$ displays a biphasic dependence on manganese (Figure 3-2B), similar to that observed when ATP is saturating in multiple-turnover. A fit of this data to the equation describing a noncompetitive inhibition model

(Equation 3-1) where manganese acts as both the activating and inhibitory cofactor yields a maximal $(k_{cat}/K_M)^{ATP}$ value of (1.2 ± 0.2) x 10^5 $M^{-1}s^{-1}$, and identical values for K_A and K_I of 2.1 ± 0.6 mM (Table 3-1). The metal affinities have a large error associated with them in the fitting program, Kaleidagraph. This suggests that multiple solutions exist that fit the model to the data. Thus, while this set of numbers is the best fit for the data, they should be considered as rough estimates of the real value.

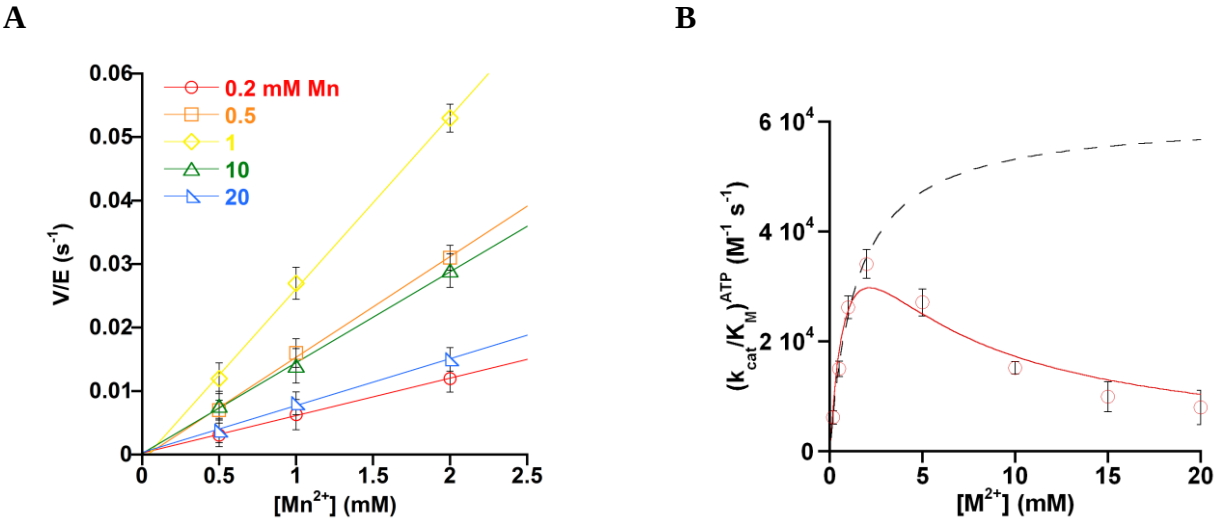

Figure 3-2: Multiple-turnover with Mn^{2+} and sub-saturating ATP. A, Representative initial rates of ligation for sub-saturating amounts of ATP that are used to calculate the value of $(k_{cat}/K_M)^{ATP}$ at different concentrations of Mn^{2+}. **B,** The value of $(k_{cat}/K_M)^{ATP}$ displays a biphasic dependence on the concentration of Mn^{2+} (○). For comparison, the $(k_{cat}/K_M)^{ATP}$ dependence on magnesium is plotted from [7].The Mg^{2+} dependence is represented by a single-site binding model (Equation 3-2, dashed black line), and the Mn^{2+} dependence is fit by a noncompetitive inhibition model (Equation 3-1, solid red line).

Inhibitory Manganese is Not Competitive with Magnesium in Multiple-Turnover

To investigate the effect of manganese on magnesium stimulated multiple-turnover ligation, we followed reactions containing saturating concentrations of magnesium and varying concentrations of manganese. The steady-state rate of product formation decreases in response to increasing levels of manganese under these conditions (Figure 3-3A). The manganese dependence of the observed multiple-turnover rate fits well to a noncompetitive inhibition model (Equation 3-1), where magnesium is the activating cofactor, A, and manganese is the inhibitory

cofactor, I. This model yields superimposable fits to the data at 5 mM and 20 mM magnesium, yielding a K_I for the multiple-turnover reaction of 0.22 ± 0.06 mM and 0.19 ± 0.04 mM, respectively. Absence of a change in the K_I for manganese over a 4-fold change in magnesium ion concentration indicates that the inhibitory manganese ion(s) do not compete with magnesium. The significantly tighter affinity for the inhibitory manganese measured in a background of magnesium in this experiment as opposed to that reported above with manganese alone (0.2 mM vs. 2.1 mM, respectively) suggests the measurement of a different inhibitory species between the two experiments. This will be evaluated further in the discussion section.

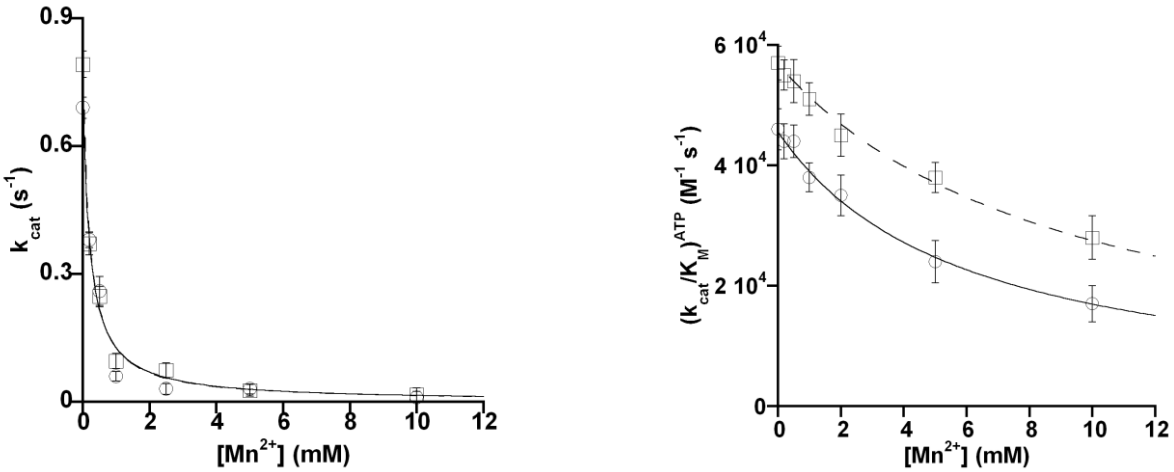

Figure 3-3: Mn^{2+} is a noncompetitive inhibitor of Mg^{2+}-dependent ligation. A, The rate constant for multiple turnover ligation (k_{cat}) with saturating DNA (1 μM) and ATP (200 μM) was measured at both 5 mM (○) and 20 mM (□) Mg^{2+} and varying amounts of Mn^{2+}. The data were fit by a noncompetitive inhibition model (Equation 3-1). Fits of the data for the two different concentrations of Mg^{2+} are superimposable and yield K_I values of 0.22 mM and 0.19 mM Mn^{2+} at 5 mM and 20 mM Mg^{2+}, respectively. **B,** The second order rate constant for ligation at sub-saturating ATP, $(k_{cat}/K_M)^{ATP}$, was determined at both 5 mM (○) and 20 mM (□) Mg^{2+} and varying concentrations of Mn^{2+}. The data were fit by a noncompetitive inhibition model (Equation 3-1) and yield K_I values of 4.1 mM and 8.4 mM Mn^{2+} at 5 mM and 20 mM Mg^{2+}, respectively.

The manganese dependence of the magnesium stimulated multiple-turnover rate under $(k_{cat}/K_M)^{ATP}$ conditions fits well to a noncompetitive inhibition model in which magnesium acts as the stimulatory metal and manganese is inhibitory (Figure 3-3B, Equation 3-1). Though the curves have different $(k_{cat}/K_M)^{ATP}{}_{max}$ values due to 5 mM magnesium being subsaturating under $(k_{cat}/K_M)^{ATP}$ conditions, the K_I values are quite similar (4.1 ± 0.7 mM and 8.4 ± 0.9 mM at 5

mM and 20 mM magnesium, respectively). This suggests that inhibition by manganese is not caused by displacement of active-site magnesium ions, but must instead be occurring via binding to some other site(s).

Stimulation of Single-Turnover Ligation by Manganese

To determine the effect of manganese on adenylyl transfer and nick-sealing, we performed single-turnover ligation reactions across a range of manganese ion concentrations. Under-single turnover conditions, adenylylated enzyme is added to substrate in the absence of ATP, ensuring that each enzyme can turnover only once. Use of saturating levels of enzyme in vast excess over substrate ensures that the observed rate constants are not affected by substrate binding. The rates for these steps were determined as described in the methods. Briefly, the level of intermediate and product present in the reaction over time is fit by a 2-step irreversible mechanism using the program Berkeley-Madonna. These fits give values for the rates of adenylyl transfer and nick-sealing, which are reported here. 3 M HCl was used as the quench in the single-turnover experiments reported here, as the EDTA/formamide quench used previously did not stop the reaction on the required time-scale (see Methods, Appendix Figure B-2). This may reflect slower dissociation of manganese than magnesium. Single-turnover reactions spanned the range of manganese concentrations from 10 μM to 10 mM. Identical rate constants were obtained from reactions performed with either 800 nM or 3200 nM LIG1 at various manganese concentrations, indicating saturating levels of enzyme (Appendix Figure B-5, Appendix Table B-1).

Similar to what was observed for k_{cat}, the rate constant for adenylyl transfer, $k_{transfer}$, displays a biphasic dependence on manganese concentration, resulting in an increase from 0 mM to 0.1 mM Mn^{2+}, and then a decrease above 0.1 mM Mn^{2+} (Figure 3-4A). Fitting the data to the equation describing a noncompetitive inhibition model (Equation 3-1), in which manganese acts as both the activating and inhibiting cofactor, yields a maximal rate constant for adenylyl transfer, $k_{transfer}$, of 8.7 ± 1.2 s^{-1}, with a K_A of 0.12 ± 0.06 mM and a K_I of 0.13 ± 0.08 mM. Similar to the values obtained from the $(k_{cat}/K_M)^{ATP}$ measurements, the numbers given here have large reported errors from Kaleidagraph, suggesting they are not a unique solution to the data. In contrast to the

adenylyl transfer step, the nick-sealing reaction displays a simple hyperbolic binding dependence on manganese concentration, similar to what is observed for magnesium (Figure 3-4B). Fitting of the nick-sealing data to a hyperbolic binding curve (Equation 3-3) yields a maximal nick-sealing rate constant, k_{seal}, of 6.4 ± 0.6 s^{-1} and a K_A for manganese of 0.44 ± 0.08 mM.

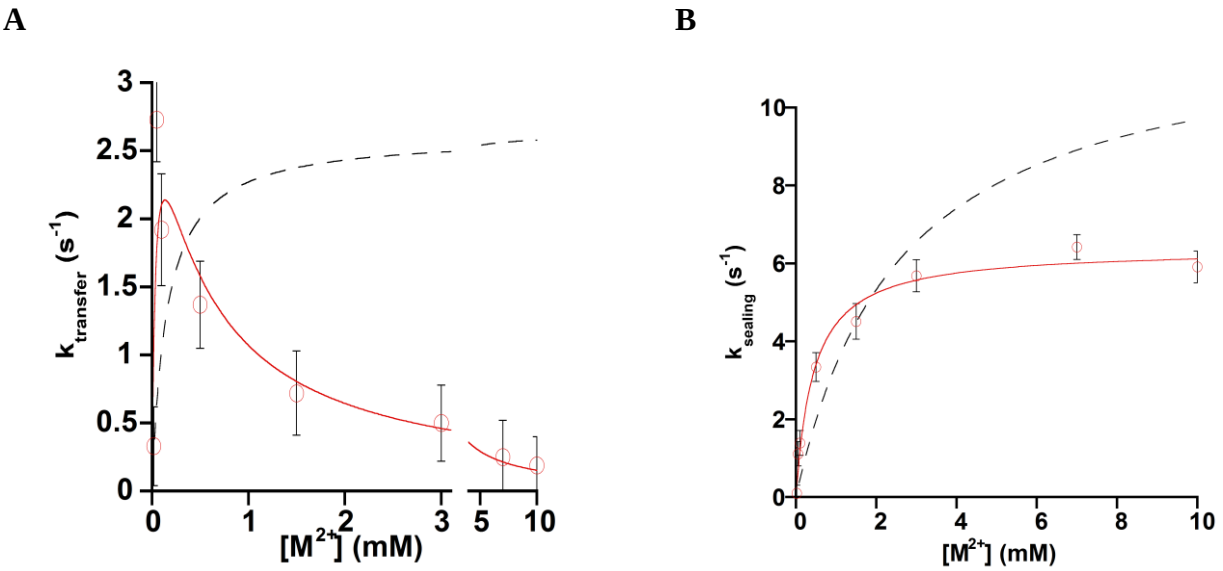

Figure 3-4: Mn^{2+} dependence of single-turnover ligation. The adenylyl transfer and nick-sealing rate constants were determined using rapid quench with 800 nM LIG1 and 80 nM nicked DNA at the indicated concentrations of Mn^{2+} (○). For comparison the magnesium dependence is plotted from [7]. **A,** The manganese dependence for adenylyl transfer is fit by a noncompetitive inhibition model (Equation 3-1, solid red line), whereas the magnesium dependence is represented by a single-site binding curve (Equation 3-2, dashed black line). **B,** The metal dependence for nick-sealing is fit by a single-site binding curve (Equation 3-2) for both manganese (solid red line) and magnesium (dashed black line).

Manganese Inhibition of Magnesium Stimulated Single-Turnover Ligation

To gain insight into the inhibitory manganese sites observed during enzyme adenylylation, we performed single-turnover reactions at a fixed concentration of magnesium and varying concentrations of manganese. As expected, the addition of manganese decreases the observed rate for adenylyl transfer (Figure 3-5A). Data obtained at either 5 mM or 20 mM magnesium fits reasonably well to a noncompetitive inhibition model for manganese (Equation 3-1), and yields a K_I of 0.25 mM at both magnesium concentrations. An identical value for the K_I at both 5 mM

and 20 mM magnesium suggests that the inhibitory manganese that affects adenylyl transfer is not competitive with magnesium.

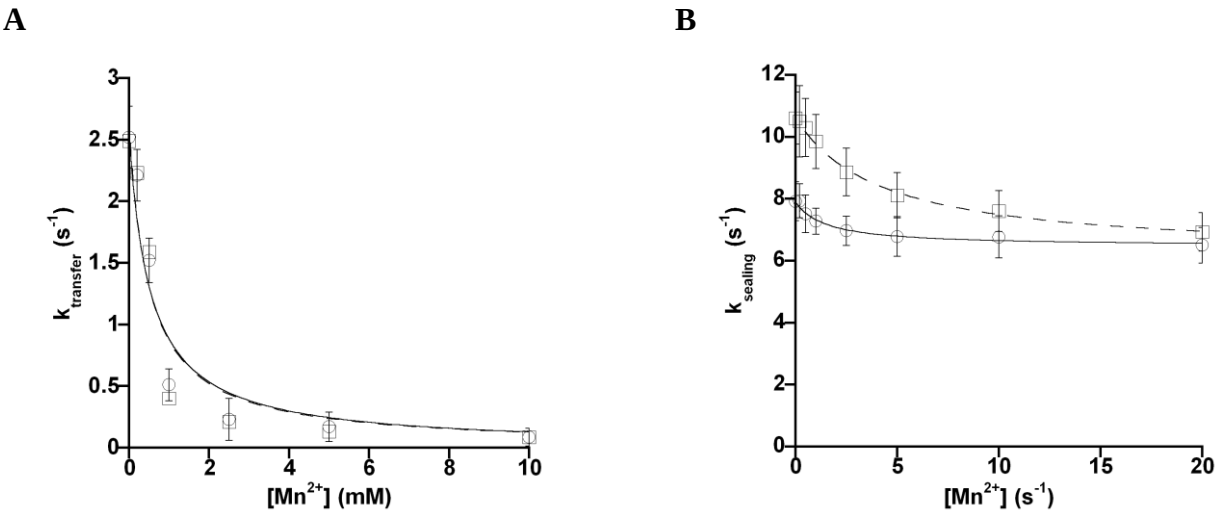

Figure 3-5: Mn^{2+} is a noncompetitive inhibitor of adenylyl transfer, but not nick sealing. Single-turnover ligation reactions were performed at both 5 mM and 20 mM Mg^{2+} and various concentrations of Mn^{2+} to evaluate the inhibitory effects of Mn^{2+} on these two steps. **A,** The data for adenylyl transfer were fit to a noncompetitive inhibition model (Equation 3-1). Fits of the data at both 5 mM and 20 mM Mg^{2+} yield nearly identical K_I values of 0.54 mM and 0.51 mM, respectively. **B,** The data for nick-sealing were fit to a competitive, single-stimulatory site model (Equation 3-3). The fit to the data at 5 mM Mg^{2+} yields a k_{seal} of 6.5 s^{-1} and a $K_{1/2}$ of 0.52 mM, and the fit to the data at 20 mM Mg^{2+} yields a k_{seal} of 6.2 s^{-1} and a $K_{1/2}$ of 0.49 mM. The value of k_{seal} at infinite $[Mn^{2+}]$ in a background of two different concentrations of magnesium approaches the value observed with manganese alone, indicating manganese competes with magnesium for the active-site and that the inhibitory manganese sites do not affect the nick-sealing step.

The manganese dependence of the magnesium stimulated nick-sealing reaction reveals an apparent partial inhibition by manganese (Figure 3-5B). This apparent inhibition occurs because stimulatory manganese ions displace magnesium ions in the active site due to their higher affinity ($K_{A,Mn}$ = 0.44 mM and $K_{A,Mg}$ = 2.6 mM), while manganese ions have a lower maximal rate for nick-sealing ($k_{seal,Mn}$ = 6.4 s^{-1} and $k_{seal,Mg}$ = 12 s^{-1}). When fit to the equation describing a single-site competitive model (Equation 3-3), the fit gives values of 6.5 s^{-1} and 6.2 s^{-1} for $k_{seal,Mn}$ at 5 mM and 20 mM magnesium, respectively, and 0.52 mM and 0.49 mM for $K_{A,Mn}$ at 5 mM and 20 mM magnesium, respectively. This experiment directly shows that manganese ions

compete with magnesium ions for binding to the active-site, and that they do not inhibit the nick-sealing reaction, unlike enzyme adenylylation and adenylyl transfer.

Discussion

Stimulatory manganese ions behave very similarly to magnesium ions

The observation of product formation during multiple-turnover ligation with only manganese metal ions indicates that manganese can substitute for magnesium in all catalytically important roles. Many of the kinetic constants obtained with manganese are quite similar to those obtained with magnesium (Table 3-1). Together, this data suggests a substantial plasticity in the LIG1 active-site with regards to metal cofactors, considering the difference in size and preferred binding partners of each metal. Manganese ions may then serve as an excellent tool to further probe the reaction mechanism and substrate interactions of LIG1. For example, comparative analysis of active-site mutations in the presence of magnesium or manganese may reveal which residues specifically interact with active-site metal ions, and/or how many active-site metal ions are required for catalysis. Similarly, characterization of DNA ligation of substrates with varying chemical moieties at the nick in the presence of either metal may elucidate how the metal ions specifically interact with the substrate. These questions are essential to understanding how LIG1 functions, and will be easier to answer now that changes in enzyme behavior in the presence of manganese can also be evaluated.

Inhibitory manganese sites reveal new metal binding sites

The inhibitory behavior of manganese ions with LIG1 is unusual. The lack of a change in the affinity of the inhibitory manganese across a 4-fold range of saturating magnesium concentrations suggests that there is a site in LIG1 specific for manganese over magnesium. Inhibition by manganese then cannot result from non-productive binding of manganese to a catalytically required metal site, but instead to some other location on the enzyme (Scheme 3-2). Perhaps even more interesting is the observation that manganese can inhibit the enzyme

adenylylation and adenylyl transfer steps, but not nick-sealing. This suggests significant rearrangement occurs between the two DNA dependent steps of adenylyl transfer and nick-sealing that either renders the enzyme insensitive to inhibition during the nick-sealing step or simply eliminates the inhibitory manganese site. While it is expected that large scale domain rearrangements occur between the enzyme adenylylation and adenylyl transfer steps [9], we currently have little information as to how much conformational rearragnement occurs between adenylyl transfer and nick-sealing.

Multiple-turnover		**Mg^{2+}** [a]	**Mn^{2+}**	**relative** [b]
Saturating Conditions				
	k_{cat} (s^{-1})	0.81 ± 0.1	1.3 ± 0.1	0.62
	K_{M}^{2+} (mM)	0.71 ± 0.2	0.50 ± 0.08	1.4
	K_I (mM)	N/A	2.1 ± 0.6	N/A
Subsaturating ATP				
	$(k_{cat}/K_M)^{ATP}$ (M^{-1} s^{-1})	(6.2 ± 1.1) x 10^4	(1.2 ± 0.2) x 10^5	0.52
	K_{M}^{2+} (mM)	1.8 ± 0.5	2.1 ± 0.5	0.86
	K_I (mM)	N/A	2.1 ± 0.6	N/A
Single-turnover				
Adenylyl transfer				
	$k_{transfer}$ (s^{-1})	2.6 ± 0.3	8.7 ± 1.2	0.30
	K_{M}^{2+} (mM)	0.15 ± 0.06	0.12 ± 0.06	1.25
	K_I (mM)	N/A	0.13 ± 0.08	N/A
Nick-sealing				
	k_{seal} (s^{-1})	12 ± 2	6.4 ± 0.6	1.9
	K_{M}^{2+} (mM)	2.6 ± 0.9	0.44 ± 0.08	5.9

Table 3-1: Comparison of kinetic constants for hLIG1 measured in the presence of magnesium or manganese. Not applicable (N/A) is reported for inhibition of the magnesium reaction as magnesium was never observed to inhibit ligation.

[a] Values reported for the LIG1 reaction in magnesium come from Taylor *et al.* [7].

[b] The relative value is determined by dividing the value obtained in the presence of magnesium by the value obtained in the presence of manganese. Values greater than 1 for rate constants indicate a faster maximal rate in manganese, while values less than 1 indicate a slower maximal rate. Values greater than 1 for metal affinity indicate a tighter affinity for manganese during the corresponding step, while values less than 1 indicate a weaker affinity.

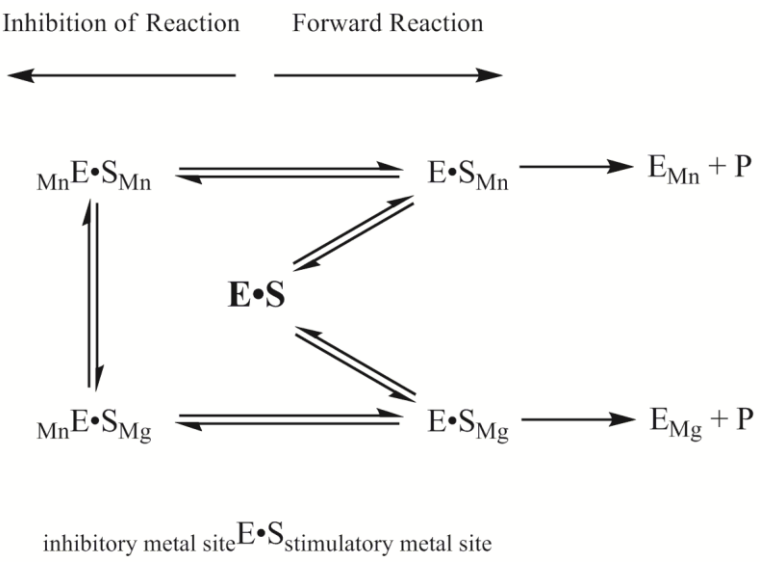

Scheme 3-2: Kinetic model for metal ion binding to hLIG1.

Significance of manganese inhibition of magnesium stimulated reaction

One very surprising result is stronger inhibition by manganese of the magnesium stimulated multiple-turnover reaction than the inhibition observed when manganese is the only metal ion present (K_I of 0.22 mM vs 2.1 mM). Under these conditions, manganese and magnesium compete for binding to the enzyme active-site. Though we know from other reactions that the enzyme is very active in magnesium or manganese alone, this experiment suggests that a hybrid active site containing both metals is either much less active, or more susceptible to inhibition by manganese. This could result from the need for two active-site metals during catalysis, and though two of the same metal correctly structures the active site for catalysis, having two different metal ions disrupts the active-site structure.

The low cellular concentration of manganese in the cell, combined with the relatively weak affinity of the inhibitory site would normally rule out any biological significance of the inhibitory behavior. However, because inhibition by manganese does not appear to be competitive with magnesium, it is possible that inhibition by manganese occurs despite the relative metal ion levels. Indeed, our results suggest manganese inhibition is more potent in the

presence of a high magnesium concentration. Previous reports have listed cadmium and zinc as inhibitors of LIG1, though the affinity reported for inhibition is also above normal physiological levels [13]. It will be interesting to see if inhibition by these metals occurs via similar means as manganese, and if these metals may affect LIG1 activity *in vivo* despite their low relative concentrations.

References

1. Lehman, I.R., *DNA ligase: structure, mechanism, and function.* Science, 1974. **186**(4166): p. 790-7.
2. Soderhall, S. and T. Lindahl, *Mammalian DNA ligases. Serological evidence for two separate enzymes.* J Biol Chem, 1975. **250**(21): p. 8438-44.
3. Simsek, D., et al., *Crucial role for DNA ligase III in mitochondria but not in Xrcc1-dependent repair.* Nature, 2011. **471**(7337): p. 245-8.
4. Gao, Y., et al., *DNA ligase III is critical for mtDNA integrity but not Xrcc1-mediated nuclear DNA repair.* Nature, 2011. **471**(7337): p. 240-4.
5. Wilson, T.E., U. Grawunder, and M.R. Lieber, *Yeast DNA ligase IV mediates non-homologous DNA end joining.* Nature, 1997. **388**(6641): p. 495-8.
6. Grawunder, U., et al., *DNA ligase IV is essential for V(D)J recombination and DNA double-strand break repair in human precursor lymphocytes.* Mol Cell, 1998. **2**(4): p. 477-84.
7. Taylor, M.R., et al., *Kinetic mechanism of human DNA ligase I reveals magnesium-dependent changes in the rate-limiting step that compromise ligation efficiency.* J Biol Chem, 2011. **286**(26): p. 23054-62.
8. Yang, S.W. and J.Y. Chan, *Analysis of the formation of AMP-DNA intermediate and the successive reaction by human DNA ligases I and II.* J Biol Chem, 1992. **267**(12): p. 8117-22.
9. Pascal, J.M., et al., *Human DNA ligase I completely encircles and partially unwinds nicked DNA.* Nature, 2004. **432**(7016): p. 473-8.
10. Frank, E.G. and R. Woodgate, *Increased catalytic activity and altered fidelity of human DNA polymerase iota in the presence of manganese.* J Biol Chem, 2007. **282**(34): p. 24689-96.
11. El-Deiry, W.S., K.M. Downey, and A.G. So, *Molecular mechanisms of manganese mutagenesis.* Proc Natl Acad Sci U S A, 1984. **81**(23): p. 7378-82.
12. Tabor, S. and C.C. Richardson, *Effect of manganese ions on the incorporation of dideoxynucleotides by bacteriophage T7 DNA polymerase and Escherichia coli DNA polymerase I.* Proc Natl Acad Sci U S A, 1989. **86**(11): p. 4076-80.
13. Yang, S.W., F.F. Becker, and J.Y. Chan, *Inhibition of human DNA ligase I activity by zinc and cadmium and the fidelity of ligation.* Environ Mol Mutagen, 1996. **28**(1): p. 19-25.

Appendix B: Figures and Tables to Accompany Chapter 3

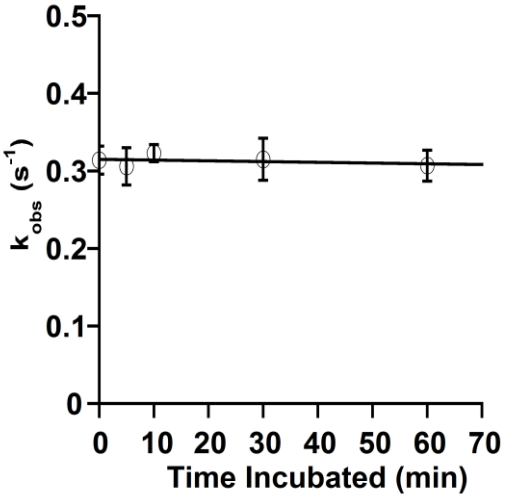

Figure B-1: LIG1 is stable under standard manganese reaction conditions. 4 nM LIG1 was incubated at 37 °C in standard reaction buffer, 200 μM ATP and 20 mM $MnCl_2$ for 0 minutes to 60 minutes prior to the start of a multiple-turnover ligation reaction. Reactions were initiated by addition of 1 μM nDNA. The initial velocity was divided by the concentration of enzyme to obtain k_{obs}. The observed multiple-turnover rate constant was unaffected by the length of incubation, indicating that LIG1 is stable under these reaction conditions.

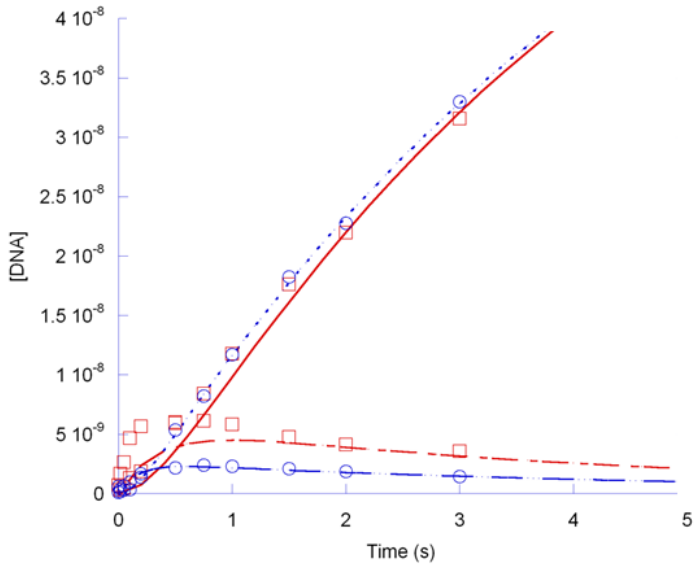

Figure B-2: Determination of proper quench solution for rapid-mixing experiments. Data from single-turnover reactions containing 80 nM substrate, 800 nM LIG1 and 10 mM Mn^{2+} quenched with either 50 mM EDTA in 90% formamide (red, squares) or 3 M HCl (blue, circles). At early time-points, the EDTA/formamide quench results in significantly more intermediate than the HCl quench. The EDTA/formamide data cannot be well-fit by a 2-step irreversible model, while the HCl data is fit well by the model. This indicates that the EDTA/formamide quench is insufficient to quench reactions on the time-scale required for rapid-mixing experiments, while 3 M HCl is sufficient.

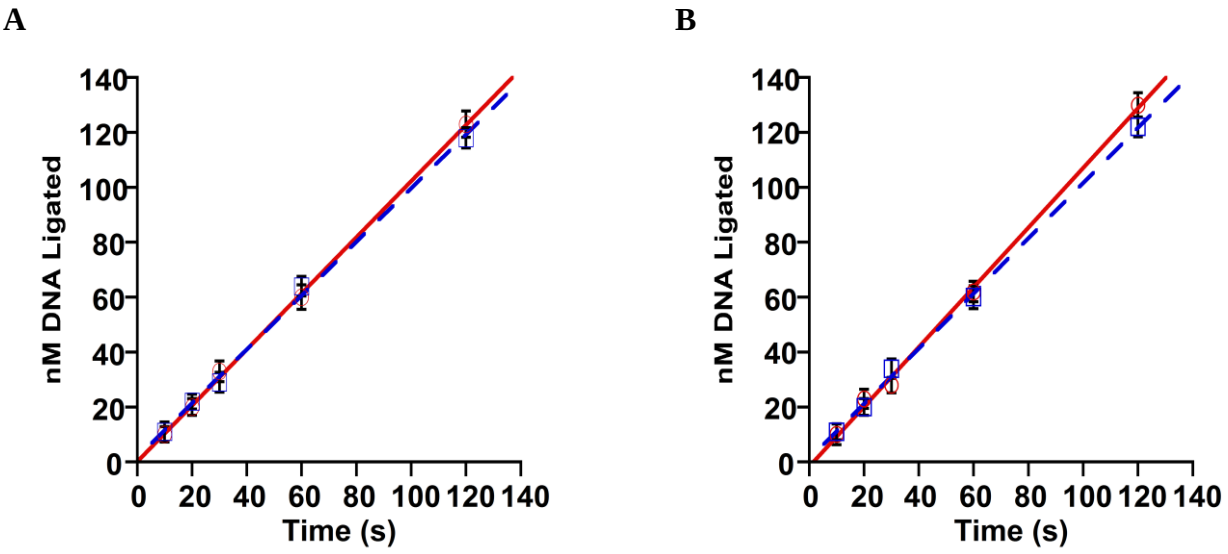

Figure B-3: DNA Evidence of DNA saturation during manganese stimulated multiple-turnover ligation. Multiple-turnover reactions performed at the lowest (200 μM, **A**) and highest (20 mM, **B**) concentrations of manganese used during multiple-turnover reactions. The rate of DNA ligation remains constant when either 250 nM (red, circles) or 1 μM DNA (blue, squares) is present in the reaction, indicating that the 1 μM concentration of DNA used for multiple-turnover reactions is saturating.

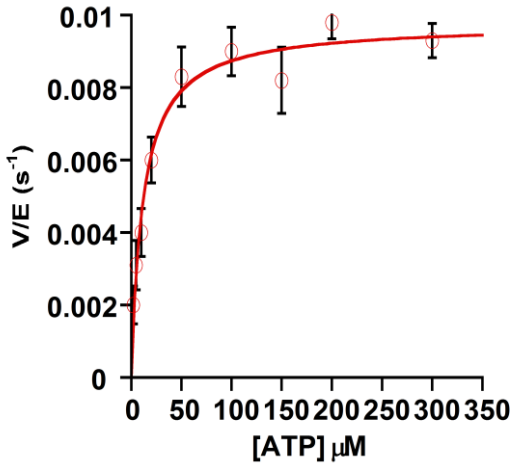

Figure B-4: ATP saturation of manganese stimulated multiple-turnover ligation. Multiple-turnover reactions were performed under standard conditions with 20 mM manganese and a range of ATP concentrations. The ATP dependence of the observed multiple-turnover rate constant fits well to the Michaelis-Menten equation, yielding a k_{max} of 0.01 s^{-1} and a K_{ATP} of 12 μM.

A

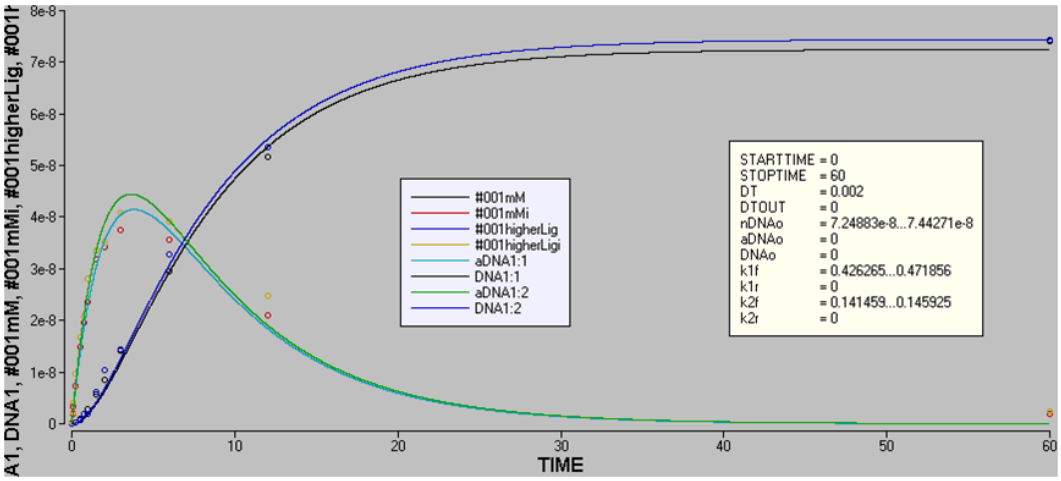
A1, DNA1, #001mM, #001mMi, #001higherLig, #001
TIME
#001mM
#001mMi
#001higherLig
#001higherLigi
aDNA1:1
DNA1:1
aDNA1:2
DNA1:2
STARTTIME = 0
STOPTIME = 60
DT = 0.002
DTOUT = 0
nDNAo = 7.24883e-8...7.44271e-8
aDNAo = 0
DNAo = 0
k1f = 0.426265...0.471856
k1r = 0
k2f = 0.141459...0.145925
k2r = 0

B

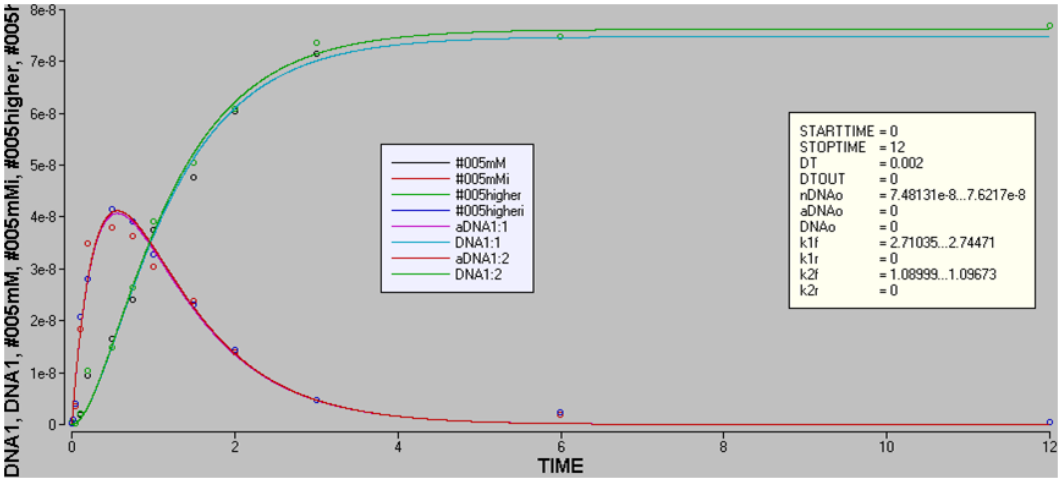
DNA1, DNA1, #005mM, #005mMi, #005higher, #005
TIME
#005mM
#005mMi
#005higher
#005higheri
aDNA1:1
DNA1:1
aDNA1:2
DNA1:2
STARTTIME = 0
STOPTIME = 12
DT = 0.002
DTOUT = 0
nDNAo = 7.48131e-8...7.6217e-8
aDNAo = 0
DNAo = 0
k1f = 2.71035...2.74471
k1r = 0
k2f = 1.08999...1.09673
k2r = 0

C

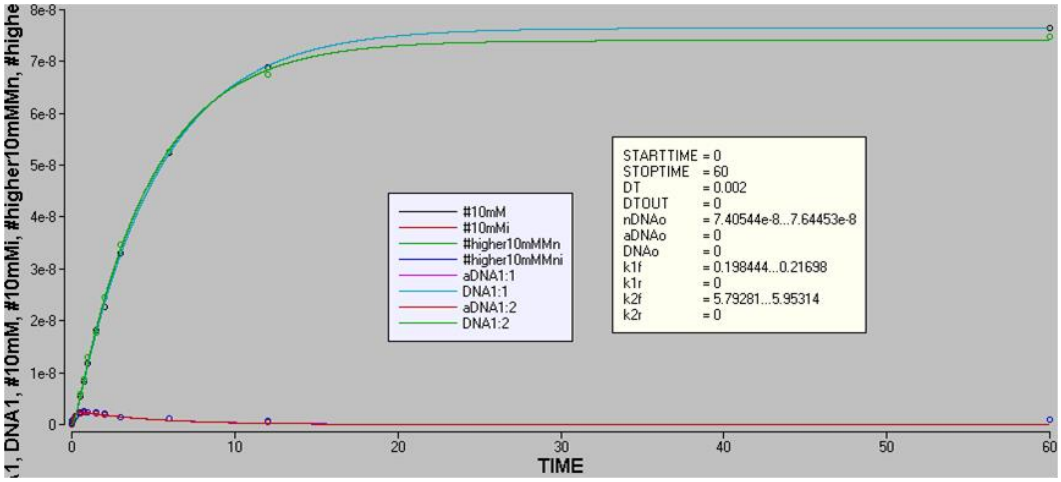
1, DNA1, #10mM, #10mMi, #higher10mMMn, #highe
TIME
#10mM
#10mMi
#higher10mMMn
#higher10mMMni
aDNA1:1
DNA1:1
aDNA1:2
DNA1:2
STARTTIME = 0
STOPTIME = 60
DT = 0.002
DTOUT = 0
nDNAo = 7.40544e-8...7.64453e-8
aDNAo = 0
DNAo = 0
k1f = 0.198444...0.21698
k1r = 0
k2f = 5.79281...5.95314
k2r = 0

Figure B-5: LIG1 saturation of manganese stimulated single-turnover ligation. Reactions were performed with 80 nM substrate and either 800 nM or 3200 nM LIG1 at the lowest (0.01mM, **A**) and highest (10 mM, **B**) concentrations of manganese studied, as well as the concentration of manganese that yields the fastest adenylyl transfer rate (0.05 mM, **C**). The two LIG1 concentrations yield identical rate constants under all manganese concentrations, indicating that 800 nM LIG1 is saturating for single-turnover reactions in manganese (Table B-1).

[Mn]	[Lig1]	$k_{transfer}$	k_{seal}
0.01 mM	800 nM	$0.43 \pm 0.053\ s^{-1}$	$0.14 \pm 0.036\ s^{-1}$
	3200 nM	$0.47 \pm 0.061\ s^{-1}$	$0.15 \pm 0.050\ s^{-1}$
0.05 mM	800 nM	$2.71 \pm 0.27\ s^{-1}$	$1.09 \pm 0.15\ s^{-1}$
	3200 nM	$2.74 \pm 0.43\ s^{-1}$	$1.10 \pm 0.26\ s^{-1}$
10 mM	800 nM	$0.20 \pm 0.018\ s^{-1}$	$5.8 \pm 0.42\ s^{-1}$
	3200 nM	$0.22 \pm 0.034\ s^{-1}$	$6.0 \pm 0.67\ s^{-1}$

Table B-1: 800 nM LIG1 saturates single-turnover reactions under all tested reaction conditions. Single-turnover reactions were performed in triplicate as described in Figure B-5. The values reported are the averages of the value for ktransfer and kseal from 3 independent experiments, and the standard deviation of that measurement.

Chapter 4: Role of Conserved Active Site Carboxylates in Enzymatic DNA Ligation

Abstract

Human DNA ligase I catalyzes the formation of a phosphodiester bond via a reaction mechanism involving three independent phosphoryl transfer steps. Each step of the reaction requires divalent metal ions, though the function of these metals during catalysis is unknown. Two potential active-site metal binding site were observed in a crystal structure of the protein bound to a DNA substrate. These sites are coordinated by the universally conserved residues D570, E621 and E720 (LIG1 numbers). Kinetic analyses of mutant enzymes with conservative carboxyl to amide substitutions reveal that mutations at any of these residues results in changes to metal affinity and maximal catalytic rate for each step of the DNA ligation reaction. The E621Q mutant retains wild-type substrate binding and is able to perform each step of the ligation reaction, however the overall rate of ligation is 10^5-fold slower than wild-type. The D570N and E720Q affect metal binding sites on opposite sides of the nick, yet the mutations result in similar changes to metal binding affinity and maximal reaction rate for the DNA dependent steps. This suggests the two residues are part of a cooperative network of interactions within the active-site. The E720Q mutation disturbs the ATP dependent reaction much more severely than the D570N mutation. The kinetic analysis done with these mutants extends previous mutational studies done with a minimal DNA ligase to the more complex human DNA ligase I and provides functional evidence that these residues coordinate metals in multiple steps of the reaction.

*The work reported here would not have been possible without the help of Neha V. Bokil and Thomas J. Jurkiw. Neha collected most of the kinetic data for D570N and E720Q data while working with me as a UROP sponsored undergraduate research assistant during the 2012-2013 school year, and as a UROP summer fellow during the summer of 2013. Tom performed a majority of the experiments with E621Q under my guidance during a fall research rotation in 2013. Patrick O'Brien made the mutant plasmids and Mark Taylor purified the mutant proteins.

Introduction

DNA ligases complete the processes of DNA replication and repair by catalyzing formation of a phosphodiester bond between adjacent DNA strands [1]. DNA based life from viruses to humans require the function of these enzymes to maintain the integrity of the genome [2-5]. All DNA ligases share a universally conserved reaction pathway which consists of three independent phosphoryl transfer reactions [1] (Scheme 4-1). During the first step of the reaction, enzyme adenylylation, the enzyme catalyzes transfer of an adenylyl group from either ATP or NAD^+ to an active site lysine. All higher eukaryotes use ATP as the nucleotide donor, while bacteria and some viruses use NAD^+ [6]. The next step of the reaction is adenylyl transfer, in which the AMP group is transferred from the enzyme to the 5' phosphate of a DNA nick. The phosphodiester bond is formed during the third step of the reaction, nick-sealing. Each of these reactions requires the presence of one or more divalent metal ions, though the role of these ions during each of the steps has not been well established [7].

A crystal structure of human DNA ligase I (LIG1) in complex with an adenylylated, nicked DNA reveals two potential metal binding sites within the active-site of the enzyme (Figure 4-1A) [8]. Both of these sites are coordinated by catalytically essential substrate groups and active-site residues that are universally conserved from viruses to humans [9] (Figure 4-1B). D570 and E621 coordinate the site on the 5' side of the nick, which places a metal ion in close proximity to the 3' hydroxyl that executes nucleophilic attack during nick-sealing. E720 and DNA substrate phosphates coordinate the site on the 3' side of the nick, which places a metal near the active site lysine and 5' phosphate. Conservative mutations of the corresponding residues in Chlorella Virus DNA ligase result in decreased enzymatic activity, suggesting the importance of these residues in catalysis [9].

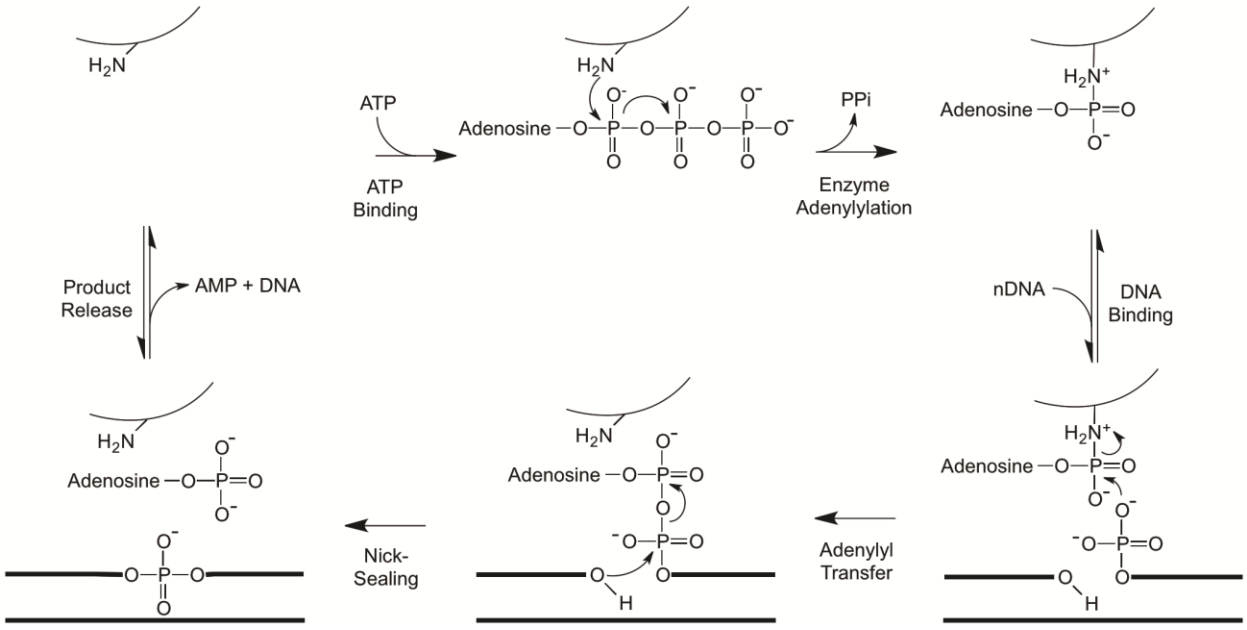

Scheme 4-1: Minimal kinetic mechanism of enzymatic DNA ligation.

Support for the two-metal active-site comes from recent work characterizing the kinetic mechanism of ligation with LIG1 in the presence of magnesium [10]. The magnesium dependencies reveal that the enzyme requires at least two magnesium ions during enzyme adenylylation, one that comes in bound to the ATP substrate, and the other captured from solution. The active-site during enzyme adenylylation is predicted to be substantially different from that pictured in the crystal structure, however, as residues important for enzyme adenylylation are oriented toward away from the active site [8, 11]. Reorientation of the OB-fold domain would drastically change the overall structure of the active-site, but could leave the observed metal sites intact. Changes in the structure of the active-site also likely occur between the two DNA dependent steps in order to accommodate the shifting location of the scissile bond. Understanding what role the predicted binding sites play during each step of DNA ligation could give insight into the arrangement of the active-site during each step of catalysis, as well as to the function of metal ions during DNA ligation.

A **B**

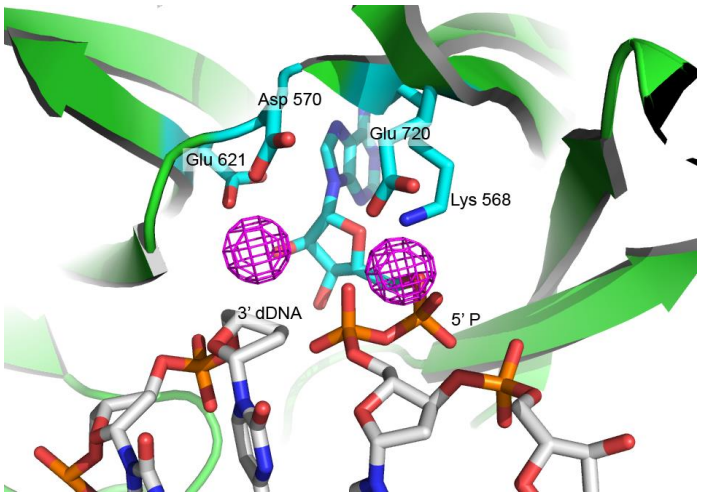


```
                                  †  *
LIG1      560   EAAFTCEYKYDGQRAQIHAL
LIG3      414   NGMFS-EIKYDGERVQVHKN
LIG4      199   HQSFYIETKLDGERMQMHKD
CDC9      411   GETFTSEYKYDGERAQVHLL
CDC17     408   QAAFTCEYKYDGERAQVHFT
ChVLIG     24   A-----TPKIDGIRSVKQ--

                                  *
LIG1      610   LPSVTSFILDTEAVAWDREK
LIG3      462   FPGGHSMILDSEVLLIDNKT
LIG4      340   KADIQICILDGEMMAYNPNT
CDC9      461   LDTTKNLILDCEAVAWDKDQ
CDC17     458   KPDARSFILDCEAVGWDRDE
ChVLIG     44   LTELLPEGSDGFISIEGATF

                                  *
LIG1      710   FLEQSVKDSCEGLMVKTLD-
LIG3      558   MITRVIQEGLEGLVLKDVK-
LIG4      417   ALNEAIDKREEGIMVKQPL-
CDC9      561   FLDESVNHSCEGLMVKMLEG
CDC17     558   FLEESVKDSCEGLMVKMLEG
ChVLIG    140   YERDVLSKGFEGVMIRKPDG
```

Figure 4-1: Metal binding sites revealed by hLIG1 crystal structure. A, Close-up of active-site of hLIG1 as crystallized in complex with adenylylated DNA [8]. The protein backbone is represented in green cartoon form, with important active-site residues and substrate DNA depicted in stick form. The lysine that goes through transient adenylylation and active site residues involved in coordinating metal sites are labeled, as are the free 3' and 5' DNA ends at the nick. Predicted metal sites are depicted with magenta lattices. **B,** Protein sequence alignment of human DNA ligase I (LIG1), DNA ligase III (LIG3) and DNA ligase IV (LIGIV), *Saccharomyces cerevisiea* (CDC9), *Schizosaccharomyces pombe* (CDC17) and Chlorella Virus DNA (ChVLIG) show conservation of residues within the active-site. Alignment performed with default settings in ClustalX using truncated versions of each protein that include only the catalytic core domains. * indicates a residue involved in coordination of proposed active-site metal sites. † indicates Lys 568, that is adenylylated in the first step of the reaction.

To investigate the role of metal ions in predicted metal binding sites of LIG1, we have made conservative carboxyl to amide mutations in the residues coordinating these sites. Comparison of the magnesium dependence of the mutants during each step of the ligation reaction to wild-type indicates during which step each residue serves as an important metal ligand. The E621Q mutation results in a functional enzyme with greatly diminished ability to perform adenylyl transfer and nick-sealing. The D570N and E720Q mutations result in a nearly identical defect in adenylyl transfer and a similar defect in nick-sealing, despite being on opposite sides of the nick. We propose that D570 and E720 form part of a network of cooperative interactions that structure the enzyme active site during the DNA dependent reactions. In contrast, D570N has little effect on enzyme adenylylation, while E720Q shows a significant decrease in the second order rate constant for ATP utilization, $(k_{cat}/K_M)^{ATP}$. This suggests that E720Q may play a role in metal binding during enzyme adenylylation, as well as the DNA dependent reactions. This work builds

on what is known about DNA ligases from work with the Chlorella Virus DNA ligase to help us understand the more complicated human DNA ligase I.

Experimental Procedures

DNA Ligase I Mutants

The D570N, E621Q or E720Q mutants were each expressed as the catalytic domain of human LIG1 (residues 232-919) in *E. coli* and purified as previously described [10]. Cells were lysed in the presence of 1 mM EDTA to preserve the adenylylated form of the enzyme, and subsequently purified over a phosphocellulose column and a NTA-nickel column. The His tag was removed with Prescission protease, and LIG1 was further purified with Q-sepharose. The final purified fractions were combined and dialyzed into storage buffer (25 mM Tris•Cl, pH 7.6, 150 mM NaCl, 1 mM DTT, and 0.1 mM EDTA). Aliquots were snap-frozen and stored at -80 ^{o}C. Purity was greater than 90% as judged by SDS-PAGE. Initial concentrations were estimated from the absorbance at 280 nm, using the calculated extinction coefficient. The concentration of active, adenylylated enzyme was determined by titration with nicked DNA substrate, as described in the paper, and this active concentration is reported throughout. Due to the low activity of E621Q, we used the concentration determined from UV-absorbance.

DNA Substrates

Oligonucleotides were synthesized by Integrated DNA Technologies or by the Keck Center at Yale University and were purified on denaturing polyacrylamide gels. The portion of the gel containing the full-length oligonucleotide was excised, crushed, and extracted by soaking overnight in 500 mM NaCl and 1 mM EDTA. The extracted oligonucleotides were desalted by binding to a C18 reverse phase column (Sep-pak, Waters) and eluted with 30% (v/v) acetonitrile. Concentrations were obtained from the absorbance at 260 nm using the calculated extinction coefficients. The three oligonucleotides used in this study had sequences 5'-CCGAATCAGTCCGACGACGCATCAGCAC, 5'-GTGCTGATGCGTC, and 5'-P-

GTCGGACTGATTCGG-FAM (P indicates 5' phosphorylation and FAM indicates the presence of a 3' fluorescein). The nicked, double-stranded DNA substrate (nDNA) was formed by mixing equimolar amounts of the three oligonucleotides in 10 mM NaMES pH 6.5 and 50 mM NaCl and cooling the mixture from 90 °C to 4 °C at a rate of 3 °C per minute.

Gel-based Ligation Assay

Ligation reactions were performed at 37 °C. Unless otherwise indicated, the standard buffer contained 50 mM NaMOPS pH 7.5 (measured at 25 °C), 1 mM dithiothreitol, 0.05 mg/mL BSA, and sufficient NaCl to maintain a constant ionic strength of 150 mM. The amounts of ATP, $MgCl_2$, nDNA, and LIG1 mutant enzyme varied, as indicated below. Preincubation controls established that each LIG1 mutant retains 100% of its activity after 1 hr in this standard buffer, and all of the kinetic data was collected within this window of time. Reactions were quenched as described below, heated to 95 °C for 5 min to denature the DNA and resolved on 20% (w/v) denaturing polyacrylamide gels containing 8 M Urea. Fluorescein-labeled oligonucleotides were detected with a Typhoon Trio$^+$ imager (GE Healthcare) with excitation at 488 nm and emission through a 520 nm band-pass filter. The images were analyzed using ImageQuantTL (GE Healthcare). The intensity of the individual DNA species was corrected for background fluorescence, and the fraction of the total fluorescence was determined by dividing the fluorescence intensity for the desired species by the signal for all other species in the sample. When necessary, this fraction was converted into its concentration by multiplying by the total concentration of DNA in the reaction.

Multiple-Turnover Ligation Assays

Steady state kinetic analysis was performed in the standard ligation buffer and the temperature was maintained at 37 °C in a circulating water-bath. Reaction mixtures were preincubated for 5 min prior to addition of LIG1. Reactions were arrested by quenching a 4 µL aliquot in 15 µL of quench solution (50 mM EDTA in 90% formamide), and the extent of ligation was determined as

described above. Initial rates were determined from the linear rate of substrate disappearance within the first 10% of the reaction. When both intermediate and product were formed during the reaction, the rate of formation for each species was determined. Values reported represent the average of at least two experiments, unless otherwise noted in the text. Equations used to fit data are described in the Models of Kinetic Parameters section and in the text. All fitting of multiple-turnover data was done using Kaleidagraph, Synergy Software.

Single-turnover Ligation Assays

Unless otherwise indicated, the typical concentrations used for single-turnover reactions were 20 mM $MgCl_2$, 800 nM nDNA and 80 nM LIG1 mutant enzyme. Reactions were quenched as described above for multiple-turnover reactions and submitted to the standard gel-based ligation assay. Levels of intermediate and product were imported into the program Berkeley-Madonna (www.berkeleymadonna.com) and the curve fitting function was used to globally fit the levels of intermediate and product by the scheme represented in Scheme 4-1. Fitting of the data to a model including reversible chemical steps did not produce significantly different results (data not shown). Fits of reactions from individual experiments provided values for the rate constants for adenylyl transfer and nick-sealing and the reported values reflect the average rates determined from at least two independent experiments at each metal concentration, unless otherwise noted in the text. These rate constants were plotted versus the concentration of metal ions. Fitting of the data is discussed in the results section.

Models of Kinetic Parameters

$$k_{obs} = \frac{k_A * [A]}{K_A + [A]} \qquad \text{Equation 4-1}$$

Equation 4-1 describes the model where a reaction is activated by binding of species A to a single stimulatory site. k_{obs} is the observed rate constant for the step being measured, k_A is the maximal rate constant, and K_A is the observed affinity for species A during the observed step. Equation 4-1 is used for fitting the magnesium dependence in Figures 4-5B, 4-5C, and 4-8. This equation takes on the form of the Michaelis-Menten equation when applied to Figure 4-7A and B, where A becomes DNA and ATP, respectively.

$$k_{obs} = \frac{k_A * [A]}{[A] + K_A + \frac{K_A [I]}{K_I}} \qquad \text{Equation 4-2}$$

Equation 4-2 describes a competitive inhibition model where the substrate can either be bound by a productive enzyme, A or a nonproductive enzyme, I. k_{obs} is the observed rate constant for the step being measured, k_A is the maximal rate constant when bound by enzyme A, K_A is the affinity between enzyme A and the substrate, and K_I is the affinity between the inactive enzyme, I, and the substrate. Equation 4-2 is used for fitting the data in Figure 4-4.

$$k_{cat} = \frac{1}{\frac{1}{k_1} + \frac{1}{k_2} + ... + \frac{1}{k_n}}$$ Equation 4-3

Equation 4-3 describes the relationship between the macroscopic rate constant for the steady-state reaction (k_{cat}) and the individual microscopic rate constants that define each step of the reaction (k_1, k_2, etc.). Equation 4-3 is used to determine the value of $k_{adenylylation}$ from the measured rate-constants for k_{cat}, $k_{transfer}$ and k_{seal}. This value is reported in Table 4-1.

Results and Discussion

Determining the adenylylation state of LIG1 mutants

Wild-type LIG1 can be purified as the adenylylated enzyme and 100% of the protein is active [10], however mutations of the residues corresponding to D570, E621 and E720 in Chlorella Virus DNA ligase (ChVLIG) are reported to affect the enzyme's adenylylation state [9]. In order to determine the adenylylation state and active concentration of each mutant, active-site titrations were performed in which varying amounts of enzyme was added to a fixed concentration of nicked DNA (nDNA) substrate in standard reaction buffer without ATP (Figure 4-2). The reaction is allowed to sit for 5 minutes and the amount of product formed then directly relates to the amount of active, adenylylated LIG1 present in the reaction. D570N and E720Q each form product in a 1.2:1 ratio of input enzyme to input substrate (Figure 4-2A, B), indicating that 80% of the purified protein measured by UV-absorption is active and adenylylated. This small discrepancy from 100% active enzyme can be explained by the contribution of the adenylyl group to the absorbance at 280 nm. Reaction times of 15 minutes do not change the amount of product formed at any DNA concentration, indicating the reaction is complete at 5 minutes (data not shown).

E621Q forms product at a 500:1 ratio of input enzyme to input substrate under the same conditions (data not shown). The amount of product formed with E621Q increases with time up to 200 minutes (data not shown) indicating that the enzyme is active, but much slower than wild-type LIG1. Pre-incubation of each mutant with ATP and magnesium prior to reaction does not alter the amount of product formed, indicating each mutant is fully adenylylated following purification (data not shown). This contrasts with what was seen with the ChVLIG mutants, in which analogous mutations were reported to decrease, or even abolish enzyme adenylylation.

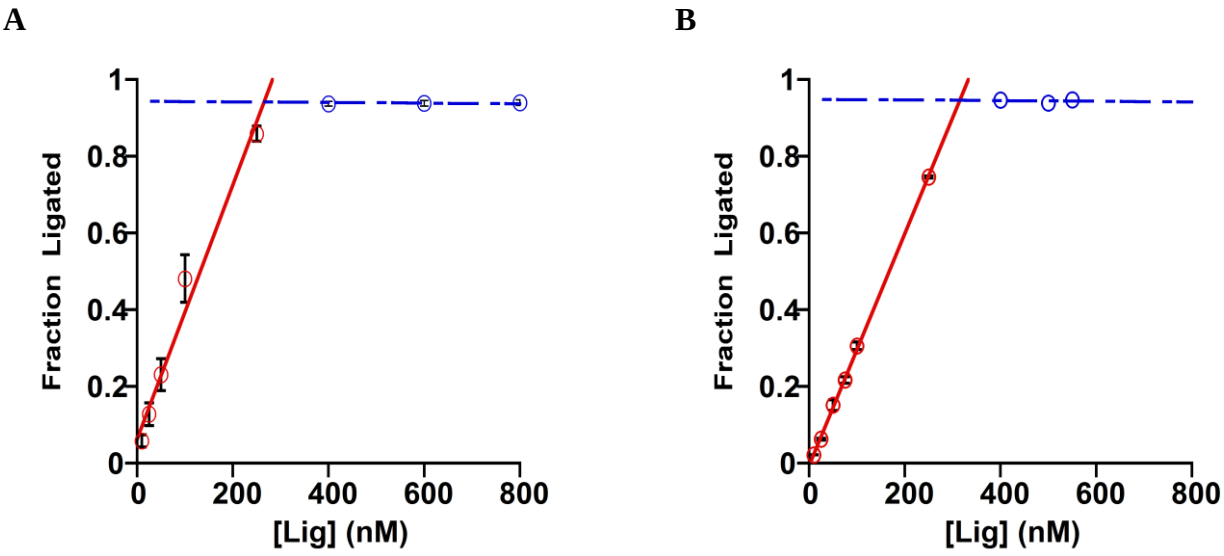

Figure 4-2: Active-site titration of D570N and E720Q LIG1 mutants. Enzyme was titrated against a fixed concentration of 250 nM DNA substrate in 20 mM $MgCl_2$ and allowed to react for 15 minutes. Titration of D570N (**A**) and E720Q (**B**) indicate ~80% of the protein measured by UV-absorption is adenylylated and active. Addition of an adenylyl group increases the extinction coefficient of the protein by 20%, indicating all enzyme is actually active.

E621Q is severely impaired for the DNA dependent reactions

We investigated the slow reaction rate observed during active-site titration experiments by performing single-turnover reactions with E621Q. Reactions containing 20 mM $MgCl_2$, 600 nM E621Q, 250 nM nDNA and no ATP show that E621Q does not complete ligation over a 48-hour time-course (Figure 4-3). The rate of product formation rapidly decreases after 6 hours, indicating the enzyme begins to lose activity at this point. Though we are unable to directly determine any rate constants from this data, comparison of the linear rate of product formation to wild-type can give a rough estimate of the relative difference between the two proteins. During the linear phase of product formation, E621Q converts 1.3% of the input DNA to product per hour, compared to 62% per second for wild-type LIG1. This rough comparison suggests E621Q is ~$1.8x10^5$-fold slower than wild-type under similar single-turnover conditions.

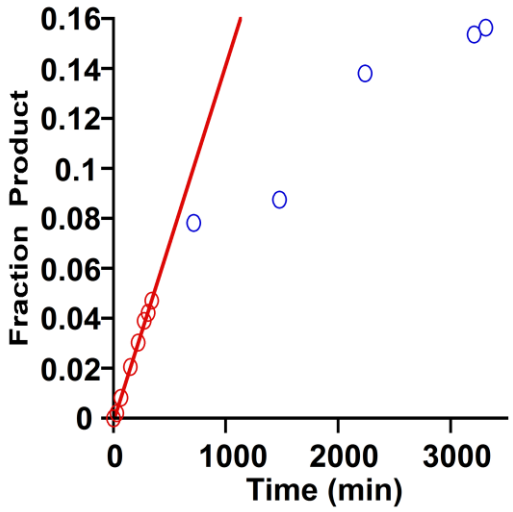

Figure 4-3: E621Q exhibits extremely slow single-turnover ligation. The formation of product was monitored during single-turnover ligation reactions containing 20 mM $MgCl_2$, 600 nM E621Q and 250 nM nDNA. The enzyme remains active up to 24 hours, but appears to begin losing activity around 6 hours into the reaction. Comparison of the linear rate of product formation (red circles and fit-line) indicates that the enzyme is at least 10^5-fold slower than wild-type under similar conditions [10].

To ensure the observed changes in reaction rate do not result from a decreased DNA substrate affinity, we competed E621Q against wild-type LIG1 under multiple-turnover conditions (Figure 4-4). These reactions contained 20 mM magnesium, 200 μM ATP, 100 nM DNA, 1 nM wild-type LIG1 and 0-1000 nM E621Q. The measured multiple-turnover rate decreases with increasing amounts of E621Q and fits well to the equation describing simple competitive inhibition (Equation 4-2), with a K_I for the inhibitor (E621Q) of 70 nM. This value for the affinity of the E621Q mutant for DNA is quite similar to the 30 nM K_M measured for wild-type LIG1 (Table 4-1) [10].

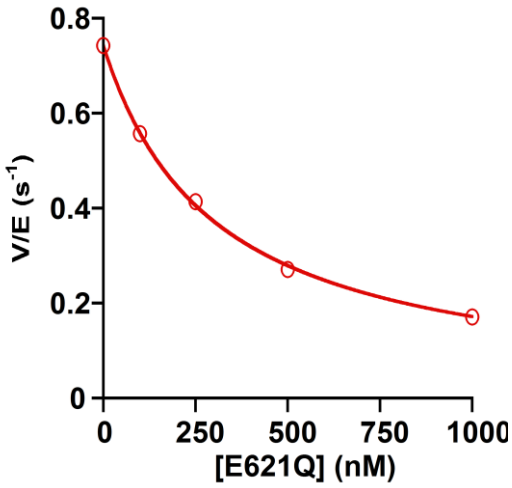

Figure 4-4: E621Q shows no significant decrease in substrate binding activity. Increasing amounts of E621Q were added to reactions containing 20 mM MgCl2, 200 μM ATP, 100 nM DNA and 1 nM wild-type LIG1. The dependence of the rate of reaction on the concentration of E621Q fits well to a competitive inhibition model (Equation 4-2) and yields a K_I for E621Q of 70 nM. This value is similar to the $K_{M,DNA}$ of 30 nM displayed by wild-type LIG1, suggesting little effect of the E621Q mutation on DNA binding.

D570N and E720Q mutations display similar effects on single-turnover ligation

To investigate the effect of the D570N and E720Q mutations on enzymatic DNA ligation, single-turnover reactions were performed with either mutant across a range of magnesium and DNA concentrations. Omission of ATP from these reactions ensures that each enzyme molecule can perform ligation only once. Each reaction with D570N and E720Q was followed to completion, and data from all reactions fit well to a 2-step irreversible model (Figure 4-5A). Identical values for rate constants were measured at both 800 nM and 1600 nM substrate with 80 nM enzyme, indicating the standard single-turnover conditions of 80 nM enzyme with 800 nM substrate are saturating (data not shown).

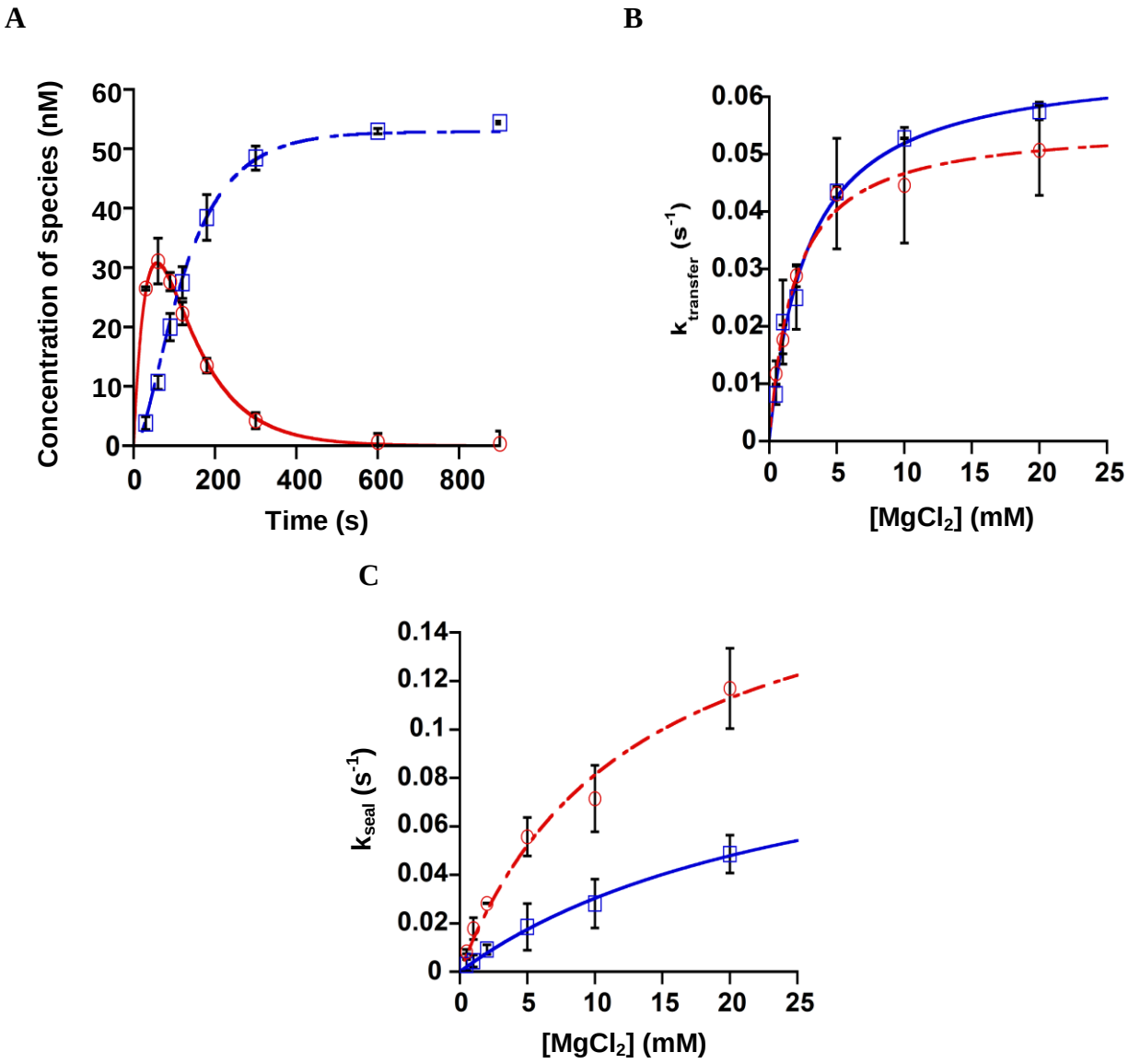

Figure 4-5: Single-turnover ligation by D570N and E720Q. Single-turnover reactions were performed with 800 nM nDNA, 80 nM mutant LIG1 and a range of $MgCl_2$. **A,** Representative data from a single-turnover reaction with E720Q at 20 mM $MgCl_2$. The time dependence of the levels of intermediate (red, circles) and product (blue, squares) fits well to the 2-step irreversible model used for single-turnover ligation (see Experimental Procedures). **B,** The magnesium dependence of $k_{transfer}$ fits well to a single-site binding model (Equation 4-1), and is almost identical between D570N (red, circles) and E720Q (blue, squares). **C,** The magnesium dependence of k_{seal} fits well to a single-site binding model (Equation 4-1) for both D570N (red, circles) and E720Q (blue, squares). The E720Q mutation results in a stronger decrease in the value of k_{seal} at magnesium saturation, as well as a more weakened affinity for magnesium. Values for kinetic constants measured in these fits reported in the text and Table 4-1.

The magnesium dependence of the single-turnover reaction was measured across a range of 0.5 mM to 20 mM magnesium. The magnesium dependence of $k_{transfer}$, the rate constant for adenylyl transfer, appears very similar between the D570N and E720Q mutants (Figure 4-5B). The data for $k_{transfer}$ fit well to a single-site binding model (Equation 4-1) and yield similar values for $k_{transfer}$ of 0.066 s^{-1} and 0.055 s^{-1} for D570N and E720Q, respectively. Both mutants also display similar values of 2.8 mM and 1.9 mM for K_{Mg} for D570N and E720Q, respectively, during adenylyl transfer. These values correspond to an ~40 fold decrease in $k_{transfer}$ and an ~10-fold decrease in metal affinity from the 2.6 s^{-1} $k_{transfer}$ and 0.15 mM K_{Mg} measured with wild-type LIG1 (Table 4-1) [10]. The nick-sealing data also fit well to a single-site binding model (Equation 4-1**)**, yielding values of 0.18 s^{-1} and 0.11 s^{-1} for k_{seal}, and 13 mM and 28 mM for K_{Mg} with D570N and E720Q, respectively (Figure 4-5C). Compared to the values of 12 s^{-1} for k_{seal} and 2.6 mM K_{Mg} measured with wild-type LIG1, each mutant displays ~100-fold decrease in k_{seal} and ~10-fold decrease in K_{Mg} during nick-sealing (Table 4-1) [10]. It should be noted that these reactions poorly define the values for k_{seal}, as the highest value of magnesium tested for these reactions, 20 mM, is close the measured K_{Mg} for both mutants. The buffering system used for these reactions is unable to control for the changes in ionic strength that would occur at higher concentrations of magnesium. Thus the values measured for k_{seal} and K_{Mg} during nick-sealing should be considered estimates.

D570N and E720Q have differing effects on enzyme adenylylation

To evaluate the effect of the D570N and E720Q mutations on enzyme adenylylation and the overall steady-state reaction, we performed multiple-turnover reactions in which ATP is included in the reaction. The standard conditions used for these reactions include 20 mM $MgCl_2$, 200 μM ATP, 4 nM enzyme and 1 μM nDNA. The rate of all multiple-turnover reactions were determined from data at less than 10% substrate disappearance, ensuring measurement of the steady-state reaction (Figure 4-6). Product formation remains linear for all steady-state reactions up to the final time-point recorded (longest reaction time of 20 minutes) indicating that the mutants are stable during the course of the reaction. To ensure saturation of the enzyme with nDNA substrate during multiple turnover, we measured the V/E values for reactions spanning

the range of 50 nM to 2 μM nDNA. The DNA dependences of the steady-state reaction rate for both the D570N and E720Q mutants fit well to the Michaelis-Menten equation describing a single-site binding interaction (Equation 4-1) (Figure 4-7A). Both mutants display a K_M for nDNA of less than 50 nM in steady-state reactions, similar to the affinity of 30 nM measured for the wild-type enzyme (Table 4-1) [10]. The lack of a difference in DNA affinity between the D570N and E720Q mutants and wild-type during either steady-state or single-turnover reactions suggests that these two mutations do not significantly affect protein-DNA binding interactions. The ATP dependence of the rate of steady-state ligation reveals a low K_M value of these mutants for ATP (Figure 4-7B). Fitting of the data to a single-site binding model yields a $K_{M,ATP}$ of 1.0 μM and 4.3 μM for D570N and E720Q, respectively. These are both considerably lower than the 12 μM affinity for ATP measured with wild-type LIG1 (Table 4-1) [10].

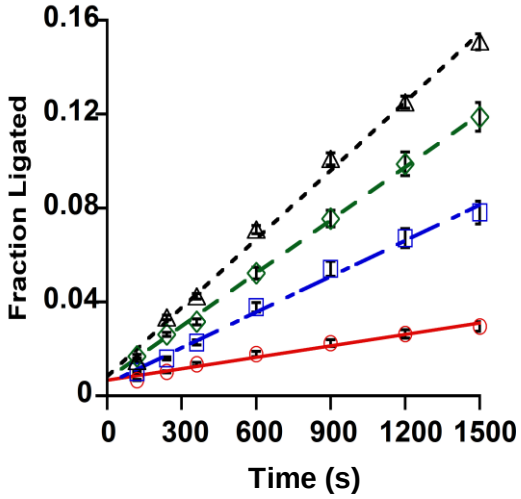

Figure 4-6: Representative steady-state time-course. Multiple-turnover reactions were performed with 20 mM $MgCl^2$, 1 μM nDNA, 4 nM D570N and either 1 μM (red, circles), 5 μM (blue, squares), 20 μM (green, diamonds) or 200 μM (black, triangles) ATP. All data was collected within the linear portion of the reaction. The reaction remains linear up to 16% product formation, indicating time-points taken within the first 10% reaction are not affected by product inhibition.

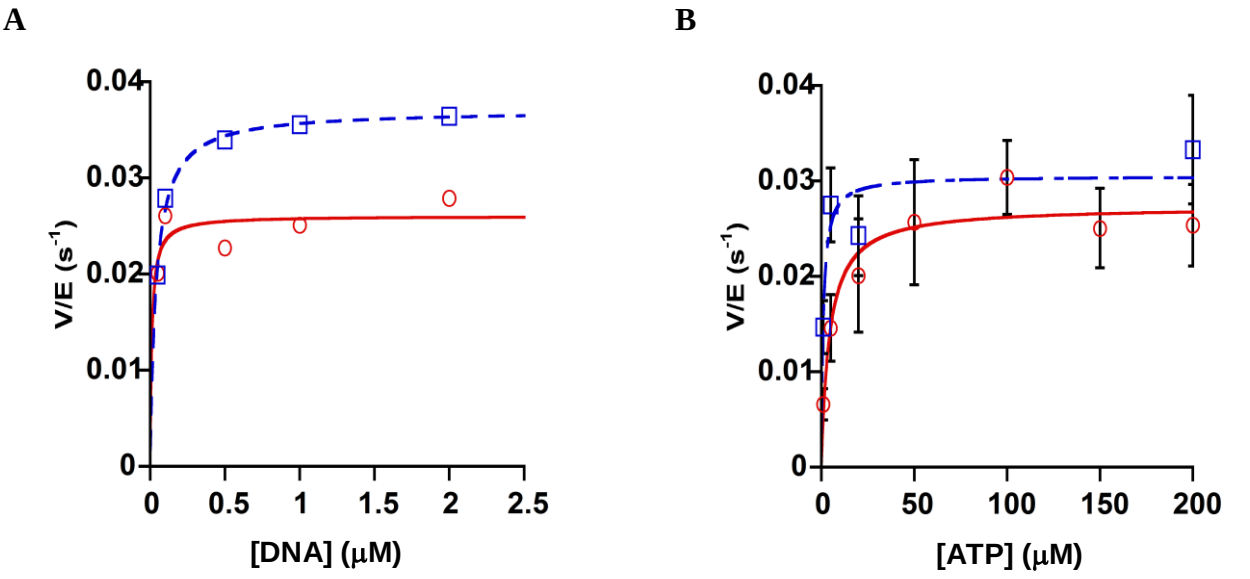

Figure 4-7: D570N and E720Q display wild-type substrate binding. A, Multiple-turnover reactions were performed with 20 mM $MgCl^2$, 200 μM ATP, 4 nM D570N (red, circles) or E720Q (blue, squares) and a range of DNA concentrations from 50 nM to 2 μM. The DNA dependences of the reaction rate for both enzymes fit well to the equation describing a single-site binding model (Equation 4-1). Both mutants display a lower than 50 nM $K_{M,DNA}$, similar to that measured for wild-type LIG1 [10]. **B,** Multiple-turnover reactions were performed with 20 mM $MgCl^2$, 1 μM nDNA, 4 nM D570N or E720Q and a range of ATP concentrations from 0.5 μM to 200 μM. The ATP dependences of the multiple turnover reaction rate for D570N (red, circles) and E720Q (blue, squares) fit well to the Michaelis-Menten equation (Equation 4-1). The K_M value for ATP measured for D570N and E720Q are considerably lower than that measured with wild-type LIG1 (1.0 μM and 4.3 μM vs. 12 μM, respectively) [10].

The apparent increase in ATP affinity can be explained either by a true change in ATP binding, or by the multiple-turnover rate being rendered less sensitive to ATP concentration due to fast DNA dependent reactions. The second order rate constant $(k_{cat}/K_M)^{ATP}$ describes the ATP dependent steps of the reaction, up to and including enzyme adenylylation. The ATP dependence at 20 mM mganesium gives $(k_{cat}/K_M)^{ATP}$ values of $3.1x10^4$ $M^{-1}s^{-1}$ and $6.3x10^3$ $M^{-1}s^{-1}$ for D570N and E720Q, respectively. Whereas the value measured for D570N is quite similar to the $5.6x10^4$ $M^{-1}s^{-1}$ $(k_{cat}/K_M)^{ATP}$ measured for wild-type LIG1 under similar conditions, E720Q shows a significant decrease in $(k_{cat}/K_M)^{ATP}$ compared to wild-type (Table 4-1) [10].

D570N and E720Q display significant defect in magnesium utilization during steady-state reactions

Multiple turnover reactions were performed at saturating DNA and ATP concentrations across a range of magnesium concentrations in order to investigate the effect of the D570N and E720Q mutations on magnesium binding during the overall multiple-turnover reaction. The magnesium dependence of the steady-state rate fits well to the equation describing a single-site binding model (Equation 4-1) and yields a maximal steady-state rate, k_{cat}, of 0.042 s^{-1} and 0.063 s^{-1} and a $K_{1/2}$ for magnesium of 7.3 mM and 35 mM for D570N and E720Q, respectively (Figure 4-8). These high values for K_{Mg}, that are similar to the values for the nick-sealing step, suggests that multiple-turnover for these mutants is limited by the rate of nick-sealing at most concentrations of magnesium. The second order rate constant for utilization of magnesium during multiple-turnover, $k_{cat}/K_{Mg^{2+}}$, gives insight into how efficiently the magnesium cofactor binds to and stabilizes the transition state. As determined from the magnesium dependence of multiple-turnover, $k_{cat}/K_{Mg^{2+}}$ is 5.8 $M^{-1}s^{-1}$ and 1.8 $M^{-1}s^{-1}$ for D570N and E720Q, respectively (Table 4-1). These values are much lower than the $1.1x10^3$ $M^{-1}s^{-1}$ measured for the wild-type enzyme, indicting a drastic decrease in the ability of magnesium to stabilize the reaction transition state (Table 4-1) [10]. This observation supports the idea that both the D570 and E720 residues play an important role in coordinating a metal ion during catalysis.

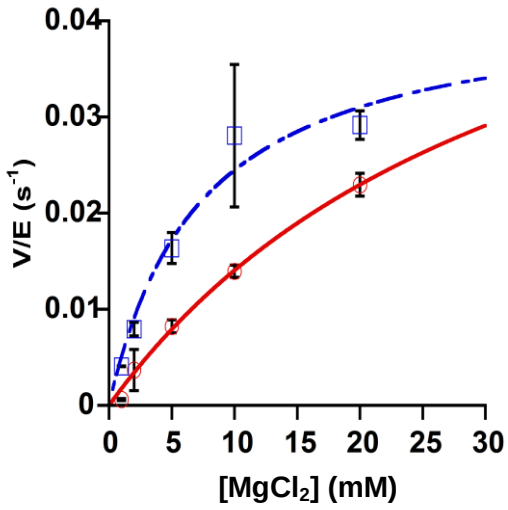

Figure 4-8: D570N and E720Q show greatly weakened metal binding during multiple-turnover reactions. Multiple-turnover reactions were performed with 200 μM ATP, 1 μM nDNA, 4 nM D570N or E720Q and a range of $MgCl_2$ from 1 mM to 20 mM. The magnesium dependence of the rate of steady-state ligation if fit by the equation describing a single-site binding model (Equation 4-1). D570N and E720Q both show a significant decrease in metal binding affinity and maximal reaction rate vs. wild-type LIG1 (K_{Mg} = 7.3 mM and 35 mM vs. 0.71 mM and k_{cat} = 0.042 s^{-1} and 0.063 s^{-1} vs. 0.81 s^{-1}, resepectively).

Conclusion

E621 plays an essential role during DNA dependent reactions

The amide to carboxyl substitution in E621Q is expected to be a relatively conservative mutation with respect to metal ion binding. The expected change would be a weakening of metal binding at the site with little effect on catalysis. The E621Q mutation in LIG1, however, has a surprisingly deleterious effect on catalysis during the DNA dependent reactions of enzymatic ligation, decreasing the observed rate constant for single-turnover reactions by a factor of 10^5. A similar decrease in the rate of DNA ligation was observed for the corresponding mutation in Chlorella Virus DNA ligase (ChVLIG) [9]. Such strong effects on the rate of reaction could indicate that the hydroxyl of E621 may play a role either in overall stabilization in the active site, or through direct or indirect activation of important catalytic groups. The carbonyl group of E621 could instead be responsible for metal ion coordination. Unfortunately, the extremely slow rate of DNA ligation with E621Q prevented a full characterization. Future work characterizing other mutations at E621 could help elucidate the obvious importance of this residue to catalysis.

D570 and E720 form a network of cooperative interactions during DNA dependent reactions

The D570N and E720Q mutations both result in a roughly 650-fold decrease in utilization for magnesium during adenylyl transfer as compared to wild-type, due to nearly identical effects on $k_{transfer}$ and K_{Mg} (Table 4-1). An identical effect at two residues that appear to coordinate two different metal sites suggests that they form a cooperative network of interactions that stabilizes the enzyme active-site. No amino acid or substrate group appears to bridge these two residues in the LIG1 crystal structure, however the oxygen atoms of the two carboxylates are spaced 0.44 nm apart, which could accomodate bridging water molecules [8]. In contrast, E720Q shows a much greater decrease in magnesium utilization during nick-sealing than D570N (12,000-fold

and 3300-fold vs. wild-type, respectively) (Table 4-1). This suggests that while the two residues appear to be equally important for adenylyl transfer, E720 plays a greater role during nick-sealing than D570.

Multiple-turnover		**WT**	**D570N**	**relative**	**E720Q**	**relative**
Saturating Conditions						
	k_{cat} (s^{-1})	0.81	0.042 ± 0.007	(19)	0.063 ± 0.01	(13)
	K_{Mg} (mM)	0.71	7.3 ± 3	(0.097)	35 ± 10	(0.02)
Subsaturating Mg^{2+}						
	k_{cat}/K_{Mg} ($M^{-1}s^{-1}$)	1.1	5.8	(190)	1.8	(610)
Subsaturating ATP						
	$(k_{cat}/K_M)^{ATP}$ ($M^{-1}s^{-1}$)	$6.8x10^4$	$3.1x10^4$	(2.1)	$6.3x10^4$	(10.8)
Enzyme adenylylation*						
	$k_{adenylylation}$ s^{-1}	1.3	0.32	(4)	fast	(ND)
Single-turnover						
Adenylyl transfer						
	$k_{transfer}$ (s^{-1})	2.6	0.066 ± 0.005	(39)	0.055 ± 0.004	(47)
	K_{Mg} (mM)	0.15	2.8 ± 0.4	(0.054)	1.9 ± 0.2	(0.079)
	$k_{transfer}/K_{Mg}$ ($M^{-1}s^{-1}$)	$1.7x10^4$	24	(710)	29	(590)
Nick-sealing						
	k_{seal} (s^{-1})	12	0.18 ± 0.03	(67)	0.11 ± 0.02	(110)
	K_{Mg} (mM)	2.6	13 ± 4	(0.2)	28 ± 7	(0.093)
	k_{seal}/K_{Mg} ($M^{-1}s^{-1}$)	$4.6x10^4$	14	(3300)	4	(12,000)

Table 4-1: Comparison of kinetic constants measured with wild-type ligase to D570N and E720Q. Relative values between the constants measured for wild-type LIG1 and the mutants are calculated by dividing the value of the wild-type constant by the value of the corresponding constant measured with the mutant enzyme. Thus, values greater than 1 for rate constants and the efficiency of magnesium utilization during single-turnover steps indicates a decrease in activity, while values less than 1 for metal affinity indicate a weakening in metal binding for the indicated step.

*The value for $k_{adenylylation}$ is determined by using the equation that relates macroscopic and microscopic rate constants (Equation 4-3), it is not directly determined by the experiments reported herein. Use of Equation 4-3 with the rate constants measured for E720Q results in a negative number for $k_{adenylylation}$, indicating the error in measurements of the other rate constants is larger than the value of $k_{adenylylation}$. This suggests enzyme adenylylation is the fastest step of the ligation reaction catalyzed by E720Q under standard conditions.

E720 appears to play a significant role during enzyme adenylylation

Compared to the large effects the D570N mutation has on the utilization of magnesium during the DNA dependent steps, changes to the same parameter for enzyme adenylylation appear quite small. D570N shows only a 2-fold decrease compared to wild-type in the second order rate-constant for utilization of ATP, $(k_{cat}/K_M)^{ATP}$ (Table 4-1). The E720Q mutation, however, shows a significant, 10-fold decrease in $(k_{cat}/K_M)^{ATP}$ compared to wild-type. The difference in importance of these two residues during adenylyl transfer coincides with their position within the active-site as pictured in the LIG1 crystal structure [8]. E720 and the metal site it is proposed to coordinate are nearby K568, the active-site lysine that becomes adenylylated during step 1 of catalysis. This positioning allows E720 to play an important role during enzyme adenylylation. D570, however, rests on the opposite side of the nick, well outside direct interaction range of the lysine residue.

Outstanding Questions

This work has extended our understanding of the role of conserved carboxylates in DNA ligase. Kinetic characterization of these mutant enzymes has revealed further information about these sites, supoorting the model of two metals being required for the DNA dependent steps. We also found differences between LIG1 mutants and those of ChVLIG, such as observing complete enzyme adenylylation following purification, unlike the ChVLIG mutants which purify with a large portion deadenylylated. This work greatly enhances our knowledge of the metal binding sites important for enzyme catalysis. Future research looking into additional mutations at these, as well as other, important active-site residues will enable us to better understand the exact function of metals in these sites.

References

1. Lehman, I.R., *DNA ligase: structure, mechanism, and function.* Science, 1974. **186**(4166): p. 790-7.
2. Sancar, A., et al., *Molecular mechanisms of mammalian DNA repair and the DNA damage checkpoints.* Annu Rev Biochem, 2004. **73**: p. 39-85.
3. Levin, D.S., et al., *Interaction between PCNA and DNA ligase I is critical for joining of Okazaki fragments and long-patch base-excision repair.* Curr Biol, 2000. **10**(15): p. 919-22.
4. Shokolenko, I.N., et al., *Mitochondrial DNA ligase is dispensable for the viability of cultured cells but essential for mtDNA maintenance.* J Biol Chem, 2013. **288**(37): p. 26594-605.
5. Grawunder, U., et al., *DNA ligase IV is essential for V(D)J recombination and DNA double-strand break repair in human precursor lymphocytes.* Mol Cell, 1998. **2**(4): p. 477-84.
6. Shuman, S., *DNA ligases: progress and prospects.* J Biol Chem, 2009. **284**(26): p. 17365-9.
7. Yang, S.W. and J.Y. Chan, *Analysis of the formation of AMP-DNA intermediate and the successive reaction by human DNA ligases I and II.* J Biol Chem, 1992. **267**(12): p. 8117-22.
8. Pascal, J.M., et al., *Human DNA ligase I completely encircles and partially unwinds nicked DNA.* Nature, 2004. **432**(7016): p. 473-8.
9. Sriskanda, V. and S. Shuman, *Role of nucleotidyl transferase motif V in strand joining by chlorella virus DNA ligase.* J Biol Chem, 2002. **277**(12): p. 9661-7.
10. Taylor, M.R., et al., *Kinetic mechanism of human DNA ligase I reveals magnesium-dependent changes in the rate-limiting step that compromise ligation efficiency.* J Biol Chem, 2011. **286**(26): p. 23054-62.
11. Sriskanda, V. and S. Shuman, *Mutational analysis of Chlorella virus DNA ligase: catalytic roles of domain I and motif VI.* Nucleic Acids Res, 1998. **26**(20): p. 4618-25.

Chapter 5: Conclusions and Future Directions

The work presented in this thesis explores the relationship between metal ions and human DNA ligase I. Our characterization of the kinetic mechanism of enzymatic DNA ligation by LIG1 in the presence of magnesium provides the first kinetic evidence for two functionally important metal ions during catalysis. This agrees with the many two-metal reaction mechanisms described for other phosphoryl transfer enzymes [1-3], and with the observance of two potential metal-binding sites within the LIG1 crystal active site [4]. We found that mutation of the residues coordinating these two potential metal sites causes a decrease in the metal binding affinity during each catalytic step, suggesting the involvement of metals at these two sites during catalysis. Characterization of enzymatic DNA ligation in the presence of manganese revealed that LIG1 is able to substitute manganese for magnesium during catalysis, similar to what has been seen with many other phosphoryl transfer enzymes [5-7]. We also found evidence for the presence of at least one inhibitory metal binding site that appears to be specific for manganese over magnesium. Like all scientific research, this work has brought forth a large number of questions even as it answered many basic questions about how metal ions interact with LIG1.

Abortive ligation

The adenylylated DNA intermediate formed during the adenylyl transfer step of DNA ligation represents a significant danger to the genome if released from the enzyme prior to completing nick-sealing. Rapid adenylylation of LIG1 prevents it from rebinding to the adenylylated intermediate, resulting in a persistent DNA break. Multiple pathways can remove the adenylyl group from DNA, allowing another chance at successful DNA ligation, including direct removal of the adenylyl group by aprataxin [8], and strand displacement of the lesion with DNA polymerase followed by single-strand cleavage with FEN-1[9]. Loss of aprataxin results in the progressive neurodegenerative disease Ataxia with Oculomotor Apraxia 1 (AOA1) [10, 11], suggesting that cells missing aprataxin are unable to efficiently repair adenylylated DNA. Neurons are likely rendered more sensitive to loss of aprataxin due to their increased metabolism

and subsequent DNA repair activity compounded with the loss of replication-dependent DNA repair pathways.

Previous work indicated LIG1 can form the adenylylated DNA intermediate at single-strand nicks created through Fenton chemistry, presumably by acting on nicks with additional damage [12]. Our work has shown that LIG1 can also form persistent adenylylated DNA at normal DNA nicks by releasing the DNA intermediate prior to completing nick-sealing. Release of the intermediate is most pronounced at sub-physiological concentrations of magnesium and decreases with increasing magnesium, however a measurable amount of abortive ligation occurs even at physiological concentrations of magnesium (.01% of ligation events resulting in abortive ligation at 1 mM free magnesium) [13]. With the million or more ligation events occurring in the genome of the average human cell per day due to DNA repair and DNA replication, even this low rate of abortive ligation results in a substantial amount of total abortive ligation events. A recent report suggests the main function of aprataxin may be to repair 5' adenylylated DNA within the mitochondria, as loss of the protein appears to more adversely affect the mitochondrial than the nuclear genome [14]. Studies of abortive ligation by LIG3 will need to be done in order to understand how significant a problem this might be within the unique environment of the mitochondria.

Substrate Specificity

The nature of substrate recognition by LIG1, and DNA ligases in general, remains one of the least understood aspects of DNA ligase function. The ability of DNA ligases to discriminate between proper ligation substrate and substrates with additional forms of damage seems almost essential to prevent the accumulation of genomic aberrations. There are, however, numerous reports of LIG1 catalyzing reactions on non-ideal DNA nicks, including abortive ligation of Fenton-chemistry induced DNA nicks [12] or nicks lacking a 3’ hydroxyl [4], and full ligation of hybrid duplexes containing mismatches or ribonucleotides [4]. In each of these cases, LIG1 appears to discriminate against the non-ideal substrate by showing a diminished rate of catalysis. Other DNA ligases appear to show similar behavior with these non-ideal substrates [15, 16].

Many of these observations have been reported as qualitative observations from different sources and different types of experiments, complicating synthesis of the data into a single model. Perhaps the most straight-forward way to understand the importance of different chemical groups at the nick and the effect of different forms of damage on ligation would be to compete substrates with chemical substitutions against one another during a DNA ligation assay. Such a systematic evaluation of how different forms of DNA damage at or near a nick affect ligation would greatly increase our knowledge of how LIG1 interacts with the nick, and how these forms of DNA damage may get exacerbated during ligation.

The crystal structure of LIG1 suggests that the nucleotide sequence of the substrate may also affect catalysis in addition to chemical groups at the nick. The DNA within the LIG1 crystal structure is highly distorted, with a 5 Å shift in the axis of the DNA backbone across the nick and a partial unwinding of the DNA helix [4]. These movements require the energetically unfavorable unstacking of adjacent base-pairs and stretching of hydrogen bonds in base-pairing interactions, which must be overcome by the energy of binding to the protein. Differences in the strength of base-stacking and base-pairing interactions due to DNA sequence can then cause changes in the rate of catalysis, as seen in studies of other DNA modifying enzymes [17]. In the case of LIG1, sequences prone to slow or abortive ligation would increase the likelihood of chromosomal breaks. Sequence specificity of LIG1 could have profound impacts on the genome by selecting over time against poorly ligatable sequences.

Preliminary work with three randomly different DNA sequences has shown that LIG1 shows a 10-fold range of k_{cat}/K_M values at physiological concentrations of magnesium, suggesting that the sequence context of the nick can have a significant effect on catalysis. The number of potential DNA sequences at a nick prohibits in-depth, manual characterization of sequence space. Characterizing only the 2 nucleotides on either side of the nick, for example, would require 256 different substrates. This type of question can only now be correctly asked by utilizing the new technique of Next-Generation DNA Sequencing. Next-Gen Sequencing can measure the rates of ligation of each of the millions of sequences formed during ligation of a substrate containing degenerate sequence on either side of the nick. The relative rates correlate

with relative ligation efficiencies of each sequence with LIG1 and to how well each sequence will be ligated within the cell. This data should reveal trends in what makes a "good" or "poor" substrate for LIG1, potentially characteristics such as the effect of individual nucleotides at the nick or overall AT or GC rich-ness for an area of the substrate. Knowing this sequence bias for LIG1 could help explain why certain sequences are more or less prevalent within the genome. One particularly interesting application would be to compare the sequences of "poor" LIG1 substrates to sequences within the genome that display an enigmatically high level of mutations. Do fragile-sites within genomes arise due to persistent DNA breaks within sequences that are poor ligation substrates? Do LIG1 and LIG3 show similar or different sequence specificity? Perhaps both ligases exist in the nucleus in order to compensate for the sequence specificity of the other. Understanding the substrate and sequence specificities of DNA ligases will provide a great deal of information into how the enzymes interact with substrates, and under what conditions DNA ligation may actually worsen DNA damage.

Alternative metals

Our characterization of the kinetic mechanism of DNA ligation by LIG1 in the presence of magnesium supports the hypothesis that magnesium is the physiologically relevant metal cofactor. LIG1 performs very efficient ligation at the estimated 1 mM concentration of free magnesium within cells, at a rate adequate to accommodate all of the single-strand breaks formed within the nucleus during DNA repair and DNA replication. The complex milieu of the cell, however, raises the possibility that other divalent metals may affect catalysis *in vivo*. Alternative metals such as manganese, cadmium and zinc have been shown to interfere with protein-substrate interactions and catalysis through displacement of active site metal ions or altering protein or substrate structures [18]. Knowledge of how these metals affect catalysis aids in understanding both the basic function of metal ions during catalysis and the complexities of how metal poisoning occurs at the cellular level.

Our characterization of the kinetic mechanism of DNA ligation in the presence of manganese revealed a new method of metal interaction with LIG1. In addition to stimulating each step of the

reaction similar to magnesium, manganese also inhibits the enzyme adenylylation and adenylyl transfer steps. The relatively low concentration of manganese within the cell, combined with the similar affinities measured for manganese and magnesium, ensures that magnesium will out-compete manganese for the active site. The observed noncompetitive inhibition by manganese, however, suggests that it may alter LIG1 function even at low concentrations.

In addition to manganese, preliminary work with cadmium, zinc and calcium indicates that these metals also stimulate and/or inhibit the enzyme in interesting ways. Cadmium and zinc are unable to stimulate any of the ligation reaction steps and only inhibit the enzyme adenylylation reaction. This observation contrasts with a previous report on inhibition of LIG1 by cadmium and zinc where the two metals were reported to inhibit all steps of the reaction with similar metal affinities during each step [19]. The discrepancy between our observations and the previous report likely results from differences in protein purification and sample preparation which lead to the previous group observing the multiple-turnover inhibition during their single-turnover experiments. Both our work and the previous report establish an inhibitory metal affinity for zinc of 350 μM and an inhibitory metal affinity for cadmium of 12 μM during the multiple-turnover reaction [19]. The inhibitory zinc affinity is relatively weak compared to the < 1 μM cellular concentration of the metal within cells, however the inhibitory cadmium displays an affinity similar or stronger than the concentration at which cells experience cadmium related toxicity (10-60 μM) [20, 21]. Cadmium poisoning leads to deficiencies in DNA replication and repair, signified by persistent DNA breaks, suggesting that inhibition of LIG1 may be one of the causative events for cadmium related cell death.

In a new pattern of metal ion interaction with LIG1, calcium stimulates adenylyl transfer and nick-sealing, but is unable to promote enzyme adenylylation. Calcium also inhibits enzyme adenylylation and adenylyl transfer, similar to what was observed with manganese. Preliminary data suggests the calcium ion affinities lie within the low millimolar range for both the stimulatory and inhibitory sites. Similar to manganese, this ensures that under normal conditions magnesium will out-compete calcium for binding to the active site due to the much higher concentration of magnesium in the cell compared to calcium (1 mM free magnesium vs. ~10 μM free calcium). However, under conditions of severe cell stress, such as during stroke, the level of

calcium within the cell is estimated to increase 10- to 100-fold [22]. Under these conditions, a significant proportion of LIG1 molecules will contain active site calcium ions, allowing calcium to promote DNA ligation. It is interesting to note that DNA fragmentation is one of the hallmarks of neuronal cell death following stroke, perhaps suggesting that calcium stimulated DNA ligation by LIG1 is more apt to lead to abortive ligation.

This small survey of divalent metals with LIG1 reveals 4 different patterns of metal interactions with LIG1 based on which steps each metal stimulates and/or inhibits. The presence of an inhibitory metal site that is not competitive with magnesium allows each metal to potentially influence LIG1 catalysis, despite relatively low inhibitory metal affinities. As metal ions likely play a significant role in the interaction between protein and substrate, it will be interesting to investigate how the presence of alternative metals might affect substrate binding and recognition. Do these inhibitory metals render LIG1 more or less sensitive to mismatches, damage or ribonucleotides at the nick? Do they affect the rate of abortive ligation? These questions are especially relevant in the context of calcium, as calcium will be able to out-compete magnesium ions for active site metal binding during calcium spikes.

References

1. Yang, L., et al., *Critical role of magnesium ions in DNA polymerase beta's closing and active site assembly.* J Am Chem Soc, 2004. **126**(27): p. 8441-53.
2. Smith, D. and N.R. Pace, *Multiple magnesium ions in the ribonuclease P reaction mechanism.* Biochemistry, 1993. **32**(20): p. 5273-81.
3. Klumpp, K., et al., *Two-metal ion mechanism of RNA cleavage by HIV RNase H and mechanism-based design of selective HIV RNase H inhibitors.* Nucleic Acids Res, 2003. **31**(23): p. 6852-9.
4. Pascal, J.M., et al., *Human DNA ligase I completely encircles and partially unwinds nicked DNA.* Nature, 2004. **432**(7016): p. 473-8.
5. Tabor, S. and C.C. Richardson, *Effect of manganese ions on the incorporation of dideoxynucleotides by bacteriophage T7 DNA polymerase and Escherichia coli DNA polymerase I.* Proc Natl Acad Sci U S A, 1989. **86**(11): p. 4076-80.
6. El-Deiry, W.S., K.M. Downey, and A.G. So, *Molecular mechanisms of manganese mutagenesis.* Proc Natl Acad Sci U S A, 1984. **81**(23): p. 7378-82.
7. Frank, E.G. and R. Woodgate, *Increased catalytic activity and altered fidelity of human DNA polymerase iota in the presence of manganese.* J Biol Chem, 2007. **282**(34): p. 24689-96.
8. Rass, U., I. Ahel, and S.C. West, *Molecular mechanism of DNA deadenylation by the neurological disease protein aprataxin.* J Biol Chem, 2008. **283**(49): p. 33994-4001.
9. Liu, Y., et al., *DNA polymerase beta and flap endonuclease 1 enzymatic specificities sustain DNA synthesis for long patch base excision repair.* J Biol Chem, 2005. **280**(5): p. 3665-74.
10. Moreira, M.C., et al., *The gene mutated in ataxia-ocular apraxia 1 encodes the new HIT/Zn-finger protein aprataxin.* Nat Genet, 2001. **29**(2): p. 189-93.
11. Date, H., et al., *Early-onset ataxia with ocular motor apraxia and hypoalbuminemia is caused by mutations in a new HIT superfamily gene.* Nat Genet, 2001. **29**(2): p. 184-8.
12. Ahel, I., et al., *The neurodegenerative disease protein aprataxin resolves abortive DNA ligation intermediates.* Nature, 2006. **443**(7112): p. 713-6.
13. Gunther, T., *Concentration, compartmentation and metabolic function of intracellular free Mg2+.* Magnes Res, 2006. **19**(4): p. 225-36.
14. Sykora, P., et al., *Aprataxin localizes to mitochondria and preserves mitochondrial function.* Proc Natl Acad Sci U S A, 2011. **108**(18): p. 7437-42.
15. Sriskanda, V. and S. Shuman, *Specificity and fidelity of strand joining by Chlorella virus DNA ligase.* Nucleic Acids Res, 1998. **26**(15): p. 3536-41.
16. Ho, C.K., J.L. Van Etten, and S. Shuman, *Characterization of an ATP-dependent DNA ligase encoded by Chlorella virus PBCV-1.* J Virol, 1997. **71**(3): p. 1931-7.
17. Stivers, J.T., *2-Aminopurine fluorescence studies of base stacking interactions at abasic sites in DNA: metal-ion and base sequence effects.* Nucleic Acids Res, 1998. **26**(16): p. 3837-44.

18. Takiguchi, M., et al., *Effects of cadmium on DNA-(Cytosine-5) methyltransferase activity and DNA methylation status during cadmium-induced cellular transformation.* Exp Cell Res, 2003. **286**(2): p. 355-65.
19. Yang, S.W., F.F. Becker, and J.Y. Chan, *Inhibition of human DNA ligase I activity by zinc and cadmium and the fidelity of ligation.* Environ Mol Mutagen, 1996. **28**(1): p. 19-25.
20. Watjen, W., et al., *Induction of apoptosis in mammalian cells by cadmium and zinc.* Environ Health Perspect, 2002. **110 Suppl 5**: p. 865-7.
21. Shimoda, R., et al., *Induction of apoptosis in cells by cadmium: quantitative negative correlation between basal or induced metallothionein concentration and apoptotic rate.* Toxicol Sci, 2001. **64**(2): p. 208-15.
22. Kristian, T. and B.K. Siesjo, *Calcium in ischemic cell death.* Stroke, 1998. **29**(3): p. 705-18.

Appendix: Berkeley-Madonna Code for Reaction Fitting

```
METHOD RK4

STARTTIME = 0
STOPTIME = 14
DT = 2e-5

{A single reaction scheme applies to all the traces.  Madonna needs to associate a set of equations with each trace.  Rather than repeat the equations for each trace, it can be done with one set using vectors indexed 1 through 3 for each trace.}

{Shorthand reaction scheme: Lig + ATP <-k1-> Lig•ATP <-k2-> aLig + nDNA <-k3> aLig•nDNA <-k4> Lig•aDNA <-k5-> Lig•DNA <-k6-> Lig + DNA}

{Explanation of variable names: Lig = deadenylylated Ligase, Lig•ATP = Ligase w/ ATP bound, aLig = adenylylated Ligase, nDNA = nicked DNA substrate, aLig•nDNA = adenylylated Ligase w/ DNA substrate bound, Lig•aDNA = Ligase w/ adenylylated (intermediate) DNA bound, DNA = product DNA, Lig•DNA = Ligase with product DNA bound}

d/dt (Lig[1..3])    =  k6f*LigDNA[i]             - k6r*Lig[i]*DNA[i]      - k1f*Lig[i]*ATP[i]      + k1r*LigATP[i]
d/dt (ATP[1..3])    =  -k1f*Lig[i]*ATP[i]        + k1r*LigATP[i]
d/dt (LigATP[1..3]) =  k1f*Lig[i]*ATP[i]         - k1r*LigATP[i]          - k2f*LigATP[i]          + k2r*aLig[i]
d/dt (aLig[1..3])   =  k2f*LigATP[i]             - k2r*aLig[i]            - k3f*aLig[i]*nDNA[i]    + k3r*aLignDNA[i]
d/dt (nDNA[1..3])   =  -k3f*aLig[i]*nDNA[i]      + k3r*aLignDNA[i]
d/dt (aLignDNA[1..3]) = k3f*aLig[i]*nDNA[i]      - k3r*aLignDNA[i]        - k4f*aLignDNA[i]        + k4r*LigaDNA[i]
d/dt (LigaDNA[1..3]) = k4f*aLignDNA[i]           - k4r*LigaDNA[i]         - k5f*LigaDNA[i]         + k5r*LigDNA[i]
d/dt (LigDNA[1..3]) =  k5f*LigaDNA[i]            - k5r*LigDNA[i]          - k6f*LigDNA[i]          + k6r*Lig[i]*DNA[i]
d/dt (DNA[1..3])    =  k6f*LigDNA[i]             - k6r*Lig[i]*DNA[i]


{"init X[i] = ##" sets value of reagent "X" in reaction "i" at t=0 to "##".  By putting in a variable name for "##", the value can be changed easily in the parameters window.}

{Explanation of variable names: "o" used as a "not" to symbolize amount of species present at time zero, deadLig = deadenylylated Ligase, LigATP = Ligase w/ ATP bound, aLig = adenylylated Ligase, nDNA = nicked DNA substrate, aLignDNA = adenylylated Ligase w/ DNA substrate bound, LigaDNA = Ligase w/ adenylylated (intermediate) DNA bound, DNA = product DNA, LigDNA = Ligase with product DNA bound}
```

```
init Lig[1..3] = deadLigo
init ATP[1] = ATP1o
init ATP[2] = ATP2o
init ATP[3] = ATP3o
init LigATP[1..3] = 0
init aLig[1] = aLigo1
init aLig[2] = aLigo2
init aLig[3] = aLigo3
init nDNA[1..3] = nDNAo
init aLignDNA[1..3] = 0
init LigaDNA[1] = LigaDNA1o
init LigaDNA[2] = LigaDNA2o
init LigaDNA[3] = LigaDNA3o
init LigDNA[1..3] = 0
init DNA[1..3] = 0
```

{"X = ##" sets value of variable "X" to "##" for the initial run. The value of "##" in this file will not change when the value of "X" is altered in the parameter window.}

```
deadLigo = 0
ATP1o = 0
ATP2o = 4e-6
ATP3o = 150e-6
ATP4o = 0
aLigo1 = 50e-9
aLigo2 = 50e-9
aLigo3 = 50e-9
aLigo4 = 50e-9
nDNAo = 500e-9
LigaDNA1o = 0
LigaDNA2o = 0
LigaDNA3o = 0
LigaDNA4o = 0
```

{"X = Y[i]" allows the variable "X" to be used in fitting the reagent "Y" from reaction "i" in curve fitting. Also allows the variable "X" to be plotted independently on the graph.}

```
DNA1 = DNA[1]
DNA2 = DNA[2]
DNA3 = DNA[3]
ATP1 = ATP[1]
ATP2 = ATP[2]
ATP3 = ATP[3]
LigaDNA1 = LigaDNA[1]
LigaDNA2 = LigaDNA[2]
LigaDNA3 = LigaDNA[3]
```

{Rate constants must be set to a value using the following form. When fitting data, these values are simply initial guesses. Rate constants automatically appear in the parameters window and in the curve fitting menu.}

```
k1f = 1e5
k1r = 2e-3
```

k2f = 0.5
k2r = 0
k3f = 1e8
k3r = 1
k4f = 2.5
k4r = 0
k5f = 12
k5r = 0
k6f = 1e8
k6r = 1